

---

Electronic Thesis and Dissertation Repository

---

12-10-2013 12:00 AM

## Specimen Size Effect on Shear Behavior of Loose Sand in Triaxial Testing

Tarek Omar  
*The University of Western Ontario*

Supervisor  
Abouzar Sadrekarimi  
*The University of Western Ontario*

Graduate Program in Civil and Environmental Engineering  
A thesis submitted in partial fulfillment of the requirements for the degree in Master of  
Engineering Science  
© Tarek Omar 2013

Follow this and additional works at: <https://ir.lib.uwo.ca/etd>



Part of the [Civil and Environmental Engineering Commons](#)

---

### Recommended Citation

Omar, Tarek, "Specimen Size Effect on Shear Behavior of Loose Sand in Triaxial Testing" (2013).  
*Electronic Thesis and Dissertation Repository*. 1755.  
<https://ir.lib.uwo.ca/etd/1755>

This Dissertation/Thesis is brought to you for free and open access by Scholarship@Western. It has been accepted for inclusion in Electronic Thesis and Dissertation Repository by an authorized administrator of Scholarship@Western. For more information, please contact [wlsadmin@uwo.ca](mailto:wlsadmin@uwo.ca).

**SPECIMEN SIZE EFFECT ON SHEAR BEHAVIOR OF LOOSE SAND IN  
TRIAxIAL TESTING**

(Thesis format: Integrated Article)

by

**Tarek Omar**

Graduate Program in Civil and Environmental Engineering

A thesis submitted in partial fulfillment  
of the requirements for the degree of  
Master of Engineering Science

The School of Graduate and Postdoctoral Studies  
The University of Western Ontario  
London, Ontario, Canada  
December 2013

© Tarek Omar 2013

## Abstract

Triaxial tests are widely used to determine the behavior and strength characteristics of soils without due attention to the differences in specimen size. Several drained and undrained monotonic triaxial compression shear tests are performed on three different specimen sizes of the same sand to investigate the influence of specimen size and scale effect on the shear behavior. The test results indicate that the behavior of loose sand is strongly influenced by the specimen size, with larger specimens exhibiting a stiffer behavior during isotropic compression, and mobilizing smaller shear strengths and effective friction angles. Triaxial testing also involves many sources of errors that could significantly affect shear strength parameters if not corrected. Extensive errors are investigated and it is found that negligence in making corrections accounting for these errors will result in an overestimation as much as 42% and 15 degrees in the critical shear strength and critical state friction angle, respectively. Furthermore, the measured critical state parameters and shear strengths are employed to compare the static and seismic slope stability of an earth embankment dam, calibrate a critical state soil constitutive model, study the soil behavior under shallow foundations, and evaluate liquefaction triggering and failure of retaining structures. The results show that all of these analyses are significantly affected by the strength parameters of the same soil determined from different specimen sizes. While using small size samples for determining shear strength parameters might result in un-conservative design, the choice of a large sample size is consequently a more accurate representation of soil strength conditions and field deformations.

### .Keywords

Triaxial testing, loose sand, scale effect, corrections, critical state, geotechnical analyses.

## Co-Authorship Statement

This thesis has been prepared in accordance with the regulations for an Integrated-Article format thesis stipulated by the School of Graduate and Postdoctoral Studies at the University of Western Ontario and has been co-authored as:

### **Chapter 2: Effects of Errors and Multiple Corrections on Triaxial Compression Testing of Loose Sands**

All the experimental work was conducted by Tarek Omar under close supervision of Dr. Abouzar Sadrekarimi. A paper co-authored by Tarek Omar and Abouzar Sadrekarimi is going to be submitted to the ASTM Geotechnical Testing Journal.

### **Chapter 3: Specimen Size Effect on Triaxial Compression Testing of Loose Sands**

All the experimental work was conducted by Tarek Omar under close supervision of Dr. Abouzar Sadrekarimi. A paper co-authored by Tarek Omar and Abouzar Sadrekarimi is going to be submitted to the Canadian Geotechnical Journal.

### **Chapter 4: Influence of Triaxial Specimen Size in Engineering Practice**

All the experimental work was conducted by Tarek Omar under close supervision of Dr. Abouzar Sadrekarimi. A paper co-authored by Tarek Omar and Abouzar Sadrekarimi is going to be submitted to the journal of Geotechnique.

## Acknowledgments

The research work presented in this thesis has been carried out under the supervision of Assistant Professor Abouzar Sadrekarimi, who has been a constant source of support and helpful guidance throughout the research and preparation of this dissertation. I would like to thank him for his consistent support and valuable advices.

I would also like to thank the graduate students in the department of civil and environmental engineering for sharing the knowledge and most of all, for being my friends as well to the administrative and laboratory staff, and to the machine shop staff at Western Engineering.

Finally, my deepest appreciation goes to my parents, my wife, my beloved daughter Heba, and my beloved son Abdelrahman for their patience and boundless support.

# Table of Contents

Abstract .....	ii
Co-Authorship Statement.....	iii
Acknowledgments.....	iv
Table of Contents .....	v
List of Tables .....	viii
List of Figures .....	ix
List of Symbols .....	xiii
Chapter 1 .....	1
1 Introduction .....	1
1.1 Statement of the Problem.....	1
1.2 Research Objective .....	3
1.3 Thesis Outline .....	4
Chapter 2.....	5
2 Effects of Errors and Multiple Corrections on Triaxial Compression Testing of Loose Sands .....	5
2.1 Introduction.....	5
2.2 Physical Index Properties of Tested Sand.....	7
2.3 Testing Equipment .....	8
2.3.1 Enlarged Platens.....	8
2.3.2 Mould Design.....	12
2.3.3 Triaxial Test System .....	14
2.4 Triaxial Compression Testing Procedure.....	17
2.4.1 Sample Preparation .....	17
2.4.2 Saturation Stage .....	21
2.4.3 Consolidation Stage .....	23

2.4.4	Shearing Stage .....	23
2.5	Corrections for Triaxial Compression Tests .....	25
2.5.1	Correction of Volume Change during Saturation .....	26
2.5.2	Correction of Volume Change due to Membrane Penetration.....	29
2.5.3	Effects of Enlarged Platens on Stress-Strain Response .....	34
2.5.4	Area Correction due to Specimen Deformation Pattern .....	36
2.5.5	Correction for Bedding Error .....	40
2.5.6	Correction for Membrane Resistance .....	42
2.6	Comparison of Corrections .....	45
2.7	Conclusion .....	47
	References.....	49
	Chapter 3.....	52
3	Specimen Size Effect on Triaxial Compression Testing of loose sands .....	52
3.1	Introduction.....	52
3.2	Experimental Methodology .....	57
3.3	Triaxial Test Results: .....	59
3.3.1	Isotropic Compression Response .....	59
3.3.2	Undrained shear behavior .....	61
3.3.3	Drained shear behavior .....	65
3.4	Influence of Specimen Size on Effective Stress Paths.....	70
3.5	Influence of Specimen Size on Effective Friction Angle .....	72
3.6	Influence of Specimen Size on Critical State Parameters.....	76
3.7	Influence of Sample Size on Undrained Shear Strength.....	78
3.8	Discussion.....	84
3.9	Conclusion .....	87
	References.....	88

Chapter 4.....	92
4 Influence of Triaxial Specimen Size in Engineering Practice .....	92
4.1 Introduction.....	92
4.2 Experimental Data .....	94
4.3 Sample Size Effect on Liquefaction Triggering Analysis .....	95
4.4 Sample Size Effect on the Calibration of a Soil Constitutive Model .....	96
4.5 Sample Size Effect on Consolidation Settlement .....	104
4.6 Sample Size Effect on Slope Stability Analysis .....	105
4.6.1 Static Slope Stability Analysis.....	107
4.6.2 Seismic Slope Stability Analysis .....	107
4.7 Sample Size Effect on Bearing Capacity of Shallow Foundations.....	109
4.8 Sample Size Effect on Lateral Earth Pressure .....	113
4.9 Conclusion .....	115
References.....	116
Chapter 5.....	119
5 Summary and Conclusions.....	119
Appendix A.....	122
Appendix B.....	126
Curriculum Vitae .....	129



## List of Tables

Table 2.1: Triaxial test data in this study .....	25
Table 2.2: Void ratio change due to flushing and backpressure saturation .....	28
Table 2.3: Effect of area correction on the critical strength .....	39
Table 2.4: Effect of bedding error on the axial displacement.....	42
Table 2.5: Effect of membrane resistance on the deviator stress.....	45
Table 2.6: Summary of the applied corrections and percentage improvement for triaxial shear testing on very loose sand.....	46
Table 3.1: Summary of the specimen sizes used in different studies .....	52
Table 3.2: Specifications of triaxial tests of this study .....	59
Table 3.3: Summary of $\phi'_{\text{yield}}$ and $\phi'_{\text{cs}}$ for different specimen sizes .....	74
Table 3.4: Effect of specimen size on critical state parameters .....	77
Table 3.5: $s_u(\text{yield})$ and $s_u(\text{critical})$ from undrained triaxial compression tests.....	79
Table 3.6: Summary of $\psi_{\text{cs}}$ , $s_u(\text{yield})/p'_c$ , $s_u(\text{cs})/p'_c$ , and $I_B$ for the undrained triaxial tests ...	83
Table 4.1: Summary of NorSand calibration parameters.....	100
Table 4.2: Factor of safety against static and seismic loads of different specimen sizes ....	108
Table 4.3: Bearing capacity factor based on $\phi'_{\text{cs}}$ of different specimen sizes.....	112

## List of Figures

Figure 2.1: Average particle size distribution of the Barco 71 sand.....	7
Figure 2.2: Schematic diagrams of the enlarged platens for different sample sizes.....	11
Figure 2.3: Photos of the enlarged platens used for different sample sizes.....	11
Figure 2.4: Schematic diagram of the tamper assembly.....	12
Figure 2.5: Schematic diagrams and photos for split moulds used for different sample sizes .....	14
Figure 2.6: Schematic diagram of the triaxial testing system. ....	15
Figure 2.7: Triaxial shear apparatus used in this study.....	16
Figure 2.8: Steps of specimen preparation using moist tamping method.....	21
Figure 2.9: Effect of membrane penetration (after K.H. Head 1992).....	29
Figure 2.10: Effect of $D_{50}$ on the normalized membrane penetration (Sivathayalan and Vaid 1998).....	32
Figure 2.11: Effect of lubricated end platens on the stress-strain and excess pore pressure responses in triaxial compression tests on loose sand .....	35
Figure 2.12: Effect of lubricated end platens on the deformation patterns of loose sand specimens in triaxial compression tests at 30% axial strain .....	38
Figure 2.13: Effect of area correction method on the stress- strain response in undrained triaxial compression tests on loose sand .....	38
Figure 2.14: Effect of membrane resistance on the stress- strain response of undrained triaxial compression tests on loose sand .....	44
Figure 3.1: Effect of specimen size on the behavior of Ticino 9 sand (Jefferies <i>et al.</i> 1990)	54

Figure 3.2: Effect of specimen size on the isotropic compression behavior of loose sand ..	61
Figure 3.3: Undrained stress – strain behavior of different specimen sizes in triaxial compression tests of loose sand .....	63
Figure 3.4: Undrained stress – axial displacement behavior of different specimen sizes in triaxial compression tests of loose sand.....	64
Figure 3.5: Excess pore water pressure developed during undrained triaxial compression tests on different specimen sizes of loose sand.....	64
Figure 3.6: Drained stress – strain behavior of different specimen sizes in triaxial compression tests of loose sand .....	66
Figure 3.7: Drained deviator stress – axial displacement behavior of different specimen sizes in triaxial compression tests of loose sand.....	67
Figure 3.8: Volumetric strain response during drained triaxial compression tests on different specimen sizes of loose sand.....	69
Figure 3.9: Volumetric dilatancy response during drained triaxial compression tests on different specimen sizes of loose sand.....	69
Figure 3.10: Effect of specimen size on drained effective stress paths .....	71
Figure 3.11: Effect of specimen size on undrained effective stress paths .....	71
Figure 3.12: Effect of specimen size on $\phi'_{mob}$ in undrained triaxial compression shear tests of loose sand.....	73
Figure 3.13: Effect of specimen size on $\phi'_{mob}$ in drained triaxial compression shear tests of loose sand.....	73
Figure 3.14: Effect of $p'_c$ and $D_{rc}$ on $\phi'_{yield}$ and $\phi'_{cs}$ mobilized in undrained triaxial compression tests on loose specimens of different sizes .....	75

Figure 3.15: Effect of specimen size on $\phi'_{\text{yield}}$ and $\phi'_{\text{cs}}$ from undrained triaxial compression tests of loose sand .....	76
Figure 3.16: Effect of specimen size on the CSLs from both drained and undrained triaxial compression tests of loose sand .....	77
Figure 3.17: Effect of specimen size on $s_u(\text{yield})$ and $s_u(\text{critical})$ in undrained triaxial compression tests on loose sand .....	79
Figure 3.18: Effect of specimen size on the changes of: (a) $s_u(\text{yield})/p'_c$ and (b) $s_u(\text{critical})/p'_c$ mobilized in undrained triaxial compression tests of loose sand with $\psi_{\text{cs}}$ .....	80
Figure 3.19: Effect of specimen size on: (a) $\phi'_{\text{yield}}$ and (b) $\phi'_{\text{cs}}$ mobilized in undrained triaxial compression tests of loose sand with respect $\psi_{\text{cs}}$ .....	81
Figure 3.20: Effect of specimen size on the changes of: (a) $s_u(\text{yield})/p'_c$ and (b) $s_u(\text{critical})/p'_c$ mobilized in undrained triaxial compression tests of loose sand with $\psi_{\text{cs}}/\lambda_{\text{cs}}$ .....	81
Figure 3.21: Effect of specimen size on: (a) $\phi'_{\text{yield}}$ and (b) $\phi'_{\text{cs}}$ mobilized in undrained triaxial compression tests of loose sand with respect to $\psi_{\text{cs}}/\lambda_{\text{cs}}$ .....	82
Figure 3.22: Effect of specimen size on $I_B$ in undrained triaxial compression tests of loose sand with respect to: (a) $\psi_{\text{cs}}$ , (b) $\psi_{\text{cs}}/\lambda$ .....	83
Figure 3.23: Changes in (a) $s_u(\%)$ and (b) $\phi'$ (degrees) with percent changes of specimen diameter (D) from $s_u$ and $\phi'$ mobilized in a 70 mm loose specimen .....	86
Figure 4.1: IL of different specimen sizes from undrained triaxial compression tests.....	96
Figure 4.2: Critical state lines for different specimen sizes in (a) void ratio – $p'$ diagram, and (b) stress path plot.....	98
Figure 4.3: Plastic hardening modulus as a function of $\psi$ for each specimen size.....	99
Figure 4.4: Dilatancy as a function of $\psi$ for each specimen size.....	99

Figure 4.5: Comparison of Ottawa sand behavior in triaxial shear tests on 70 mm specimens with NorSand predictions .....	101
Figure 4.6: Comparison of Ottawa sand behavior in triaxial shear tests on 50 mm specimens with NorSand predictions .....	101
Figure 4.7: Comparison of Ottawa sand behavior in triaxial shear tests on 38 mm specimens with NorSand predictions .....	102
Figure 4.8: Effect of specimen size on modeling sand behavior with NorSand.....	103
Figure 4.9: Effect of specimen size on $s_u(\text{critical})/p'_c$ and $s_u(\text{yield})/p'_c$ estimations by the NorSand soil model.....	103
Figure 4.10: Isotropic compressibility of different specimen sizes .....	104
Figure 4.11: Pre-failure cross section of LSFD (Seed et al. 1975).....	106
Figure 4.12: Specimen size effect on factors of safety (FOS) from static and seismic slope stability analyses .....	109
Figure 4.13: Bearing capacity factor as a function of specimen size.....	113
Figure 4.14: Lateral active earth pressure coefficient, $k_a$ , as function of specimen size.....	114

## List of Symbols

<b>A<sub>0</sub></b>	Initial specimen cross-sectional area
<b>A<sub>c</sub></b>	Specimen cross-sectional area after consolidation
<b>A<sub>e</sub></b>	Specimen cross-sectional area at end of the test
<b>A<sub>f</sub></b>	Specimen cross-sectional area at peak strength
<b>A<sub>s</sub></b>	Specimen cross-sectional area after saturation
<b>B</b>	Skempton's pore water pressure parameter
<b>C</b>	Contraction behavior
<b>CO<sub>2</sub></b>	Carbon dioxide
<b>CPT</b>	Cone penetration test
<b>CSL</b>	Critical state line
<b>C<sub>c</sub></b>	Coefficient of curvature
<b>C<sub>u</sub></b>	Coefficient of uniformity
<b>c<sub>c</sub></b>	Compression index
<b>c<sub>v</sub></b>	Coefficient of consolidation
<b>D</b>	Drained shear
<b>D<sub>rc</sub></b>	Relative density at end of consolidation
<b>D<sub>rs</sub></b>	Relative density at end of saturation
<b>D<sub>max</sub></b>	Maximum particle size
<b>D<sub>50</sub></b>	Mean particle size
<b>D<sub>10</sub></b>	Particle size corresponding to 10% finer soil-size particles
<b>d<sub>c</sub></b>	Diameter of specimen after consolidation
<b>d<sub>s</sub></b>	Diameter of specimen after saturation
<b>d<sub>1/3</sub></b>	Average specimen diameter within the middle third portion
<b>d<sub>max</sub></b>	Maximum diameter of specimen after shear
<b>E<sub>m</sub></b>	Young's modulus of membrane material
<b>E<sub>w</sub></b>	Modulus of water
<b>e</b>	Void ratio
<b>e<sub>max</sub></b>	Maximum void ratio
<b>e<sub>min</sub></b>	Minimum void ratio
<b>e<sub>c</sub></b>	Void ratio at end of consolidation

$e_{cs}$	Void ratio at critical state
$e_s$	Void ratio at end of saturation
<b>FOS</b>	Factor of safety
$G_s$	Specific gravity of solid particles
<b>H</b>	Plastic hardening parameter
<b>HRDT</b>	Hall radial displacement transducer
<b>h</b>	Height of specimen
<b>IL</b>	Instability line
$I_B$	Undrained brittleness index
$I_r$	Shear rigidity number
$K_a$	Coefficient of active lateral earth pressure
<b>LSFD</b>	Lower San Fernando Dam
<b>LVDT</b>	Linear variable displacement transducer
<b>NCL</b>	Normal compression line
$N_\gamma$	Bearing capacity factor
<b>M</b>	Stress ratio at the critical state
$p'$	Mean effective stress
$p'_c$	Consolidation stress
$q$	Deviator stress
$q_{ult}$	Ultimate bearing capacity
<b>SPT</b>	Standard penetration test
$s_u$	Shear strength
$s_u(\text{yield})$	Undrained yield shear strength
$s_u(\text{cs})$	Undrained critical shear strength
$t_{50}$	Time required to reach 50% degree of consolidation
$t_{90}$	Time required to reach 90% degree of consolidation
$t_m$	Thickness of the rubber membrane
<b>UD</b>	Undrained shear
$U_n$	Maximum under compaction ratio
$u$	Pore-water pressure
$V_c$	Specimen volume after consolidation

$V_o$	Initial specimen volume
$V_s$	Specimen volume after saturation
$\chi_{tc}$	Dilatancy parameter
$\sigma_1$	Total vertical stress
$\sigma'_1$	Effective vertical stress
$\sigma_3$	Total confining stress
$\sigma'_3$	Effective confining stress
$\psi$	Critical state parameter
$\phi'_{cs}$	Critical state friction angle
$\phi'_{mob}$	Mobilized friction angle
$\phi'_{yield}$	Yield friction angle
$\varepsilon_a$	Axial strain
$\varepsilon_r$	Radial strain
$\varepsilon_v$	Volumetric strain
$\dot{\varepsilon}$	Shear strain rate
$\delta_a$	Axial shear displacement
$\nu$	Poisson's ratio
$\Delta e$	Change in specimen void ratio
$\Delta h_s$	Change in specimen height during saturation
$\Delta q$	Membrane resistance
$\Delta \sigma_3$	Increment of cell pressure
$\Delta u$	Excess pore water pressure
$\Delta v_e$	Volume change due to membrane penetration
$\Delta v_s$	Volume change during saturation
$\lambda_{cs}$	Slope of CSL
$\Gamma$	Void ratio at $p'=1$ kPa in $e-\ln p'$ space



# Chapter 1

## 1 Introduction

### 1.1 Statement of the Problem

Triaxial shear tests are widely used to determine the strength characteristics of soils subject to a wide range of stress paths and loading conditions. Although some researchers (Marsal 1967; Marachi *et al.* 1969; Ladd 1978; Scott 1987; Been and Jefferies 1991; Hu *et al.* 2010; Chew *et al.* 2011) have studied the effect of sample size on the behavior of cohesionless soils using triaxial testing, the impact of specimen size on the shear strength parameters and design is largely overlooked in engineering practice. Previous investigations of specimen-size effects in triaxial tests have mainly focused on the testing of dense sands (Scott 1987; Been and Jefferies 1985; Garga 1988; Hazarika *et al.* 2010) or coarser granular materials containing large particles such as rockfill (Marsal 1967; Marachi *et al.* 1969; Seif el Dine 2009; Hu *et al.* 2010) which require the construction of a large-sized triaxial apparatus. Therefore, there is need for additional experimental work in order to investigate the influence of sample size on the shear behavior of very loose sands and develop new guidelines for specimen size in triaxial testing. A comprehensive and systematic experimental program of several static triaxial compression shear tests is conducted to investigate the sample size effect on the consolidation, drained and undrained shear behavior of loose Ottawa sand specimens. Three different specimen diameters of 38, 50, and 70 mm of the same sand were tested and sheared up to 30% strain using an automated stress path triaxial compression testing system.

Reliability of shear strength parameters considerably depends on the accuracy of the triaxial shear testing results. Although limitation and errors accompanying triaxial testing are

evaluated by many researchers (Bishop and Henkel 1962; Lade 1977; Baldi and Nova 1984; Seed 1987; Kramer and Sivaneswaran 1989; Zhang 1997), there is need to recognize the errors that can significantly affect test results, and techniques or corrections to account for these errors. In addition it is required to identify how the corrections interact and if it is required to account for all the corrections and determine the correction that has the most significant effect on the sand shear behavior. Therefore, extensive errors investigation is accomplished for the triaxial test results in this study to improve the estimation of shear strength parameters. As non-uniform deformation at the critical state is an important factor that may affect the behavior of sand as well, enlarged and lubricated end platens are used to minimize non-uniformity caused by end restraint which required the design and construction of a set of special moulds and platens.

Most practicing engineers are unaware of the significant effect of specimen size. Accordingly, this phenomenon is either totally neglected in using laboratory test results on a small specimen in engineering design and analysis, or laboratory test results are simply distrusted and the design or analysis is based on empirical interpretations of in-situ field tests (e.g. SPT or CPT) which could also involve a wide range of uncertainties. Therefore, there is need to investigate the influence of specimen size and scale effect from laboratory triaxial shear testing on engineering analysis and design of soil structures. The measured critical state parameters and shear strengths are used to compare the static and seismic slope stability of Lower San Fernando dam as a typical geometry of an embankment dam that underwent liquefaction flow failure, calibrate NorSand model as a critical state soil constitutive model that is widely used to predict soil behavior, study the soil behavior under shallow or strip foundations, and evaluate liquefaction triggering and failure of retaining structures.

## 1.2 Research Objective

The main objective of this research is to examine the effect of sample size in triaxial shear testing on the deformation and strength behavior of very loose sand. Other objectives of this work include:

1. Design and construct moulds and enlarged platens for each specimen size to accommodate the radial expansion of the specimen at large shear strains and reduce specimen non-uniform deformation and bulging and ensure uniform stress distribution within the specimens.
2. Investigate the errors accompanying triaxial testing and study their influence on the sand shear behavior and determine the most significant error.
3. Investigate the influence of specimen size on engineering analysis and design of soil structures.
4. Develop a new guideline for specimen size in triaxial testing.

Specially-designed moulds and platens were constructed in the machine shop of Western University. The sand used in this study is clean uniformly-graded quartz fine sand (SP as per ASTM D2487-11 Unified Soil Classification System) from Ottawa, Illinois. The experimental work included 24 strain – controlled, drained and undrained, monotonic loading tests performed on very loose specimens with 0% relative density.

### 1.3 Thesis Outline

This thesis has been prepared in "Integrated-Article" format. It is organized into 5 chapters.

A brief description of the following four chapters is as follows:

**Chapter 2:** evaluates the significance of applying corrections to the triaxial test results and presents the improvement achieved on the shear strength parameters. The specimen preparation method and the applied triaxial procedure as well as the design of especially split moulds and enlarged platens are described in this chapter. The influence of using free end on the deformation pattern is also presented.

**Chapter 3:** investigates the specimen size effect on drained and undrained sand shear behavior. The influence of specimen size on the isotropic compression behavior, the mobilized friction angles, the critical state parameters, and the yield and critical strengths are discussed. The relation between the measured shear strength parameters with the critical state parameter ( $\psi$ ) is presented. The undrained brittleness index ( $I_B$ ) is also utilized to compare the degree of strain-softening and liquefaction flow exhibited for different specimen sizes.

**Chapter 4:** implements the results obtained from testing different specimen sizes in evaluating the liquefaction triggering resistance, comparing the static and seismic slope stability of an earth embankment dam, calibrating a critical state soil constitutive model, investigating the soil behavior under shallow or strip foundations, and finally evaluating the stability analyses of retaining structures.

**Chapter 5:** presents a brief summary of the performed research works accompanied with conclusions and recommendations for future study.

## Chapter 2

# 2 Effects of Errors and Multiple Corrections on Triaxial Compression Testing of Loose Sands

## 2.1 Introduction

Laboratory shear tests conducted to understand sand behavior have been improved with the continuous development of the testing devices. There are certain principle requirements that should be accounted for in the devices used to measure the shear behavior of sands in order to obtain reliable results. The most commonly used devices for measuring the shear behavior of laboratory soils are direct shear, triaxial, and ring shear devices.

Reliability of shear strength parameters significantly depends on the accuracy of the triaxial shear testing results. Therefore, it is important to recognize the factors that can affect test results, and techniques to reduce or correct for these factors. In fact, the basic principles and limitations of triaxial testing have been admirably described by Bishop and Henkel (1962) and reevaluated by several researchers (Lade 1977; Baldi and Nova 1984; Seed 1987; Kramer and Sivaneswaran 1989; Zhang 1997). Furthermore, the effects of non-uniform deformations on test results have been widely investigated (Rowe and Barden 1964; Bishop and Green 1965; Finno *et al.* 1996). The non-uniform deformation at large strains, often required to achieve critical state conditions, can develop due to the formation of shear bands or the effect of end restraint. The increase in the initial modulus of elasticity and peak shear strength is a product of end restraint effects caused by the use of rough ends and therefore, researchers supported the use of free ends with lubricated sample-platen interfaces which improves the uniformity at all strain levels (Riemer and Seed 1997).

In addition, triaxial shear tests involve many sources of errors that could significantly affect test results if not corrected. The most significant errors in the experimental investigation of granular soils are the variation of specimen cross-sectional areas during loading, and the volume change due to back-pressure saturation or membrane penetration resulting from the variation in the confining stress (Zhu and Anderson 1998). In addition, the bedding error resulting from using layers of latex membranes in the enlarged and lubricated end platens technique should be considered in the measured axial deformation (Sarsby *et al.* 1980). The membranes' resistance to the applied axial and radial stresses may also influence the measured shear strength.

In this study, monotonic triaxial compression tests are performed on very loose Ottawa sand specimens to determine the volumetric response and shear behavior for different specimen sizes. Specially-designed moulds and platens are used to reduce end restraint effects and improve specimens' uniform deformation. Corrections for the aforementioned errors were made to the test results to account for the volume change due to back pressure saturation (ASTM D4767-11) and membrane penetration (Baldi and Nova 1984), axial deformation due to bedding error (Sarsby *et al.* 1980), stress correction due to membrane resistance (ASTM D7181-11), and the change of specimen cross-sectional area during shear (Garga and Zhang 1997). The specimen preparation method and the applied triaxial procedure are described in this chapter. The design of especially split moulds and enlarged platens are presented as well as the influence of using free end technique on the deformation pattern and shear strength. The significance of applying corrections to the triaxial test results and the improvement achieved on the shear strength parameters are discussed and evaluated. It is worth mentioning that as with any other laboratory testing procedure there are a number of challenges in carrying out triaxial compression tests using enlarged platens, particularly on

loose sands and at large shear displacements. These factors, as well as the steps which are taken in this experimental procedure to correct for these challenges are discussed in the following paragraphs.

## 2.2 Physical Index Properties of Tested Sand

Clean, uniformly-graded Ottawa sand (with a commercial name of “Barco 71”) with round to sub-round particle shapes is used in the tests of this study. The large hardness of the quartz particles minimizes the amount of particle crushing experienced during loading. Sieve analysis was performed and the average particle size distribution is presented in Figure 2.1. The sand is classified as Fine Sand, SP as per the ASTM D2487 standard procedure (the unified soil classification system). The mean grain size ( $D_{50}$ ) was determined as 0.22 mm and the calculated coefficient of uniformity ( $C_u$ ) and coefficient of gradation ( $C_c$ ) is 1.71 and 1.07, respectively. Specific gravity of the sand particles ( $G_s$ ), and maximum and minimum void ratios of respectively 2.65, 0.821, and 0.487 were measured following the ASTM-D854 and D4253 standard procedures, respectively.

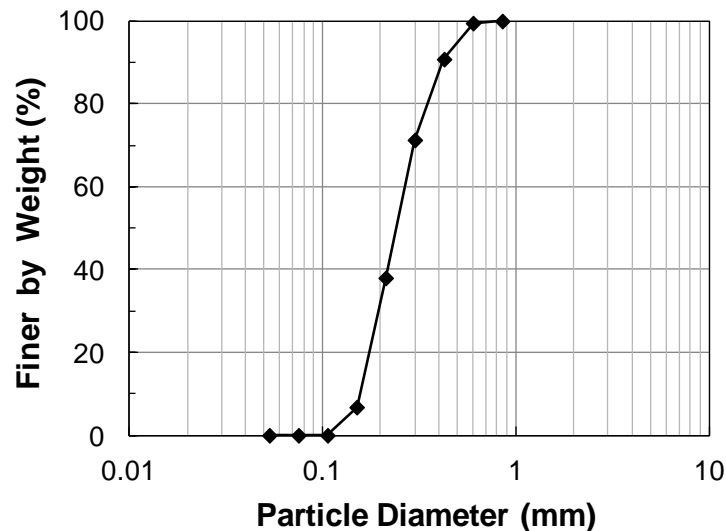


**Figure 2.1:** Average particle size distribution of the Barco 71 sand

## 2.3 Testing Equipment

### 2.3.1 Enlarged Platens

Enlarged and lubricated end platens are introduced in the experimental work of this study to minimize strain localization and bulging deformation in the specimens. A sand specimen is supposed to deform as a right circular cylinder throughout a triaxial compression shearing tests, but it often exhibits bulging deformation at its middle portion as a result of friction at the specimen boundaries (Bishop and Green 1965). Specimen bulging produces non-uniform stresses and strains in a triaxial test which could significantly affect the strength, strain-softening, pore pressure or volume change behavior of a soil specimen particularly at large deformation associated with critical states.

Different methods have been pursued to reduce the effect of specimen boundaries, but the lubricated end platens developed by Rowe and Barden (1964) has been the most effective method (Zhang 1997). In this method, the platens are covered with layers of lubricated (with vacuum grease) latex discs. The vacuum grease among the latex discs allows nearly frictionless sliding of the discs to minimize end restrains. Using an X-ray imaging technique, Kirkpatrick and Belshaw (1968) investigated the strain field within specimens of dry sand in triaxial compression tests performed with and without lubricated end platens. They observed that rough end platens promoted the development of rigid cones at the specimen ends, which are mainly responsible for global geometric softening, while lubricating the platens prevented the formation of these cones and maintained the uniformity of specimen's deformation up to large strain levels. Zhang and Garga (1997) studied the influence of lubricated platens on the stress-strain behavior of loose and dense Unimin and Ottawa sands. They found that the tests with lubricated platens presented lower deviator stresses and higher



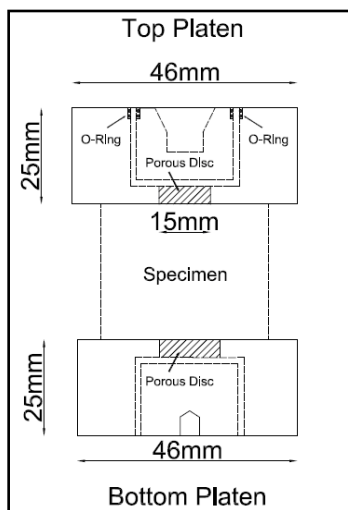
pore pressures than tests conducted using regular end platens. They also observed that the lubricated ends can significantly reduce end restraint in dense samples, while the improvement achieved by lubrication becomes smaller in loose samples.

In the experiments of this study, enlarged end platens are employed to accommodate the radial expansion of the specimen at shear strains of up to 30%. As illustrated in Figure 2.2(d), the lubricated ends consist of two sheets of 0.3 mm thick rubber discs which are separated with a thin layer of high vacuum silicone grease. The rubber discs are cut to the specimen diameter with a central hole cut to the diameter of the porous stone to allow drainage. An additional layer of high vacuum silicon grease was smeared on the rubber discs in order to provide a smooth and frictionless sliding on the specimen platens.

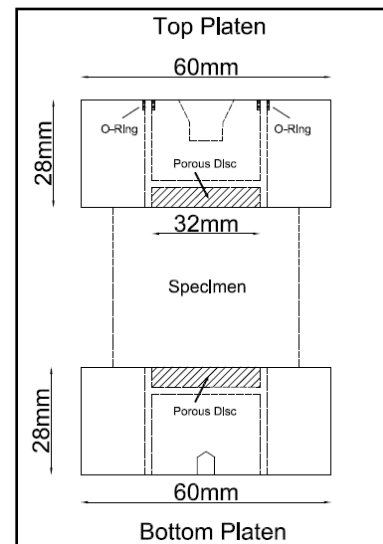
The slenderness or the height to diameter ( $h/d$ ) ratio of a specimen is another factor that could affect the bulging deformation. Bishop and Green (1965) illustrate that specimens with a slenderness ratio of 1 and lubricated ends could deform uniformly during drained loading, while specimens with a slenderness ratio of 2 with lubricated ends displayed a bulging deformation similar to the samples with regular ends. Accordingly, specimen bulging at large shear strains is largely reduced with smaller slenderness ratios (Hettler and Vardoulakis 1984).

Three different specimen diameters of 38, 50, and 70 mm with a slenderness ratio ( $h/d$ ) of 1 were tested in this study. Trial tests on specimens with a slenderness ratio of 2 exhibited significant bulging at large shear strains, regardless of whether the specimen ends were enlarged and lubricated or not. Therefore, it was decided to adopt a slenderness ratio of 1 along with lubricated and enlarged end platens to minimize the effects of specimen end restraint and allow for homogeneous stress distribution throughout the triaxial shear tests.

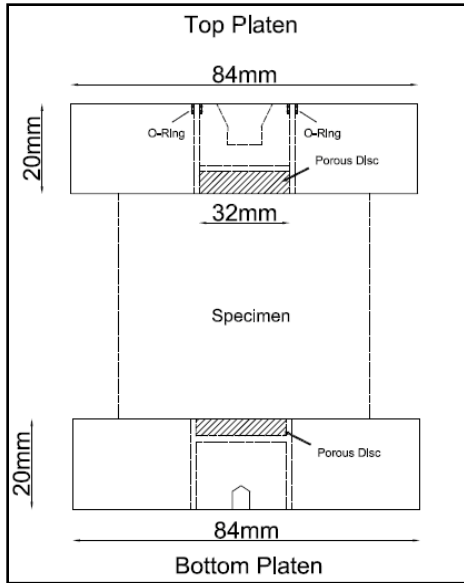
This is particularly necessary for critical state testing which require large shear strains. Accordingly, specially designed split moulds, to accommodate the enlarged platens, were constructed and used for preparing the specimens. As a result, although bulging was significantly reduced resulting in more homogeneous specimen deformations, it never completely disappeared. At this stage, a wide experimental investigation was made to further minimize specimen bulging and it was determined that rigid stainless steel platens would further reduce bulging. This was likely because the hard quartz sand particles microscopically penetrated into the soft acrylic platens producing additional end friction. This micro-penetration was eliminated by using hard stainless steel platens and therefore reduced end friction. Stainless steel end platens were subsequently replaced with the acrylic platens. Figures 2.2 and 2.3 show the schematic diagrams and photos of the enlarged end platens used in the experimental work.



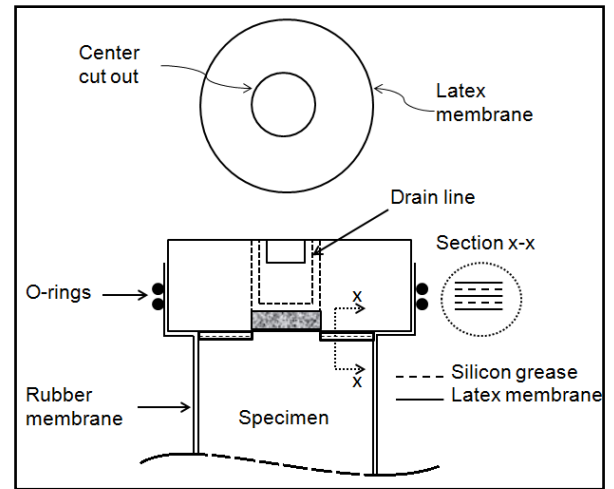
(a) Enlarged platens for 38mm specimens



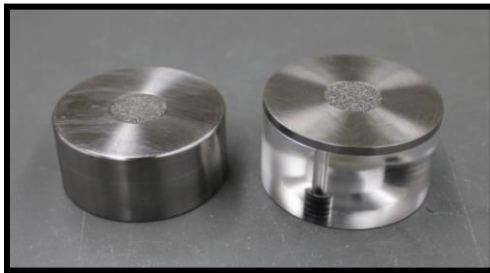
(b) Enlarged platens for 50mm specimens



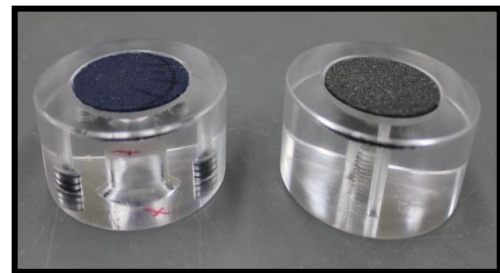
(c) Enlarged platens for 70mm specimens



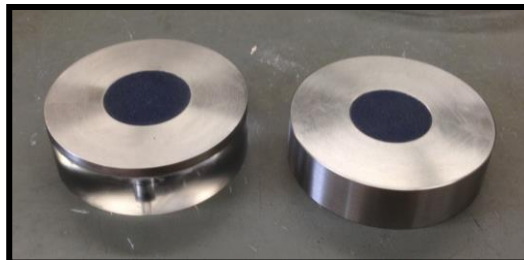
(d) Free end arrangement

**Figure 2.2:** Schematic diagrams of the enlarged platens for different sample sizes

(a) Enlarged platens for 38 mm specimens



(b) Enlarged platens for 50 mm specimens



(c) Enlarged platens for 70 mm specimens

**Figure 2.3:** Photos of the enlarged platens used for different sample sizes

### 2.3.2 Mould Design

Aluminum split moulds were constructed with internal diameters and heights equal to those of the three specimen sizes. The top and bottom ends of the moulds were bored larger to accommodate the enlarged specimen platens. Vacuum vent was constructed at the mid height of each mould to provide suction intended to hold the membrane tight against the wall during the moist tamping process. Collars that conformed to the top of each mould were constructed to allow sufficient space for tamping the sample top layers. A special tamper assembly consisting of a tamping rod scaled in millimeters covered with a clear resin, tamping foot, guide plate, and tamper lock was designed and constructed for tamping the moist sand at predetermined layer thicknesses. Figure 2.4 shows the design details of the tamper assembly. Figure 2.5 shows the schematic diagrams and photos of the different mould sizes used in the experimental work.

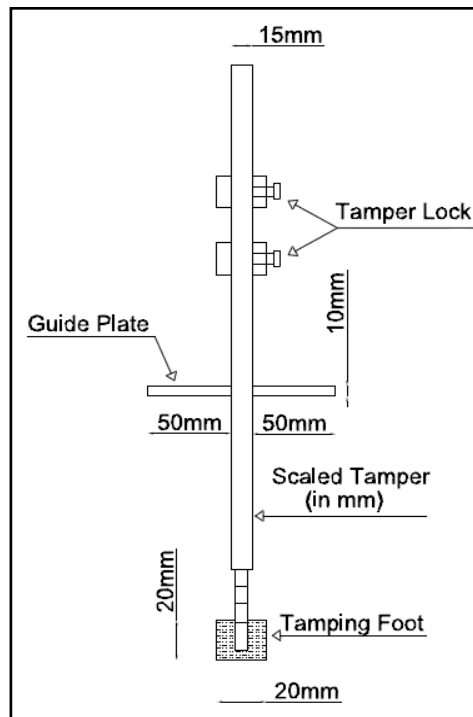
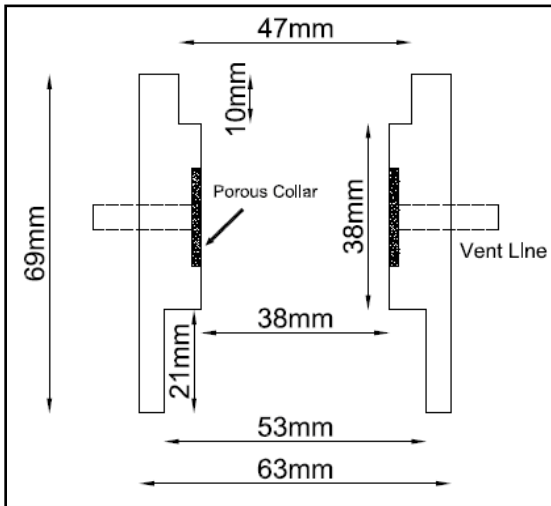
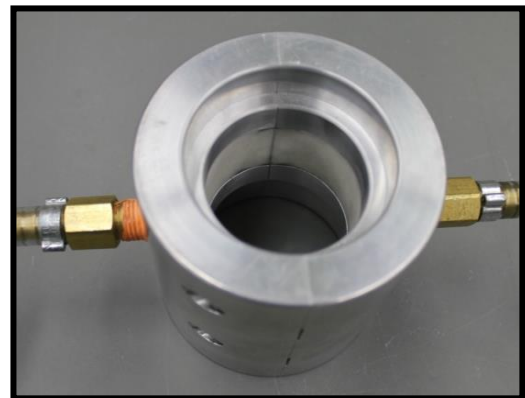
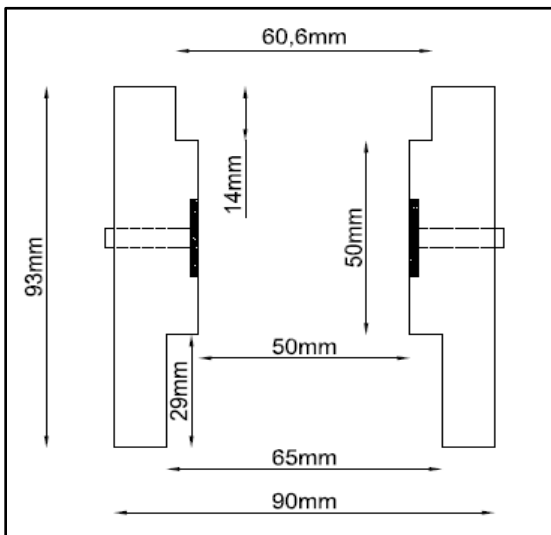


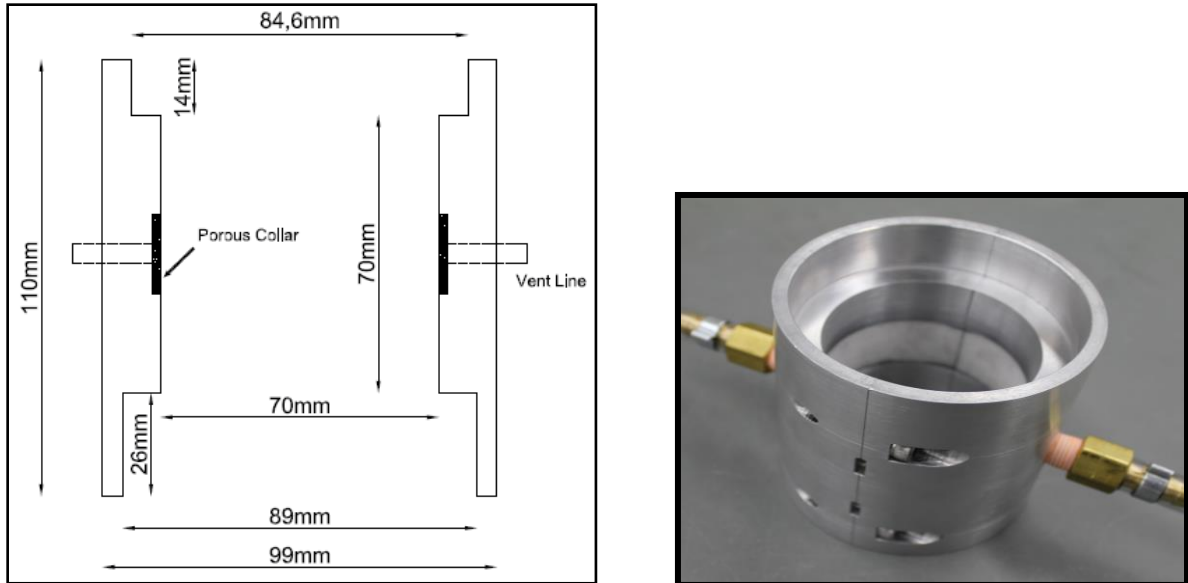
**Figure 2.4:** Schematic diagram of the tamper assembly



(a) - 38 mm Split mould



(b) - 50 mm Split mould



(c) - 70 mm Split mould

**Figure 2.5:** Schematic diagrams and photos for split moulds used for different sample sizes

### 2.3.3 Triaxial Test System

The triaxial tests of this research were conducted using an automated stress path triaxial compression testing system (SIGMA-1<sup>TM</sup> 5K model) manufactured by GeoTac, Texas, USA. The main components of this apparatus include a triaxial cell, a loading frame, two electromechanical pressure pumps, and a data acquisition system. The system also includes an external load cell, deformation sensor, and three fluid pressure sensors. Figure 2.6 provides a brief schematic diagram of the triaxial testing system.

The application of the axial load was provided by the loading frame which can apply the axial load in displacement-control (up to a rate of 25.4 mm/minute) or load-control (up to a maximum axial load of 9,000 N) modes. The load measurements were taken externally by a load cell placed on the loading frame. All tests of this study were conducted using the displacement control mode at a rate of 5%/hour. The axial deformation of the sample during

shear was measured externally by a linear variable displacement transducer (LVDT) on the loading ram of the triaxial cell.

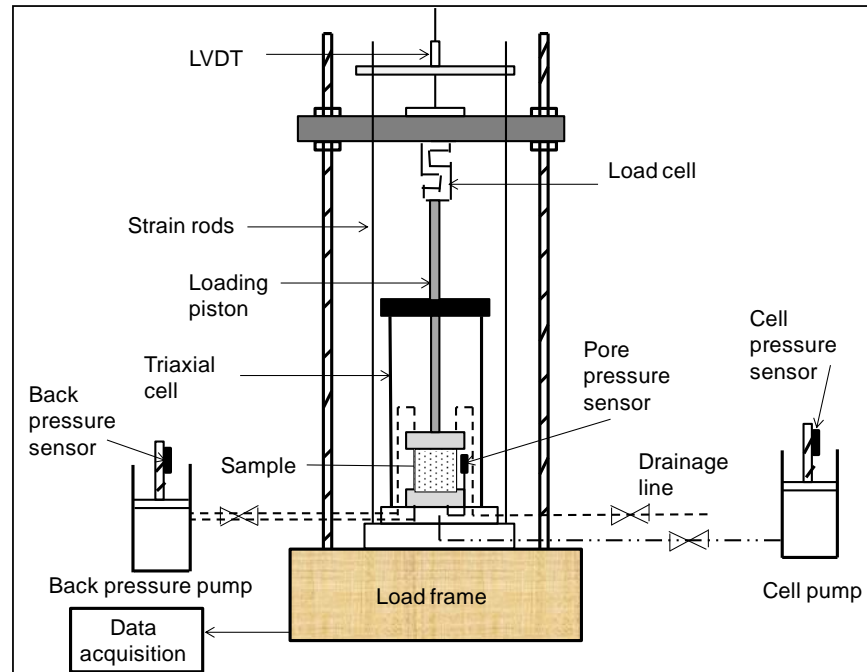


**Figure 2.6:** Schematic diagram of the triaxial testing system.

The two electromechanical pumps (referred to as the cell and pore pressure pumps) are used to control and measure the volume and pressure of the cell fluid and specimen's pore water. The cell pump has a capacity of 180 ml and drives the water into the triaxial cell through a connection at the cell base to generate the desired confining pressure. A pressure sensor with a maximum capacity of 2000 kPa is attached to the pump to measure the applied confining pressure. The pore pump has a capacity of 80 ml and drives the water into the specimen through the top and bottom platens to apply the back pressure saturation. A pressure sensor with a maximum capacity of 2000 kPa is attached to the pump to measure the applied back pressure. Both pumps could be operated under volume-control or pressure-control modes.

The volume and water pressures in both pumps are measured at a resolution of 1 mL and 0.1 kPa, respectively and transferred by an analog to digital data-controller to the computer. A separate water pressure sensor with a maximum capacity of 1400 kPa is also connected to the specimen through the bottom platen to measure the pore water pressure within the specimen for example during backpressure saturation or undrained shear. All sensors were calibrated at the commencement of the testing program. Calibration factors of each sensor are provided in appendix (A).

The triaxial testing system includes a series of interconnected modules which control the cell and pore pressure pumps as well as the load frame. All the modules are connected to a computer for command, feedback and data acquisition. The system records the output voltages of the sensors, which are then converted to engineering units using the calibration factors for further analysis and interpretation. Figure 2.7 shows a photo of the triaxial device.

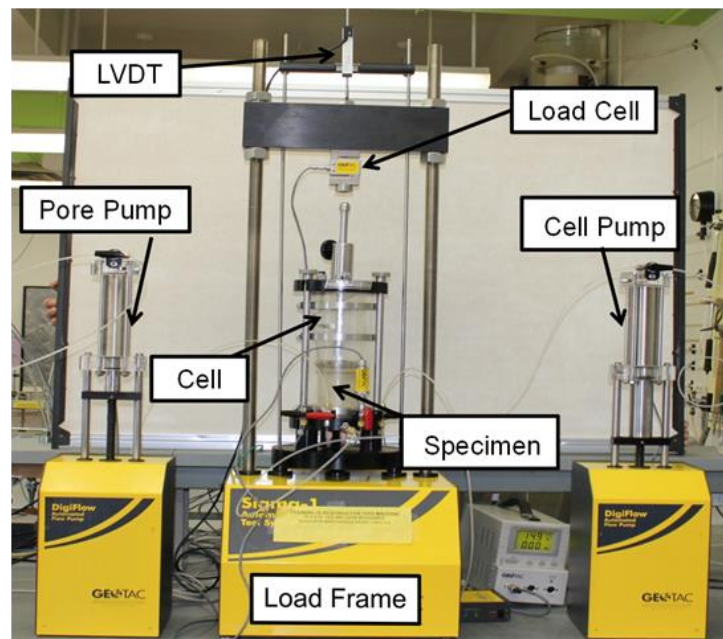


**Figure 2.7:** Triaxial shear apparatus used in this study



## 2.4 Triaxial Compression Testing Procedure

In the triaxial tests of this study, the cylindrical specimen is sealed in a water-tight rubber membrane and enclosed in a cell in which it could be subjected to stress changes made in two stages: (1) an increase in the cell pressure resulting in an equal all-round change in stress and (2) an increase in axial load resulting in a change in deviator stress. Monotonic triaxial compression shear tests were conducted according to the procedure described below.

### 2.4.1 Sample Preparation

There are several laboratory preparation methods (moist tamping, air pluviation, and water pluviation) that are generally used to produce sand samples. Moist tamping is the most popular laboratory method to prepare very loose sand specimens and consists of placing sand layers of specified thickness into a mould and tamping each layer with a flat tamper. The air pluviation method consists of pluviating dry sand through air into a sample mould from a constant fall height. Different soil densities are achieved by changing the fall height and tapping the sides of the specimen mould. Water pluviation method is similar to the air pluviation method except that the sand is pluviated through de-aired water rather than air.

It is difficult to ensure a uniform density distribution in reconstituted laboratory specimens of sand, and moist tamping is the only method that achieves relatively high void ratios in the laboratory (Gilbert and Marcuson 1988). The moist tamping method is the method in which the surface tension between the soil particles is employed to maintain a very loose sand structure (Castro 1969). Because of this tension between particles, unsaturated sands can be placed using moist tamping at a very loose soil structure even at void ratios greater than the

maximum void ratio of the dry sand obtained from the recommended ASTM D2049 procedure (Ishihara 1993).

In order to obtain very loose specimens that would exhibit entirely contractive and strain-softening behavior and achieve the critical state condition, all samples with different sizes were prepared by the moist tamping method. In the traditional method of the moist tamping technique, the specimens are prepared in a number of layers of equal dry weight and each layer is compacted to the same target density. This results in the lower layers of the specimen becoming denser than the global specimen density as compaction of each overlying layer also slightly compacts the underlying layers (Sadrekarimi and Olson 2012). Therefore, in order to minimize the density variations and void ratio non-uniformities within the specimens, the under compaction technique introduced by Ladd (1978) was employed to achieve a relatively uniform density throughout the specimen height. This method involves the compaction of each layer slightly looser than the target global unit weight, with the bottom layer compacted the least and the top layer compacted the most, so that the final unit weight of each layer, even with the effects of compaction of the successive overlying layers, would be equal to the target global unit weight.

Very loose cylindrical specimens were prepared in diameters of 38, 50, and 70 mm with a length to diameter ratio of 1 to reduce non-uniformity at larger strains. The procedure used to prepare a moist tamped specimen is illustrated in Figure 2.8. This procedure is briefly described as follows:

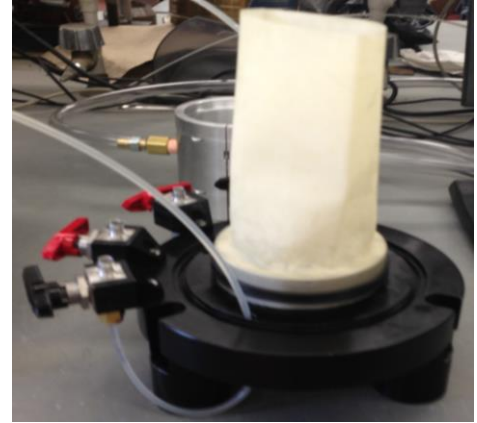
- (1) the designated split mould was secured around the bottom platen over the pedestal of the triaxial cell and the membrane was gently stretched and folded around the mould and a vacuum pressure was applied over the entire mould diameter so the membrane fitted tightly

inside the mould; (2) two latex membranes of the same specimen diameter and with 0.3 mm thicknesses were smeared with a thin layer of silicon grease and placed over the bottom platen in order to reduce soil friction at the bottom of the specimen; (3) the dry sand was weighted and mixed properly with de-aired water at a water content of 5% by weight; (4) the moist unit weight and void ratio of each layer was calculated based on the target overall relative density of zero with a maximum under compaction ratio ( $U_n$ ) of 10 for the bottom layer and the percent under compaction for each layer was determined based on the assumption that it linearly decreased from the bottom to the top layers; (5) each layer was weighed, poured into the mould, tamped to a predetermined equal height in a circular pattern using the developed scaled tamper, and scarified prior to placing the next layer with special care for tamping the top layer to ensure a level surface; (6) two latex membranes similar to those used for the bottom of the specimen were placed on the top of the soil prior to the placement of the upper platen and the membrane was gently stretched and folded around the mould and sealed with two O-rings; (7) a small vacuum (about 4 to 5 kPa) was applied by the pore pressure pump in order to provide confinement and hold the specimen in place during dismantling of the mould; (8) three readings of sample height and diameter were measured to determine the actual initial volume and thus void ratio of the specimen; (9) the cylindrical triaxial cell was assembled and placed in the load frame, filled with de-aired water, and the vacuum pressure was replaced by an external cell pressure of 10 kPa.

The initial vacuum pressure was necessary to maintain the specimen before the application of the external cell pressure, otherwise the specimen collapsed upon the removal of the specimen mould.



1) – Enlarged platen over the pedestal



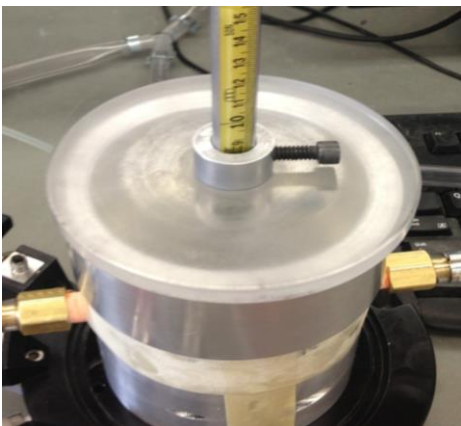
2) – Placement of membrane



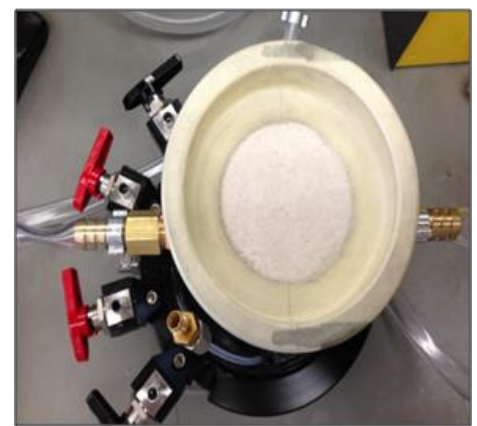
3) – Folding of the membrane around the mould



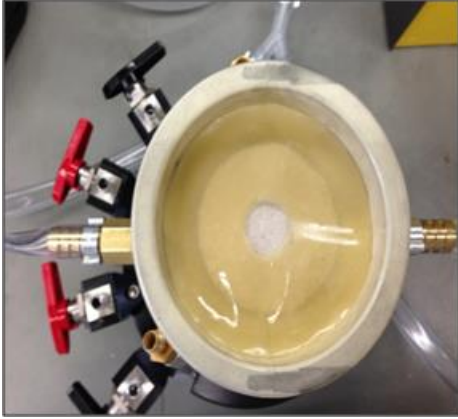
4) - Measurement of sand



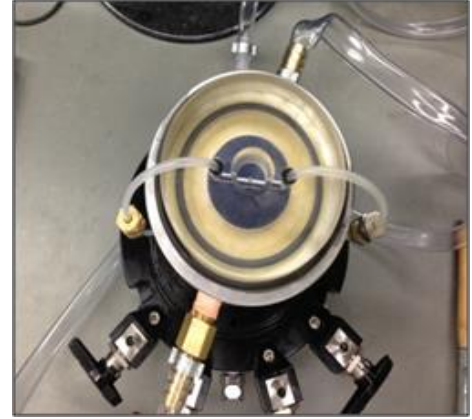
5) – Tamping process



6) –Compacted layers



7) - Two lubricated latex membranes



8) – Placement of top platen



9) – Complete specimen



10) Specimen placed in the cell

**Figure 2.8:** Steps of specimen preparation using moist tamping method

#### 2.4.2 Saturation Stage

It was important to ensure that the porous stones were boiled in deaired water for about 15 minutes prior to placement inside the platens. This helped to eliminate entrapped gas in the porous stone discs and specimen saturation. Furthermore, the pumps and sensors were saturated by flushing water to minimize errors in the measurement of specimen volume or pore water pressure resulting from the compression of entrapped air.

As complete saturation of the specimen was required to ensure accurate volume change and pore pressure measurement, carbon dioxide (CO<sub>2</sub>) was first percolated through all specimens under a small confining pressure of about 5 kPa for about 30 minutes. Compared to air, CO<sub>2</sub> is more soluble in water (forming carbonic acid) which reduces the time and pressure required to adequately saturate the specimen (Mulilis *et al* 1978). Subsequently, the top and bottom specimen drain lines were flushed using the backpressure pump at a very slow rate of 1 mL/min to ensure minimal disturbance to the specimen or dislodging the soil. The pore pressure was monitored carefully during CO<sub>2</sub> percolation and flushing with water to ensure that no pore pressure built up inside the specimen and the effective stress on the specimen was never lost during saturation.

The saturation procedure was continuing with a backpressure saturation phase as recommended by Black and Lee (1973). A back pressure of 200 kPa was applied to the specimen pore water to drive the carbon dioxide and any remaining air into solution. The process was done by raising the specimen pore pressure (using the backpressure pump) while simultaneously maintaining a constant difference effective stress of 10 kPa between the cell pressure and pore pressure. The pore pressure was increased at a rate slow enough to allow pore pressure equalization throughout the specimen. Skempton's pore water pressure parameter B was used to verify the degree of specimen saturation. This was done by closing the drainage valves and applying a small increment of cell pressure ( $\Delta\sigma_{3B}$ ) while also measuring the increase in specimen's pore pressure ( $\Delta u_B$ ). The B value was calculated as the rise in specimens pore water pressure divided by the increment in cell pressure ( $B = \Delta u_B / \Delta\sigma_{3B}$ ). A B = 1 indicates full (100%) saturation of the specimen. All specimens of this study were saturated until a B value of at least 0.98 was achieved.

### 2.4.3 Consolidation Stage

Isotropic consolidation commenced subsequent to the completion of specimen saturation by increasing the confining pressure while maintaining a constant specimen pore pressure. Confining pressures were utilized with values of 100 kPa, 200 kPa, 300 kPa, and 500 kPa. As the piston remained locked during isotropic consolidation, a gap formed between the specimen top platen and tip of the axial loading piston. The amount of displacement applied to close this gap and make contact between the piston tip and the specimen top was used as the axial deformation of the specimen following isotropic consolidation. The volume of water driven out of the sample during the consolidation stage was also measured as the difference in pore pump volume before and after the consolidation and hence, the consolidation void ratio was readily computed for each test.

### 2.4.4 Shearing Stage

The specimens were sheared following isotropic consolidation to the target confining stress. During shear the total cell pressure was kept constant while advancing the axial loading piston on the specimen cap at a constant strain rate up to an axial strain of 30%. The shear strain rate was chosen to ensure full pore pressure equalization during undrained shearing and full excess pore pressure dissipation during drained shearing based on the following ASTM guidelines:

$$\text{CIU test (ASTM D 4767): } \quad \dot{\epsilon} = 4\%/(10 t_{50}) \quad (2.1)$$

$$\text{CID test (ASTM D 7181): } \quad \dot{\epsilon} = 4\%/(16 t_{90}) \quad (2.2)$$

Where  $t_{50}$  and  $t_{90}$  are the amounts of time required to reach 50% and 90% degrees of consolidation, respectively. These were estimated from an initial trial triaxial test using the tested sand where the theory of consolidation was applied and a coefficient of consolidation ( $c_v$ ) of  $5.4 \times 10^{-5}$  m<sup>2</sup>/sec was determined using the equation:

$$c_v = 2.3 k \sigma'_n (1 + e_c) / \gamma_w c_c \quad (2.3)$$

While the coefficient of permeability,  $k$ , was estimated using Hazen's equation:

$$k = 0.1 D_{10}^2 = 1.96 \times 10^{-3} \text{ cm/sec} \quad (2.4)$$

Shear strain rates of 6.3%/hour and 5.9%/hour were calculated, and therefore a fixed shearing rate of 5%/hour was adopted in both drained and undrained triaxial shear tests. Specimen drainage was not permitted during the undrained tests while the specimen pore pressure was kept at the value of the backpressure during drained shear tests so all the shear-induced pore water pressure was dissipated. Measurements of excess pore pressures during the undrained shearing were taken by the pore pressure sensor, while volume change during shearing was measured and recorded by the back pressure pump in the drained tests. The void ratio at each strain level was calculated from the volume change measurements during the drained shear tests while a constant specimen volume was maintained in the undrained tests.

Table 2.1 summarizes the specifications of the specimens, loading conditions, and the applied shear strain rate of this study.



**Table 2.1:** Triaxial test data in this study

Test #	Specimen Size (mm)	Drainage Condition <sup>a</sup>	$p'_c$ (kPa)	$e_c$	$D_{rc}$ (%)	Strain rate $\dot{\epsilon}$ (mm/min)
MT-1	70	D	500	0.771	15	0.058
MT-2			300	0.779	13	
MT-3			200	0.785	11	
MT-4			100	0.797	7	
MT-5	70	UD	500	0.775	14	
MT-6			300	0.782	12	
MT-7			200	0.791	9	
MT-8			100	0.797	7	
MT-9	50	D	500	0.761	18	0.042
MT-10			300	0.769	16	
MT-11			200	0.773	14	
MT-12			100	0.786	10	
MT-13	50	UD	500	0.769	16	
MT-14			300	0.775	14	
MT-15			200	0.785	11	
MT-16			100	0.795	8	
MT-17	38	D	500	0.76	18	0.032
MT-18			300	0.766	16	
MT-19			200	0.775	14	
MT-20			100	0.786	10	
MT-21	38	UD	500	0.766	16	
MT-22			300	0.773	14	
MT-23			200	0.784	11	
MT-24			100	0.794	8	

<sup>a</sup> D: drained shear test; UD: undrained shear test.

## 2.5 Corrections for Triaxial Compression Tests

Triaxial shear tests involve several sources of errors that could be significant in evaluating test results if not corrected. The major errors resulting from sample volume changes occur during back-pressure saturation, membrane penetration, and the variation of specimen cross-sectional area during consolidation and shear. Additional errors result from the membrane rubber resistance to the axial and radial stresses, and the bedding errors resulting from using

latex membranes in the enlarged and lubricated end platens technique. These errors have a direct effect on the calculated stresses and the specimen's void ratio. The methods to account for these errors and the applied corrections along with the obtained results are described in the following paragraphs.

### 2.5.1 Correction of Volume Change during Saturation

In conventional triaxial tests, the specimen void ratio before shear is calculated based on the initial sample dimensions taken before assembling the cell and the void ratio changes during backpressure saturation and consolidation stages. The correct assessment of these void ratio changes is particularly critical in the testing of very loose sands because of their higher sensitivity to void ratio and could affect the position of the critical state line. The sample volume changes due to the flushing and backpressure saturation could be measured as the volume change of the cell fluid or by measuring the axial and radial deformation using sensors. Freezing the sample at the end of the test is the commonly applied method due to its high accuracy in estimating the sample volume changes. Imaging technique using either a high resolution camera or a 3D laser scanner can be also utilized. The ASTM standard method D4767-11 suggests calculating the volume change during saturation as below:

$$\Delta v_s = 3 V_o (\Delta h_s / h_o) \quad (2.5)$$

Where  $V_o$  is the initial specimen volume,  $\Delta h_s$  is change in height of the specimen during saturation, and  $h_o$  is the initial specimen height. Sladen and Oswell (1989) tested Syncrude tailing sand and measured void ratio changes due to saturation of as large as 0.15 using the specimen freezing technique. Zhang (1997) tested Unimin sand with initial relative densities

varying from 2% to 54% and monitored the axial and radial deformation during saturation using a linear variable displacement transducer (LVDT) and a hall radial displacement transducer (HRDT), respectively. He found that the entire saturation procedure resulted in a void ratio change of 0.008 to 0.026 which increased with increasing specimen void ratio where the looser the sample, the larger the volume change.

As described earlier, the saturation of moist tamped samples in this study was undertaken by flushing the samples with carbon dioxide followed by de-aired water, and then applying backpressure saturation. The sample dimensions were measured after applying a low suction (5 kPa) and removing the mould. Since the purpose of this study is to investigate the effects of measuring errors and corrections on critical state testing, all specimens were prepared at an initial void ratio of 0.821 which represents relative density of 0% and the volume changes occurring during backpressure saturation were obtained by measuring the axial strain ( $\epsilon_a$ ) of the specimen while making contact between the axial shaft and the specimen top cap, and calculating the radial strain ( $\epsilon_r$ ) and thus the volumetric strain ( $\epsilon_v$ ) of the specimen from its Poisson's ratio ( $\nu = -\epsilon_r/\epsilon_a$ ) from the following relationships:

$$\epsilon_v = \epsilon_a + 2 \epsilon_r = 1.68 \epsilon_a \quad (2.6)$$

$$\Delta v_s = \epsilon_v (V_o) = 1.68 \epsilon_a (V_o) = 1.68 \Delta h_s (A_o) \quad (2.7)$$

Where  $A_o$  is the initial specimen cross sectional area and  $\Delta h_s$  is the height change during saturation. An average Poisson's ratio of 0.34 was measured for all specimens from specimen deformations measured during consolidation.

The calculated volume changes during saturation indicated that the void ratio decreased by an average of 1.1% (0.008-0.01) after back pressure which corresponds to about (2.4-3%) in terms of relative density changes and were considered in the calculation of the specimens' void ratios at the critical state. Accordingly, neglecting saturation volume changes would lead to overestimation of the specimens' void ratio and eventually an incorrect critical state line and to about (2-3%) uncertainty in the critical strength that could be resulted from the differences in the cross-sectional area of the specimen before shear and therefore, this change in void ratio during saturation should not be ignored. Table 2.2 summarizes the void ratio changes after saturation of backpressure 200 kPa for the all conducted tests.

**Table 2.2:** Void ratio change due to flushing and backpressure saturation

Test #	$e_s$	$\Delta e$	$D_{rs}$ (%)
MT-1	0.813	-0.008	2.4
MT-2	0.812	-0.009	2.7
MT-3	0.812	-0.009	2.7
MT-4	0.813	-0.008	2.4
MT-5	0.812	-0.009	2.7
MT-6	0.813	-0.008	2.4
MT-7	0.812	-0.009	2.7
MT-8	0.813	-0.008	2.4
MT-9	0.812	-0.009	2.7
MT-10	0.811	-0.010	3.0
MT-11	0.812	-0.009	2.7
MT-12	0.812	-0.009	2.7
MT-13	0.813	-0.008	2.4
MT-14	0.811	-0.010	3.0
MT-15	0.812	-0.009	2.7
MT-16	0.812	-0.009	2.7
MT-17	0.811	-0.010	3.0
MT-18	0.812	-0.009	2.7
MT-19	0.812	-0.009	2.7
MT-20	0.811	-0.010	3.0
MT-21	0.812	-0.009	2.7
MT-22	0.811	-0.010	3.0
MT-23	0.811	-0.010	3.0
MT-24	0.812	-0.009	2.7

## 2.5.2 Correction of Volume Change due to Membrane Penetration

In triaxial tests on granular soils, volume change due to membrane penetration occurs when the latex membrane penetrates into the surface irregularities of the specimen when applying the effective confining stress. The amount of the resulting volume change is equal to the difference between the total volume of water driven out of the sample and the actual volume change of the soil skeleton (Newland and Allely 1959). This phenomenon was first recognized by Newland and Alley (1957) and since then it has been of considerable interest to numerous researchers (Pickering 1973, Frydman *et al.* 1973, Kiekbusch and Schuppener 1977, Ramana and Raju 1982, Lade and Hernandez 1982, Seed *et al.* 1989, Ansal and Erken 1996). Figure 2.9 illustrates the membrane penetration effect on a granular soil sample under low and high effective confining pressures.

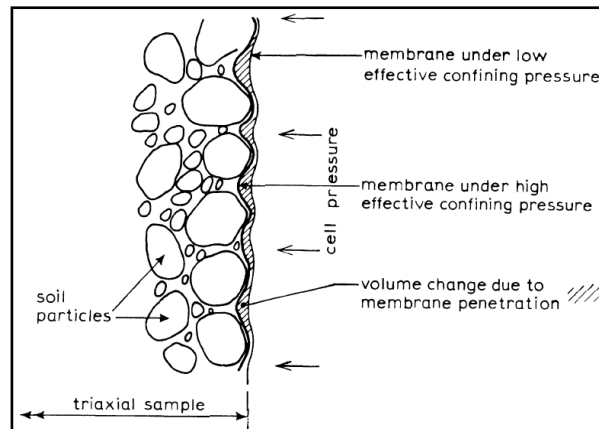


**Figure 2.9:** Effect of membrane penetration (after K.H. Head 1992)

It can be observed from the above figure that the membrane penetrates into the surface cavities when the effective confining stress increases and tends to return to its original state when the effective confining stress is reduced. The impact of membrane penetration on the stress-strain behavior of soils has been recognized by several researchers (Newland and Allely

1959, Roscoe *et al.* 1963, Frydman *et al.* 1973, Raju and Sadasivan, 1974, Baldi and Nova 1984, Seed and Anwar 1989, Kramer and Sivaneswaran 1989, Nicholson *et al.* 1993). In a drained triaxial test, the effective confining stress ( $\sigma'_3$ ) is constant and membrane penetration has only a minor influence on the volume change due to the slight changes of surface area, while in an undrained triaxial test,  $\sigma'_3$  changes substantially and the measured pore water pressure is significantly affected due to the membrane penetration (Roscoe *et al.* 1963). The amount of membrane penetration is a function of many factors including the effective confining pressure, grain size, grain shape, gradation, density of the sample, the surface area of the sample in contact with the rubber membrane, and the characteristics of the rubber membrane such as thickness and extension modulus. Hence, no single approach can precisely account for all these factors in order to accurately estimate membrane penetration for different sands (Raju and Sadasivan 1974).

However, several methods are developed to account for the volume changes due to membrane penetration. For example, Frydman *et al.* (1973) studied membrane penetration for granular soils with different particle sizes. They tested soils at  $\sigma'_3$  ranging from 50 to 800 kPa and found that the volume change due to membrane penetration ( $\Delta v_e$ ) was directly proportional to the logarithm of  $\sigma'_3$ . Further investigation by Lade and Hernandez (1977) showed that  $\Delta v_e$  was directly related to the mean diameter of the soil particles ( $D_{50}$ ). Baldi and Nova (1984) investigated the membrane penetration in triaxial testing and found that membrane penetration depends strongly on  $D_{50}$ ,  $\sigma'_3$ , and the diameter of the specimen ( $d$ ) as well as the membrane characteristics. According to their analysis, a quantitative correction was developed to account for membrane penetration in a typical triaxial test as below:

$$\Delta v_e = \left( \frac{D_{50}}{2 \times d} \right) \times \left[ V_s \times \left\{ \frac{\sigma'_3 \times D_{50}}{E_m \times t_m} \right\} \right]^{\frac{1}{3}} \quad (2.8)$$

Where  $\Delta v_e$  is the volume change due to membrane penetration,  $V_s$  is the specimen volume after saturation,  $E_m$  is the Young's modulus for the membrane material, and  $t_m$  is the thickness of the membrane. Nicholson *et al.* (1993) found that the influence of sample density on membrane penetration was relatively small in comparison to the influence of  $D_{50}$ . Zhang (1997) studied the effect of membrane thickness on the amount of membrane penetration for two sands and found that membrane thickness significantly affected the amount of penetration in both sands. The thinner the membrane the higher the volume change was due to membrane penetration.

Sivathayalan and Vaid (1998) investigated sets of experimental data produced using different techniques by several researchers and normalized the unit membrane penetration by dividing the recorded volumetric membrane penetration by the contact surface area between the sample and the membrane and then plotted that versus the logarithm of  $\sigma'_3$ . They found that the slope ( $S$ ) of the developed relationship was a function of  $D_{50}$  of the sand, with an average of  $0.0115 D_{50}$  for a wide range of particle sizes. Figure 2.10 shows the linear plot of  $S$  versus  $D_{50}$  which illustrates the normalized unit membrane penetration data and indicates that all data fall within a narrow band for particle sizes ranging from about 0.1 to 1.0 mm.

The membrane penetration in this study was calculated using Baldi and Nova (1984) equation as it accounts for all factors that could influence the membrane penetration (confining pressure, grain size, sample diameter, and membrane thickness and modulus). For comparison purpose, the calculated volumetric membrane penetration, using different

particle sizes, was normalized to the contact surface area and presented in the same plot of Figure 2.10 which demonstrates that the calculated membrane unit penetration is in good agreement and within the same linear function of  $D_{50}$  as proposed by Sivathayalan and Vaid (1998).

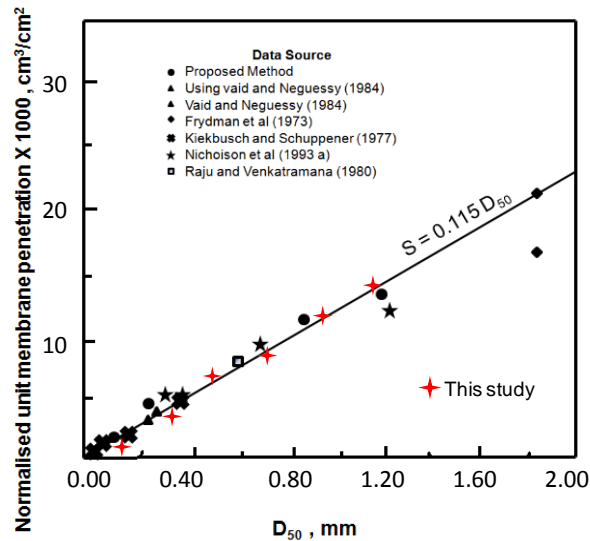


**Figure 2.10:** Effect of  $D_{50}$  on the normalized membrane penetration (Sivathayalan and Vaid 1998)

The membrane penetration volume change in an undrained test mainly depends on the change of the effective confining stress, with the higher consolidation pressure developing larger membrane penetration volume change. Instead of correcting for the effect of membrane penetration, a fewer number of studies have attempted to reduce the amount of membrane penetration during shear by isolating the direct contacting surface between the membrane and the soil specimen. For example, Lade and Hernands (1977) placed square plates inside the membrane, while Kiekbusch and Schuppener (1977) coated the membrane surface with liquid rubber. Such methods produce unknown amounts of disturbance to the



samples and result in a thick composite membrane whose axial load resistance is very difficult to evaluate (Zhu and Anderson 1998). Therefore, to eliminate the effect of membrane penetration on the results of undrained triaxial tests, several researchers have proposed to compensate for the membrane penetration volume change by injecting an equivalent volume of water into the soil specimen (Ramana and Raju 1982, Seed and Anwar 1989, Nicholson *et al.* 1993a). The injection process can be performed either manually or automatically using a computer-controlled system and the volume of water to be injected into the specimen is predetermined based on one of the available information relationship (Baldi and Nova 1984; Sivathayalan and Vaid 1998) between volumetric penetration and effective confining pressure for a given soil.

Correction for membrane penetration during the isotropic consolidation was considered in all tests performed in this study by correcting the recorded volume change after consolidation and accordingly, the consolidation void ratios. The  $D_{50}$  of the tested sand,  $t_m$ , and  $E_m$  of the used rubber membrane were measured as 0.22 mm, 0.3 mm, and 1350 kPa. The changes in the consolidation void ratios due to the membrane penetration was not significantly as only an average of 0.36% (0.002-0.003) was calculated, which corresponds to about (0.6-0.9%) in terms of relative density changes. This can be attributed to the fine gradation of the tested sand that limited the penetration of the membrane into the surface irregularities. However, as the critical state line is very sensitive to void ratio changes, it was considered for accurate estimation of the specimens' void ratios at the critical state.

During the drained shearing, the effective confining stress  $\sigma'_3$  is constant and hence the membrane penetration occurring during the consolidation stage does not change during the drained shearing and continue with the same magnitude up to the test end.

During the undrained shearing, the specimen volume is considered constant throughout the test as all the drainage lines are closed. However, the increase in the generated pore pressure would push the membrane to move out of the voids causing a partially drainage state and as a result, the measured excess pore pressure could be significantly affected and smaller than that if no penetration had occurred. This effect on the developed pore pressure is depending on the magnitude of the membrane penetration. Considering the very high modulus of water  $E_w$ , (2.2 GPa for fully saturated soil), the measured excess pore water pressure could be lower by about 200-700 kPa due to the excess pore water pressure that could be developed due to the membrane penetration ( $\Delta u = E_w \times \epsilon_v$ ), where  $\epsilon_v$  is the volumetric strain corresponding to the membrane penetration. However,  $E_w$  could be much lower than 2.2 GPa as the specimens are not fully saturated ( $B < 1$ ) and also due to the use of flexible drain tubes and accordingly, the expected response of pore pressure due to the membrane penetration could be much less than the over mentioned values. Actually, and since we are measuring pore pressure that represents the specimen behavior, this is not a testing error to be corrected. The membrane penetration in the conventional undrained triaxial shearing tests indicates the inadequacy for 100% constant volume or fully undrained condition even without measuring this slight volume change.

### 2.5.3 Effects of Enlarged Platens on Stress-Strain Response

As explained earlier, enlarged and lubricated end platens were employed in the experimental work of this study to allow free radial expansion of the specimen and minimize the bulging deformation during shear. A series of pilot tests were conducted on 50 mm specimens without lubricated platens and the results were compared with the final experiments in order

to quantify the improvements gained by lubricating the platens at large axial strains. Two undrained triaxial compression tests were performed for each case at isotropic consolidation stresses of 100 kPa and 300 kPa corresponding to relative densities of 8% and 14%, respectively. The stress-strain responses and the measured excess pore water pressures are shown in Figure 2.11. According to this figure, the shear-induced excess pore pressure is enhanced with lubricated end platens, resulting in about an average 13% reduction in the final deviator stress. This reduction occurs as friction at specimen boundaries is reduced which leads to more uniform specimen deformation and stress distribution.

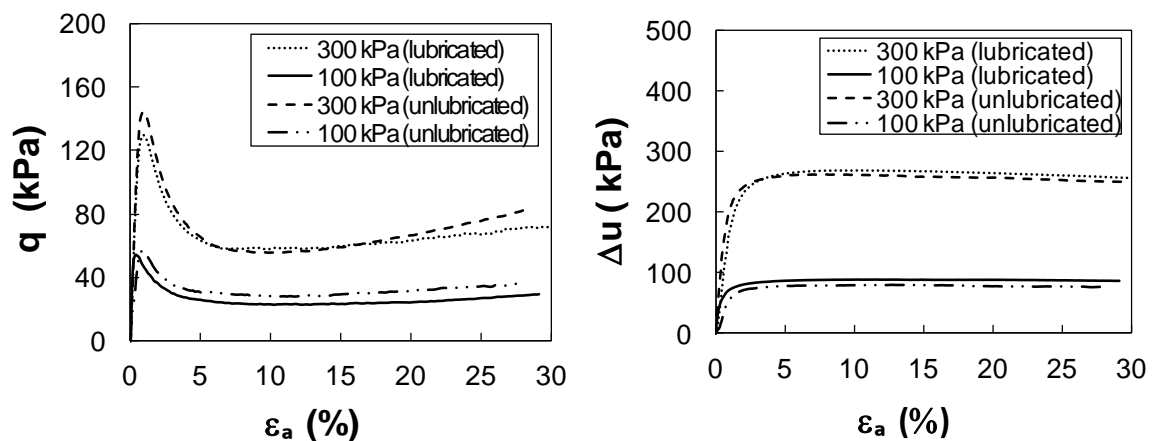


**Figure 2.11:** Effect of lubricated end platens on the stress-strain and excess pore pressure responses in triaxial compression tests on loose sand

Accordingly, an average error of about 10% in the critical strength and 4 degrees in the critical state friction angle were calculated if rough ends were used. These results are also supported with those observed by some other investigators (Olson and Campbell 1964, Ueng *et al.* 1988). However, Lee (1978) observed an opposite effect of lubrication where larger shear strength and less pore pressure were obtained with lubricated ends. Castro *et al.* (1982) found that the shear strength and pore pressure were basically the same with and without

lubricated ends, and Zhang (1997) observed that lubricated ends significantly reduced the end restraint of dense specimens.

#### 2.5.4 Area Correction due to Specimen Deformation Pattern

The axial stress on a specimen is computed by dividing the axial force by the cross-sectional area of the specimen. The cross-sectional area is calculated based on the assumption that the sample deforms as a right circular cylinder during shear. As it is necessary to shear sand samples to large axial strains for critical state testing, the triaxial samples deform substantially during the test and may significantly bulge. This bulging deformation makes the calculation of the cross-sectional area difficult and results in errors in the calculated deviator stresses and accordingly the critical strengths of the sands. Therefore, it is necessary to consider an effective cross-sectional area that takes into account the bulged shape of the specimen with a proper deformation pattern. Several methods for calculating the effective cross sectional area are summarized in the following paragraphs (Zhu and Anderson 1998):

In the cylindrical deformation correction method the specimen is assumed to deform as a right circular cylinder during shear (La Rochelle et al. 1988). This correction is recommended by the ASTM standard test method (ASTM D4767). The corrected area is calculated as  $A = A_o (1 - \varepsilon_v)/(1 - \varepsilon_a)$  where  $A$  is the effective area of the specimen,  $A_o$  is the specimen's initial area,  $\varepsilon_v$  is the volumetric strain, and  $\varepsilon_a$  is the axial strain. At a more complex level, the specimen is assumed to deform as a parabola (similar to a barrel) and the effective area is computed at the mid-height of the specimen. The resulting area correction is given as  $A = A_o \times \left[ -0.25 + \sqrt{(25 - 20\varepsilon_a - 5\varepsilon_a^2)/4} (1 - \varepsilon_a) \right]^2$ . For more bulging deformation, the effective area of the specimen is calculated by  $A = A_f + (A_{ce} -$

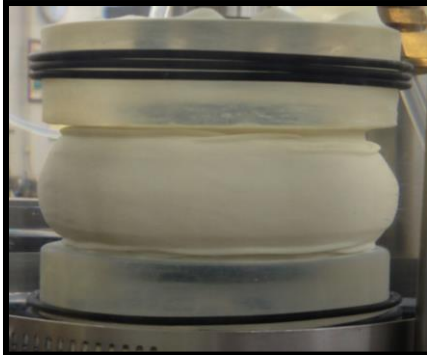
$A_f) [(\varepsilon - \varepsilon_f)/(\varepsilon_e - \varepsilon_f)]$ , where  $A_f$  and  $A_{ce}$  are the cross-sectional areas at the peak strength and at the end of the test, respectively, and  $\varepsilon_e$  and  $\varepsilon_f$  are the axial strains at the end of the test and at the peak strength, respectively.

Zhang and Garga, (1997) also developed a method to correct the cross-sectional area of triaxial sand samples. They performed triaxial tests where the samples' diameters were physically measured with a caliper at different strain levels and the deformation profile of the specimen was investigated in each test. They found that the maximum diameter occurred at the middle of the sample and the specimen diameter changes with height at different axial strains were parabolic. Therefore, they suggested using the average diameter within the middle third portion of the sample  $d_{1/3}$  to calculate the deviator stress as follows:

$$d_{\frac{1}{3}} = d_{max} - \frac{1}{12} (d_{max} - d_c) \quad (2.9)$$

$$d_{max} = \frac{d_c}{4} \left[ \left\{ 30 \frac{(1 - \varepsilon_v)}{(1 - \varepsilon_a)} \right\} - 5 \right]^{\frac{1}{2}} - 1 \quad (2.10)$$

The choice of the appropriate method depends on careful observation of specimen deformation during and after testing Figure 2.12 shows the influence of the employed lubricated ends in this study on the observed deformation patterns of the specimens at the tests end of 30% strain level. According to these photos, the lubricated end platens reduced but did not eliminate specimen bulging associated with the friction between the platens and the samples which exhibited a slightly parabolic shape at the end of the tests. Therefore, the method developed by Zhang and Garga (1997), where a parabolic deformation mode of the samples is assumed, was employed to account for the enlarged areas of the specimen.



a) – Without lubrication



b) - With lubrication

**Figure 2.12:** Effect of lubricated end platens on the deformation patterns of loose sand specimens in triaxial compression tests at 30% axial strain

The area correction method recommended by the ASTM standard D4767 assumes that the specimen deforms as a right circular cylinder and therefore it is not appropriate for the experiments of this study. However, a right cylindrical deformation would occur if the specimen ends were perfectly frictionless and therefore this correction could be used to replicate stress-strain response of an ideal specimen with no boundary effects. Figure 2.13 compares the stress-strain response of the loose sand specimens using these methods.

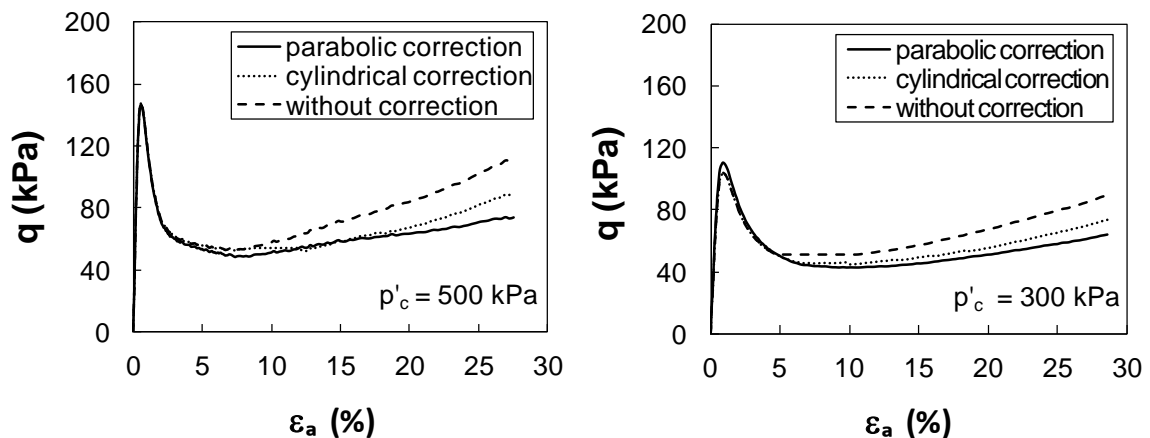


**Figure 2.13:** Effect of area correction method on the stress- strain response in undrained triaxial compression tests on loose sand

Comparing the deviator stress with and without applying area correction, the deviator stress at the end of the tests without applying any area correction was higher by about an average of 28% than that calculated using the parabolic area correction and by about 24% if area corrected considering the specimen deformed as a right circular cylinder. This further supports that the lubricated platens reduced but did not eliminate the end friction. This percentage of error is significant and can lead to overestimate the critical strength value if the actual deformation mode of the specimen is not taken into account in selecting the appropriate correction method. For example, the critical strength of the 70mm specimen tested under a 300 kPa consolidation stress was measured to be 28.1 kPa without applying any area correction and reduced to 23.5 kPa considering the specimen deformed as a right circular cylinder and to much lower value of 22.3 kPa considering parabolic area correction which means that the critical strength and critical state friction angle were overestimated by 26% and 9.5 degrees, respectively, if area correction was not applied. Table 2.3 summarizes the critical strength with and without correcting the specimens' cross-sectional area.

**Table 2.3:** Effect of area correction on the critical strength

<b>Specimen Size</b>	<b>P'<sub>c</sub> (kPa)</b>	<b>D<sub>rc</sub> (%)</b>	<b>Uncorrected s<sub>u</sub>(critical) (kPa)</b>	<b>Corrected s<sub>u</sub>(critical) (kPa)</b>	<b>Correction (%)</b>
70 mm	500	14	40.2	31.2	29
	300	12	28.1	22.3	26
	200	9	23.6	19.2	23
	100	7	14.8	12.2	21
50 mm	500	16	45.2	35.3	28
	300	14	34.8	27.8	25
	200	11	28.8	23.5	23
	100	8	16.9	14.1	20
38 mm	500	16	47.7	37.0	29
	300	14	41.3	33.0	25
	200	11	30.9	25.4	22
	100	8	20.2	16.9	20

### 2.5.5 Correction for Bedding Error

The homogenous deformation and uniform distribution of stress during the performed triaxial tests was most closely achieved by using enlarged lubricated end platens with specimens that had a length to diameter ratio of one. The use of lubrication rubber membrane layers at the top and bottom of the specimens resulted in bedding errors with the application of the axial load as the rubber layers compressed and penetrated into the sand. These errors directly affect the precise measurement of the axial strain. Lee and Seed (1964) found that, although the lubrication grease may lose its effectiveness with time, the resulting bedding errors could be still significant. Sarsby *et al.* (1980) studied the compression of rubber membrane layers in triaxial tests and the importance of correcting the measured vertical displacement for the compression of these rubbers. They found that the bedding errors were a logarithmic function of the effective axial stress  $\sigma'_1$ . Tatsuoka *et al.* (1984) performed triaxial tests with various numbers of lubricated rubber layers and found that multiple layers of greased rubbers give slightly better lubrication than single layers, but more bedding errors which should not be ignored. Russell and Khalili (2004) conducted a series of one-dimensional compression tests on sands with and without a lubricated layer separating the sample from the loading platen and the bedding error was found to be a logarithmic function of  $\sigma'_1$  as shown in Equation (2.11) and previously observed by Sarsby *et al.* (1980).

$$\Delta = 0.0352 \ln \sigma'_1 - 0.0713 \quad (2.11)$$

Where,  $\Delta$  is the error in the vertical displacement due to the use of one lubricated layer of rubber (mm) and  $\sigma'_1$  is the effective vertical stress (kPa). To improve the accuracy of axial



displacement measurement during shear in all the drained and undrained triaxial tests performed in this study, the deformation of the two latex membrane sheets is accounted for by deducting the membrane compression from the measured axial displacement of the specimen. Equation (2.11) was employed to estimate the amount of membrane deformation resulted from the axial stress applied on the specimen. Note that as the rubber membrane was already compressed following the consolidation stage, it was necessary to include the rubber compression due to the effect of all-surround consolidation pressure and then applying the correction to the measured axial displacement during shear after deducting the calculated membrane compression due to the consolidation pressure. While the latex membrane compresses due to the axial stress, it also expands in the radial direction and hence has no influence on the measured volume change during consolidation or drained shearing. In addition, the rigid top and bottom platens reduce the penetration of the latex membrane into the specimen voids and so this would have no effect on the specimen void ratio.

The bedding error, if not corrected, could significantly affect the measured axial strain. The maximum bedding deformation for the experimental work in this study was calculated to be 0.38 mm and could have 5.1% effect on the measured axial displacement if not corrected. This error would increase with increasing the number of latex rubber layers. In addition to the error in axial displacement, ignoring this deformation would result for error in estimating the specimen shear modulus. Table 2.4 summarizes the calculated maximum membrane compression ( $\Delta$ ) and its effect on the axial displacement ( $\delta_a$ ). It can be observed that the bedding error is more significant in the drained tests due to the steady increase in the effective vertical stress  $\sigma'_1$ . The bedding error is also increases with the confining pressure.

**Table 2.4:** Effect of bedding error on the axial displacement

Test #	Specimen Size	Drainage Condition <sup>a</sup>	$p'_c$ (kPa)	Max $\Delta$ (mm)	Max $\Delta/\delta_a$ (%)
MT-1	70 mm	D	500	0.364	1.6
MT-2			300	0.331	1.9
MT-3			200	0.304	2.3
MT-4			100	0.257	3.4
MT-5	70 mm	UD	500	0.313	0.45
MT-6			300	0.281	0.86
MT-7			200	0.253	1.2
MT-8			100	0.208	1.8
MT-9	50 mm	D	500	0.373	1.7
MT-10			300	0.339	2.6
MT-11			200	0.31	3.4
MT-12			100	0.262	4.2
MT-13	50 mm	UD	500	0.315	0.77
MT-14			300	0.284	1.12
MT-15			200	0.256	1.53
MT-16			100	0.214	1.92
MT-17	38 mm	D	500	0.377	2.9
MT-18			300	0.342	3.4
MT-19			200	0.314	3.7
MT-20			100	0.267	5.1
MT-21	38 mm	UD	500	0.317	0.99
MT-22			300	0.286	1.48
MT-23			200	0.258	1.85
MT-24			100	0.217	2.6

<sup>a</sup> D: drained shear test; UD: undrained shear test.

### 2.5.6 Correction for Membrane Resistance

The rubber membrane used to seal a specimen in triaxial testing can take a portion of the load applied on the specimen. During consolidation, the cell pressure applies axial and radial stresses on the sample. Most of this pressure is carried by the sample, while a small part of the load is taken by the surrounding membrane. During shearing, an additional axial load is applied on the sample, and again the membrane carried a part of the additional axial load. This could be particularly significant in measuring the reduced undrained strength of loose

soils after strain-softening and liquefaction. Henkel and Gilbert (1952) noticed this phenomenon and tried to correct for it. They conducted a series of triaxial tests using three different membrane materials. They found that the strength contributed by the rubber membrane was independent of specimen strength and cell pressure, but proportional to the stiffness of the membrane. They subsequently proposed two theories to determine the axial stress contribution of the membrane. In the first theory it is assumed that the confining cell pressure is sufficiently large to hold the membrane firmly against the specimen and the membrane acts as a reinforcing compression shell around the specimen. Whereas the second theory assumes that the rubber membrane is loosely held on the specimen (with some possible wrinkles), and acts as a rubber belt around the specimen. Duncan and Dunlop (1968) found that the restraint exerted by the rubber membrane induced indeterminate forces, which were most important when the displacements were large and the external forces were small. They considered the axial and volumetric strains in their proposed correction method. The ASTM standard method D7181-11 also provides a membrane resistance correction and recommends applying the correction if the calculated error in deviator stress by membrane resistance is greater than 5%. According to ASTM D7181-11 the shear stress carried by the membrane can be calculated by the following equation:

$$\Delta q = 4 \frac{E_m t_m \varepsilon_a}{d_c} \quad (2.12)$$

Where  $E_m$  is the Young's modulus of the membrane material (kPa),  $t_m$  is the thickness of the membrane (mm), and  $d_c$  is the diameter of specimen after consolidation (mm). A membrane resistance correction was applied according to Equation 2.12 for all the experiments performed in this study. For accurate estimation of membrane resistance, the Young's

modulus of the latex membrane material was determined from an extension test as recommended by ASTM D7181-11. The test involved stretching a one inch wide loop of the membrane with weights and measuring the force per axial deformation of the membrane. A modulus of about 1350 kPa was obtained. Figure 2.14 compares the influence of membrane resistance on the stress-strain responses of 38 mm loose sand specimens.

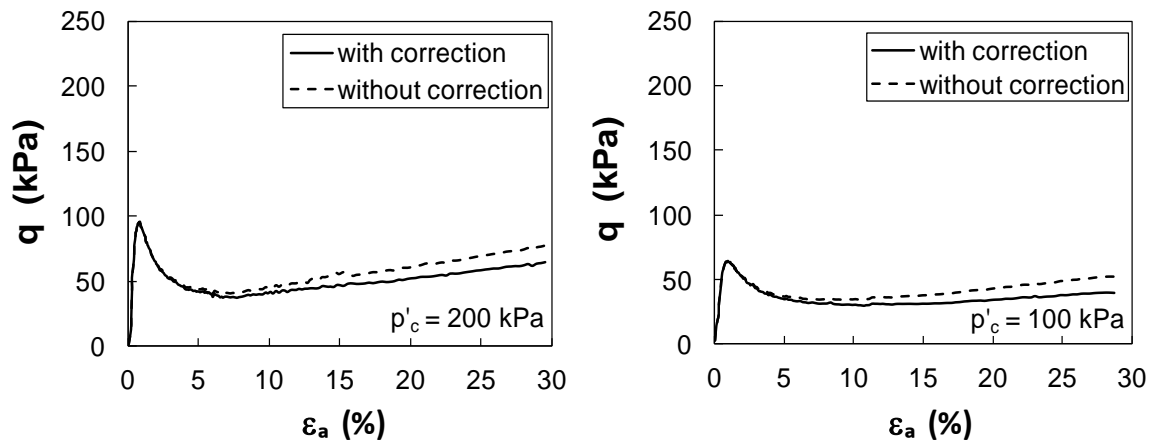


**Figure 2.14:** Effect of membrane resistance on the stress- strain response of undrained triaxial compression tests on loose sand

As shown in Figure 2.14, the contribution membrane resistance increases with the strain level ( $\sigma = E\varepsilon$ ) and thus correction for membrane resistance is particularly important at large strains where the reduced critical strength is mobilized in undrained shear tests. Neglecting this correction could lead to an average error in the measured critical strength up to 8% and up to 3 degrees in the critical state friction angle. For example, an undrained critical strength of about 35.9 kPa was measured in the 38mm specimen at  $p'_c = 300$  kPa, which includes an additional resistance of 2.9 kPa (9% of the total) provided by the membrane. Therefore, membrane resistance should be considered for accurate evaluation of the measured deviator stresses particularly at the critical state.

Table 2.5 summarizes the calculated membrane resistance and its effect on the measured deviator stress for the undrained tests.

**Table 2.5:** Effect of membrane resistance on the deviator stress

<b>Specimen Diameter</b>	<b><math>p'_c</math> (kPa)</b>	<b><math>D_{rc}</math> (%)</b>	<b>Membrane resistance <math>\Delta q</math> (kPa)</b>	<b>Corrected deviator stress <math>q_{cs}</math> (kPa)</b>	<b>Correction (%)</b>
70 mm	500	14	6.3	70.2	9
	300	12	5.6	50.5	11
	200	9	4.4	43.7	10
	100	7	3.1	27.8	11
50 mm	500	16	9.0	82.0	11
	300	14	7.8	64.9	12
	200	11	7.7	55.0	14
	100	8	4.3	33.0	13
38 mm	500	16	12.2	87.0	14
	300	14	12.5	78.0	16
	200	11	9.0	60.0	15
	100	8	7.2	40.0	18

## 2.6 Comparison of Corrections

The errors accompanied the triaxial testing of very loose sand and the applied techniques or corrections to account for these errors have been briefly reviewed. Generally, the difference between the corrected and uncorrected data increases with the increasing of the axial strain and accordingly, the shear strength and the internal friction angle could be largely overestimated. However, in order to identify how the corrections interact and if it is required to account for all these corrections and determine the correction that has the most significant effect on the sand shear behavior, the discussed errors and the applied correction methods with their references as well as the percentages of achieved improvements of the related parameters are summarized in Table 2.6 for all the performed tests in this study.

**Table 2.6:** Summary of the applied corrections and percentage improvement for triaxial shear testing on very loose sand

Applied correction	Associated Parameter	Error mechanism	Range of Improvement	Average Improvement	Correction Reference
Enlarged and lubricated platens	$s_u(\text{critical})$ %	End restraints	- (8 – 12)	- 10	Rowe (1962)
	$\phi'_{cs}$ (degrees)		- (3.1 – 4.2)	-3.6	
Area correction	$s_u(\text{critical})$ %	Specimen bulging	- (20 – 29)	- 24.5	Zhang and Garga (1997)
	$\phi'_{cs}$ (degrees)		- (7.8 - 10)	-8.9	
Membrane resistance	$s_u(\text{critical})$ %	Membrane resistance	- (6 – 10)	- 8.0	ASTM D7181-11
	$\phi'_{cs}$ (degrees)		- (2.5 – 3.6)	-3.1	
Volume change	$e_{\text{critical}}$ %	Saturation	0.4	-1.1	ASTM D4767-11
		Membrane penetration	-0.08	0.36	Baldi and Nova(1984)
Bedding error	$\epsilon_a$ %	Latex compression	5	-2.5	Sarsby <i>et al.</i> (1980)

From the above analysis, it can be observed that each correction improved a certain parameter and the critical shear strength and friction angle as well as the critical void ratio was influenced by more than one correction. The negative sign indicates the overestimation of the related parameter if the corresponding correction was not applied. It can also be observed that the specimen cross-sectional area correction is the most significant error affects the strength of the tested sand and must be corrected based on the observation of soil deformation pattern during and after testing. However, the improvement of each parameter was calculated with applying the other corrections. Therefore, the corrections effect on these parameters could be either propagated or cancel each other. Accordingly, the critical strength and friction angle found to be much overestimated if the corrections to the area

variation and the membrane resistance were not considered or the enlarged end platens were not employed. The combined improvement indicate that the critical strength and friction angle of the tested loose sand could be overestimated as large as 32% and 12 degrees, respectively, if these corrections were not applied and up to 42% and 15.6 degrees, respectively, if the enlarged lubricated platens were not used. On the other hand, the critical void ratio of the tested loose sand could be overestimated as much as 0.9% as the volume change due to the membrane penetration reduced the effects of volume change during saturation and this could be much larger when testing coarser sands or granular materials.

## 2.7 Conclusion

The experimental errors affecting the shear behavior of loose sand have been thoroughly reviewed in this study, which illustrated the significant effects of end restraint and triaxial data corrections on loose sand shearing behavior. The non-uniform deformations at large strain, which is often required to achieve critical state, may significantly affect the critical strength of sands. It was demonstrated that lubricated and enlarged end platens are helpful mechanisms to minimize the effects of end restraint and promote uniform deformations during shear. As a result of these improvements, accurate volume change in drained shear tests as well as lower deviator stresses and higher pore pressures were measured in the undrained shear tests. It was found that rough end platens could result in an average of 10% and 13% overestimation in the critical strength and friction angle, respectively. The importance of lubrication was found to increase with increasing specimen density. While lubrication improved specimens' deformation uniformity, it did not completely eliminate them and the final specimen shapes were slightly parabolic and an area correction

conforming to the shape of the deformed specimens was used to account for this barreling deformation of the specimen and correct the measured axial stress on the specimens. Accordingly, the critical strength and friction angle was reduced by an average of 24% and 32%, respectively. It was further indicated that neglecting membrane resistance would lead to overestimate of the critical strength and friction angle by an average of 8% and 11%, respectively. The propagation of all these errors, if not corrected, could overestimate the critical strength and friction angle of the tested loose sand by an average of 42% and 15.6 degrees, respectively. In addition, the bedding error due to the compression of the latex membrane used in the enlarged platens technique increased the measured axial strain by an average of 2.5%. Another important factor affecting the behavior of sands is its void ratio. The volume change during back pressure saturation and due to membrane penetration could significantly affect the critical void ratio and the location of the critical state line and accordingly, the measured critical state parameters. The results of this study indicated that ignoring the volume change during saturation could lead to an overestimation of the sample void ratio up to 0.01 which corresponds to about 3% in terms of relative density. The membrane penetration into the surface cavities lead to an overestimation of specimens volume change during consolidation and thus underestimation of the void ratio by about 0.003 which represents 0.9% changes in specimen's relative density. The relatively minor influence of membrane penetration on the volumetric strain could be related to the fine gradation ( $D_{50} = 0.22$  mm) of the tested sand that minimized the penetration of the membrane into the surface irregularities among the sand particles. The results of the corrections also indicated that the change in the specimen cross sectional area at large strain is the most significant source of error observed in this comprehensive study on loose sand and choosing the appropriate correction method requires a special attention of the engineer.



## References

- Ansari, A. M., and Erken, A. (1996). "Post-testing correction procedure for membrane compliance effects on pore pressure" *J. Geotech. Eng.*, Vol. 122 (1), pp: 27–38.
- ASTM, D2487-06 "Standard practice for classification of soil for engineering purposes (Unified Soil Classification System)" ASTM International, West Conshohocken, PA.
- ASTM, D4253-06 "Standard test methods for maximum index density and unit weight of soils using vibratory table" ASTM International, West Conshohocken, PA.
- ASTM, D4767-11 "Standard test method for consolidated un-drained triaxial compression test for soils" ASTM International, West Conshohocken, PA.
- ASTM, D7181-11 "Standard test method for consolidated drained triaxial compression test for soils" ASTM International, West Conshohocken, PA.
- Baldi, G., and Nova, R. (1984). "Membrane penetration effects in triaxial testing" *J. Geotechnique*. Vol. 110 (3), pp: 403-420.
- Black, D. K., and Lee, L. L. (1973). "Saturating laboratory samples by back pressures" *J. Soil Mech. and Found. Eng.*, Vol. 99 (MSI), pp: 75-93.
- Bishop, A. W., and Green, G. E. (1965). "The influence of end restraint on the compression strength of a cohesionless soil" *J. Geotechnique*. Vol. 15 (3), pp: 243- 266.
- Bishop, A. W., and Henkel, D. J. (1962). "The measurement of soil properties in the triaxial test" St. Martin's Press, Inc., New York, 225 pp.
- Castro, G. (1969). "Liquefaction of sands" Ph.D. Thesis, Harvard University, Cambridge, MA. Harvard Soil Mechanics Series, No. 81.
- Castro, G., Poulos, S. J., France, J. W., and Enos, J. L. (1982). "Liquefaction induced by cyclic loading". Report to the National Science Foundation, Washington, D.C.
- Duncan, J. M., and Dunlop, P. (1968). "The significance of cap and base restraint". *J. Soil Mech. and Found.* Vol. 94 (1), pp: 271-290.
- Finno, R. J., Harris, W. W., Mooney, M. A., and Viggiani, G. (1996). "Strain localization and undrained steady state of sand" *J. Geotech. Eng.*, Vol. 122 (6), pp: 462–473.
- Frost, J. D., and Park, J. Y. (2003). "A critical assessment of the moist tamping technique" *J. Geotech. Testing*. Vol. 26, pp: 1-14.
- Frydman, S., Zeitlen, J. G., and Alpan, I. (1973). "The membrane effects in triaxial testing of granular soils" *J. Testing and Evaluation*. Vol.1, pp:37-41.
- Garga, V., and Zhang, H. (1997). "Volume changes in undrained triaxial tests on sands" *Can. Geotech. J.* Vol. 34, pp: 762-773.
- Gilbert, P. A., and Marcuson, W. F. (1988). "Density variation in specimens subjected to cyclic and monotonic loads" *J. Geotech. Eng.*, Vol. 114 (1), pp: 1-20.
- Head K. H. (1992). "Manual of soil laboratory testing" Vol. 3, Effective stress tests, second edition, John Wiley & Sons, New York, pp.428.

- Henkel, D. J., and Gilbert, G. D. (1952). ‘The effect of rubber membrane on the measured triaxial compression strength of clay samples’ *J. Geotechnique*. 3 (1), pp: 20-29.
- Hettler, A and Vardoulakis, I. (1984). ‘Behaviour of dry sand tested in a large triaxial apparatus’ *J. Geotechnique*. Vol. 34 (2), pp: 183-198.
- Ishihara, K. (1993). ‘Liquefaction and flow failure during earthquakes’ *J. Geotechnique*. Vol. 43 (3), pp: 351-415.
- Kiekbusch, M., and Schuppener, B. (1977). ‘Membrane penetration and its effect in pore pressure’ *J. Geotech. Eng.* Vol. 103 (11), pp: 1267–1279.
- Kirkpatrick, W. and Belshaw, D. J. (1968). ‘On the interpretation of the triaxial test’ *J. Geotechnique*. Vol.18 (3), pp: 336-350.
- Kramer, S. L., and Sivaneswaran, N. (1989). ‘A non-destructive specimen-specific method for measurement of membrane penetration in the triaxial test’ *J. Geotech. Testing*. Vol. 12 (1), pp: 50-59.
- Ladd, C. C. (1978). "Preparing test specimen using under-compaction" *J. of Geotech. Testing*. Vol.1, pp: 16-23.
- Lade, P. V. (1977). ‘Membrane penetration effects in undrained tests’. *J. Geotech. Eng.*, Vol. 103 (2), pp: 109-125.
- Lade, P. V. and Hernandez, S. B. (1977). ‘Membrane penetration effects in undrained tests’ *J. Geotech. Eng.*, Vol. 103 (2), pp: 109-125.
- Lee, K.L. (1978). ‘End restraint effects on undrained static triaxial strength of sand’. *J. Geotech. Eng.*, Vol.104 (6), pp: 687–704.
- Lee, K. L., and Seed, H.B. (1964). ‘Importance of free ends in triaxial testing’ *J. Soil Mech. and Found.* Vol. 90 (6), pp: 173–175.
- Mulilis, J. P., Townsend, F. C., and Horz, R. c. (1978). ‘Triaxial testing technique and soil liquefactions’. *Dynamic Geotech. Testing*. Vol. 654 (STP), pp: 256-279.
- Newland, P. L., and Allely, B. H. (1957). ‘Volume changes during drained triaxial tests on granular materials’ *J. Géotechnique*. Vol. 7, pp: 17–34.
- Newland, P. L. and Allely, B. H. (1959). ‘Volume changes during undrained triaxial tests on saturated dilatant granular materials.’ *J. Geotechnique*. Vol.9, pp: 174-182.
- Nicholson, P. G., Seed, R. B., and Anwar, H. A. (1993a). ‘Elimination of membrane compliance in undrained triaxial testing’ *Canad. Geotech. J.* Vol. 30, pp: 727–738.
- Olson, R. R., and Campbell, L. M. (1964). ‘Discussion on importance of free ends in triaxial testing’ *J. Soil Mech. and Found. Eng.*, Vol. 90 (6), pp: 167-173.
- Ramana, K. V. and Raju, V. S. (1982). ‘Membrane penetration in triaxial tests’ *J. Geotech. Eng.*, Vol. 108 (GT2), pp: 305–310.
- Raju, V.S., and Sadasivan, S.K. (1974). ‘Membrane penetration in triaxial tests on sands’ *J. of Geotech. Eng.*, Vol. 100 (4), pp: 482–489.
- Riemer, M., F., and Seed, R. B. (1997). ‘Factors affecting apparent position of steady state line’ *J. Geotech. and Geoenviron. Eng.*, Vol. 123 (3), pp: 281–288.

- Roscoe, K. H., Schofield, A. N., and Thurairajah, A. (1963). "An evaluation of test data for selecting a yield criterion for soils" Proc. of the Symposium on Laboratory Shear Testing of Soils, ASTM, Special Technical Publication No. 361, pp: 111–128.
- Rowe, P.W., and Barden, L. (1964). "Importance of free ends in triaxial testing" J. soil mech. and found., Division, Vol. 90 (1), pp: 1–27.
- Russell, A. R. and Khalili, N. (2004a). "Cavity expansion in unsaturated sands". In Proc. of the 4<sup>th</sup> European Congress on Computational Methods in Applied Sciences and Eng.
- Sadrekarami, A., and Olson, S.M. (2009). "A new ring shear device to measure the large displacement shearing behavior of sands" J. Geotech. Vol. 32 (3), pp: 197–208.
- Sadrekarami, A., and Olson, S.M. (2012). "Effect of sample preparation method on critical state behavior of sands" J. Geotech. Testing. Vol. 35 (4), pp: 548-562.
- Sarsby, R.W., Kalteziotis, N., and Haddad, E.H. (1980). "Bedding error in triaxial tests on granular media" J. Geotechnique. Vol. 30 (3) pp: 302-309.
- Seed, H. B. (1987). "Design problems in soil liquefaction" J. Geotech. Eng., Vol. 113 (8), pp: 827-845.
- Seed, R. B., and Anwar, H. A. (1989). "Development of a laboratory technique for correcting results of undrained triaxial shear tests on effects of membrane compliance" Stanford University, Geotech. Research Report No. SU/GT/86–02.
- Seed, R. B., Anwar, H. A., and Nicholson, P. G. (1989). "Elimination of membrane compliance effects in undrained testing" Proceed. of the 12th Intern. Conf. on Soil Mech. and Found. Eng., Vol. 1, pp: 111–114.
- Sivathayalan, S., and Vaid, Y., P. (1998)" Truly undrained response of granular soils with no membrane-penetration effects" Can. Geotech. J. Vol. 35, pp: 730–739.
- Sladen, J. A., and Oswell, J. M (1989). "The behaviour of very loose sand in the triaxial compression test" Can. Geotech. J. Vol. 26, pp: 103-113.
- Tatsuoka, F., Molenkamp, F., Torii, T., and Hino, T. (1984). "Behaviour of lubrication layers of platens in element tests" Soils Found., Vol. 24 (1), pp: 113-128.
- Terzaghi, K., Peck, R., B., and Mersi, G. (1996). "Soil mechanics in engineering practice" Jhon Wiley & Sons, Inc., 3<sup>rd</sup> Edition. 549 pp.
- Ueng, T., Tzou, Y., and Lee, C. (1988). "The effect of end restraint on volume change and partial preakage of sands in triaxial tests" Advanced Triaxial Testing of Soil and Rock. ASTM. STP 977, PP: 679-691.
- Vaid, Y.P., and Sivathayalan, S. (1996b)." Errors in estimates of void ratio of laboratory sand specimens" Can. Geotech. J., 33 (6), pp: 1017–1020.
- Zhang, H. (1997). "Steady state behavior of sands and limitations of the triaxial tests" Ph.D dissertation, University of Ottawa, Ottawa, Canada
- Zhang, H. and Garga, V. K. (1997). "Quasi-steady state: a real behaviour" Can. Geotech. J. Vol. 34 pp: 749–761.
- Zhu, J., H., and Anderson, S., A. (1998). "Corrections for triaxial tests on undisturbed soils" J. Geotech. Testing. Vol. 26 (3), pp: 277-284.

## Chapter 3

### 3 Specimen Size Effect on Triaxial Compression Testing of loose sands

#### 3.1 Introduction

Triaxial tests are widely used to determine the strength characteristics of soils subject to a wide range of stress paths and loading conditions. Different studies employ different specimen sizes in triaxial compression tests, however the behavior of a particular soil from different studies are often compared without due attention to the differences in specimen size and its effect on soil behavior. For example, Table 3.1 presents a summary of the different specimen sizes used in different triaxial testing studies of sand behavior.

**Table 3.1:** Summary of the specimen sizes used in different studies

Sample size (mm)		Material	Researcher
Diameter	Height		
38	76	Leighton Buzzard sand	Scott (1987)
50	100	Unimin sand	Garga (1988)
50.8	101.6	Ottawa and Mississippi sands	Sadrekarami (2010)
70	70	Athabasca oil sand	Wong (1999)
71	140	Granular material	Marachi <i>et al.</i> (1969)
71	140	Ottawa sand	Frost (2000)
74	150	Monterey sand	Ladd (1978)
75	150	Banding sand	Castro (1969)
75	150	Dune sand	Konrad (1990)
75	150	Lunar soil	Arslan <i>et al.</i> (2010)
76	150	Erkask 330/0.7 sand	Been and Jefferies (1991)
100	200	Leighton Buzzard sand	Scott (1987)
100	200	Sydeny sand	Hu <i>et al.</i> (2010)
102	200	Silty sand	Yamamuro and Lade (1997)
250	500	Loire river sand	Hu <i>et al.</i> (2010)
300	675	Ticino 9 sand	Jefferies <i>et al.</i> (1990)
300	600	Granular material	Seif el Dine (2009)
915	1370	Granular material	Marachi <i>et al.</i> (1969)
1000	1500	Loire river sand	Hu <i>et al.</i> (2010)

Several researchers have studied the effect of sample size on the behavior of cohesionless soils using triaxial shear tests (Marsal 1967; Marachi *et al.* 1969; Ladd 1978; Scott 1987; Been and Jefferies 1991; Hu *et al.* 2010; Chew *et al.* 2011), direct shear tests (Parsons 1936; Palmeira and Milligan 1989; Hight and Lerouiel 2003; Cerato and Lutenegeger 2006; Wu *et al.* 2007; Bareither *et al.* 2008), and numerical modeling investigations (Oie *et al.* 2003; Liang *et al.* 2009; Arslan *et al.* 2010; Shen 2011; Frossard *et al.* 2012). For example, Parsons (1936) study on the effect of specimen size in direct shear testing on both Ottawa sand and crushed quartz indicates that a reduced friction angle is mobilized in a larger shear box, and that this difference is more significant in Ottawa sand specimens than in crushed quartz sand specimens. Scott (1987) performed drained triaxial compression tests on dense Leighton Buzzard sand specimens of diameters 38 mm and 100 mm which were consolidated to similar void ratios and effective confining pressures. He found a higher peak strength and initial shear modulus in the larger specimen whereas smaller post peak shear strength was mobilized in the larger specimen at the end of the tests at an axial strain of 15%. Shear bands developed in both specimens indicating that shear banding could occur irrespective of sample size. Garga (1988) studied the size effects on the strength of dense basaltic soils using 100 and 500 mm square direct shear tests and 36 and 63.5 mm cylindrical specimens in undrained triaxial compression tests. The shear strength ratios were used to compare the results and a reduction in the peak and critical strengths were found with increasing specimen size.

Jefferies *et al.* (1990) investigated the influence of sample size on the drained shearing behavior of Ticino 9 sand. Four different cylindrical specimens of diameters 35, 75, 150, and 300 mm were prepared by dry pluviation and sheared from the same isotropic

consolidation pressure of 100 kPa. Figure 3.1 compares the measured stress-strain and volumetric strain behaviors of these specimens.

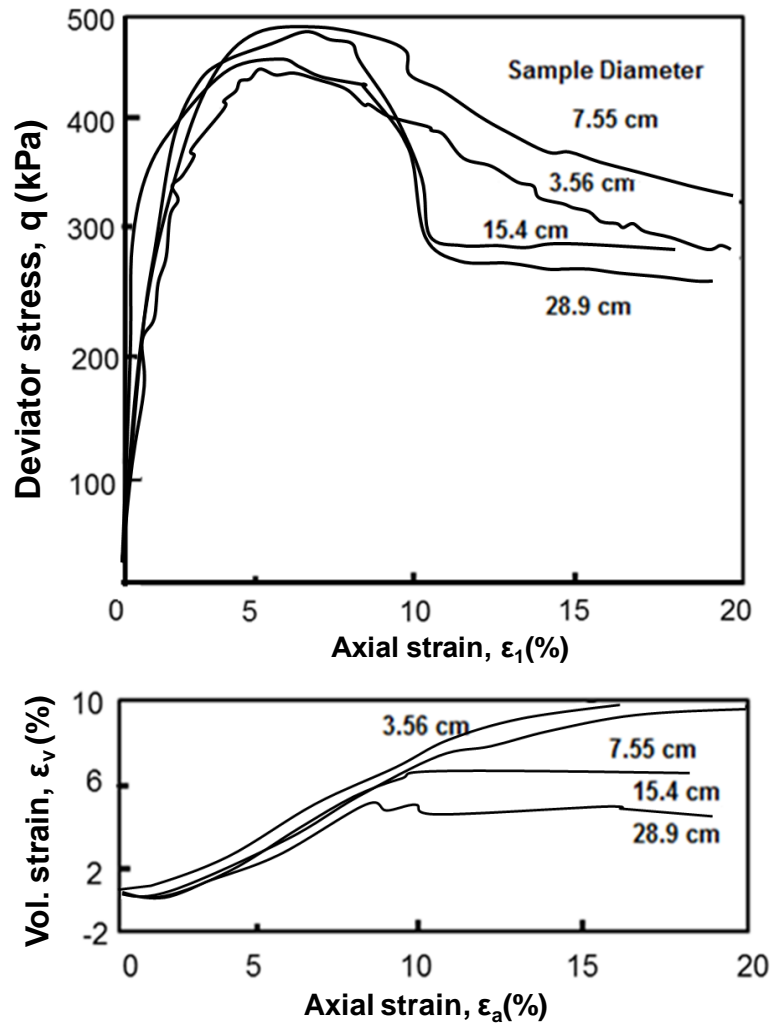


**Figure 3.1:** Effect of specimen size on the behavior of Ticino 9 sand (Jefferies *et al.* 1990)

According to Figure 3.1, the smaller specimen exhibits the greatest volumetric strain despite its smallest peak deviator stress. In addition, critical state conditions at which both the deviator stress and volumetric strain become constant are reached in the larger specimens while the smaller specimens (35.6 mm and 75.5 mm) are still strain-softening. This can be

attributed to the difference in the amounts of shear displacements applied in each specimen size. At the same axial strain, the larger specimens undergo greater shear displacements than the smaller specimens and thus subject the particles to larger amount of rearrangement and reorientation while there is insufficient space in the smaller sample for the movement and reorientation of the particles.

Cerato and Lutenecker (2006) tested five different sands in three square shear boxes with different lengths of 60, 101, and 305 mm, respectively. They found that the specimen size had a significant impact on the measured friction angle with the values obtained from testing the 60 mm specimens being up to ten degrees higher than those measured from the 305 mm specimens. Similar results have been documented by many other studies on the effect of shear box size on the results of direct shear tests (Hight and Leroueil 2003; Wu *et al.* 2007; Bareither *et al.* 2008; Dadkhah *et al.* 2010; Moayed and Alizadeh 2011). Wang and Gutierrez (2010) performed discrete element analyses to examine the impact of specimen length and height on sand behavior. The results were presented in terms of stress ratio, box height, and box length. They found that the peak stress ratio ( $\tau/\sigma'_v$ ) increased with decreasing box length or box height. Hu *et al.* (2010) developed a set of triaxial cells of various sizes to study the size effect on Loire River sand and Calcareous rockfill, and found that pre-peak behavior in drained triaxial compression tests was not affected by the specimen size, whereas the post-peak behavior depended on the size of the specimens which controlled strain localizations. It was also observed that for well-graded angular sands, the friction angle decreased as sample size increased.

While the aforementioned studies have focused on the specimen size effect on soil behavior, some other investigators have compared the behavior of granular materials with different

ranges of particle sizes as an alternative approach for studying specimen scale effect (Tatsuoka 1997; Okuyama *et al.* 2003; Oie *et al.* 2003; Islam *et al.* 2011; Farbodfar 2013). In this method, while the specimen size does not change, among granular soils with parallel particle size distributions (similar coefficients of uniformity,  $C_U$  and curvature,  $C_C$ ) a larger mean particle size ( $D_{50}$ ) replicates a smaller specimen size. For example, Fabodfar (2013) performed series of direct shear tests on three sands of more-or-less parallel particle size distributions but with different mean particles size ( $D_{50} = 0.19, 0.49, \text{ and } 2.77 \text{ mm}$ ) to examine the influence of sand gradation and specimen size on the sand strength parameters. He found that the peak shear strength and the mobilized friction angle increased with increasing  $D_{50}$ . Based on the analogy between  $D_{50}$  and specimen size, his results imply that the peak shear strength and the mobilized friction angle decrease with increasing specimen size.

As summarized above, although many studies have observed that larger specimens often result in smaller shear strengths and friction angles, the impact of specimen size on the shear strength parameters and design is largely overlooked in engineering practice. In addition, previous investigations of specimen-size effects in triaxial tests have mainly focused on the testing of dense sands (Scott 1987; Been and Jefferies 1985; Garga 1988; Hazarika *et al.* 2010) or coarser granular materials containing large particles such as rockfill (Marsal 1967; Marachi *et al.* 1969; Seif el Dine 2009; Hu *et al.* 2010) which also require the construction of a large-sized triaxial apparatus. In this study, a comprehensive and systematic experimental program is conducted to investigate the sample size effect on the consolidation, drained and undrained shear behavior of very loose Ottawa sand specimens.



## 3.2 Experimental Methodology

An experimental program for testing loose Ottawa sand with different specimen sizes is implemented to study the size effect on the consolidation and stress-strain behaviors and shear strength parameters. Static triaxial compression tests were performed on cylindrical specimens prepared to 38, 50, and 70 mm diameters. Non-uniform deformations in triaxial testing often result from the mechanical boundary restraints as a result of the friction between a specimen and the end platens (Bishop and Green 1965; Lee 1978). This end restraint could affect the pore pressure or volume change measurements and lead to incorrect shear strength parameters under different consolidation stresses. In order to reduce specimen non-uniform deformation and bulging at large strains (Rowe and Barden 1964; Bishop and Green 1965; Dangus *et al.* 1988), the specimens were prepared with equal lengths and diameters (length to diameter ratio of one) and the end restraints were nearly eliminated by employing enlarged and lubricated end platens covered with two layers of lubricated latex sheets.

The sand used in this investigation is clean uniformly-graded quartz sand from Ottawa, Illinois. This sand is composed of round to sub-round particles with a specific gravity of 2.65 and maximum and minimum void ratios of 0.821 and 0.487, respectively measured using the ASTM standards D854 and D4243, respectively. The sand is classified as Fine Sand, SP as per the ASTM D2487 standard procedure (the unified soil classification system) with mean grain size ( $D_{50}$ ) of 0.22 mm. The specimens were prepared by tamping moist sand layers (at a moisture content of 5%) of predefined sand weights to specific equal thicknesses into the specimen mold. Very loose specimens (at relative densities of 0%) were developed to reach an unequivocal critical state at which the effective stress, shear stress and

specimen volume do not change. The under compaction technique (Ladd 1978) was employed to define the weight of each layer in order to form uniform specimens.

Monotonic triaxial compression tests of this study were conducted using an automated stress path triaxial compression machine. The key components of this apparatus include a 1) triaxial cell which allows the testing of samples up to 70 mm in diameter which is mounted on a 20 kN loading frame, 2) an external load cell to measure the load acting on the sample, 3) an LVDT to measure the vertical displacement of the sample, 4) three pressure transducers for the measurement of the cell pressure, pore pressure, and back pressure, 5) pressure pumps for the measurement of volume change, and 6) a data-acquisition unit dedicated for intelligent data acquisition. Back pressure was applied as recommended by Bishop and Henkel (1962) to saturate the specimen until a pore pressure parameter (B) of at least 0.97 was achieved. The specimen was then isotropically consolidated to the target effective confining stresses. All samples were subsequently sheared at a rate of 5% / hour (0.032, 0.042, and 0.058 mm / min for 38mm, 50mm, and 70mm specimen, respectively) to about 30% axial strain in order to reach a critical state. Table 3.2 summarizes the specifications of the specimens and loading conditions of this study.

For accurate evaluation of the size effect on the measured shear strength parameters, corrections were made to the test results to account for the volume change due to back pressure saturation (ASTM D4767-11) and membrane penetration (Baldi and Nova 1984), axial deformation due to bedding error (Sarsby 1980), stress correction due to membrane resistance (ASTM D7181-11), and the change of specimen cross-sectional area during shear (Garga and Zhang 1997).

**Table 3.2:** Specifications of triaxial tests of this study

Specimen Size	Test #	Drainage Condition <sup>a</sup>	p' <sub>c</sub> (kPa)	e <sub>c</sub>	D <sub>rc</sub> (%)
70 mm	MT-1	D	500	0.771	15
	MT-2		300	0.779	13
	MT-3		200	0.785	11
	MT-4		100	0.797	7
	MT-5	UD	500	0.775	14
	MT-6		300	0.782	12
	MT-7		200	0.791	9
	MT-8		100	0.797	7
50 mm	MT-9	D	500	0.761	18
	MT-10		300	0.769	16
	MT-11		200	0.773	14
	MT-12		100	0.786	10
	MT-13	UD	500	0.769	16
	MT-14		300	0.775	14
	MT-15		200	0.785	11
	MT-16		100	0.795	8
38 mm	MT-17	D	500	0.76	18
	MT-18		300	0.766	16
	MT-19		200	0.775	14
	MT-20		100	0.786	10
	MT-21	UD	500	0.766	16
	MT-22		300	0.773	14
	MT-23		200	0.784	11
	MT-24		100	0.794	8

<sup>a</sup> D: drained shear test; UD: undrained shear test.

### 3.3 Triaxial Test Results:

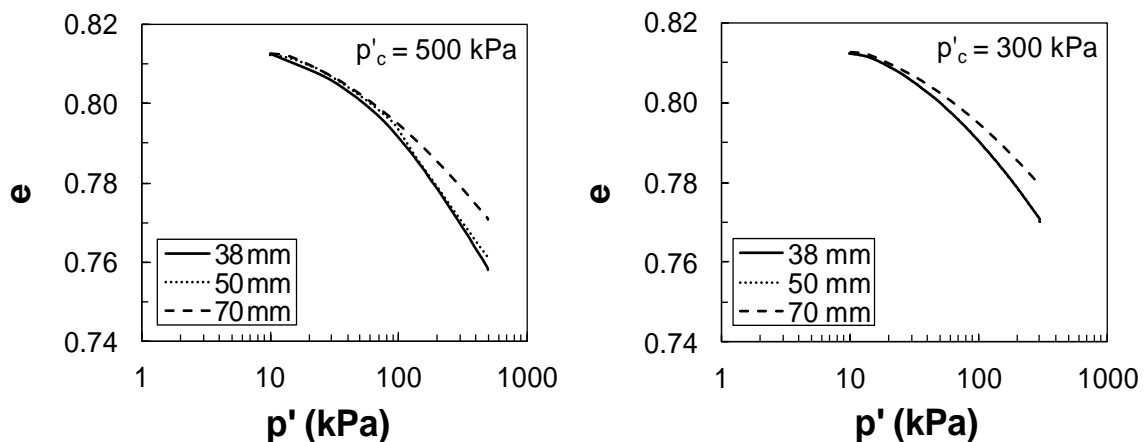
The results of the triaxial tests of this study are presented in the following paragraphs and compared for different specimen sizes during isotropic compression and shear.

#### 3.3.1 Isotropic Compression Response

As discussed earlier, all the triaxial specimens were prepared at very low relative densities ( $D_r = 0\%$ ) corresponding to void ratios of 0.821 which reached about  $D_r = 2.4\%$  following

saturation as a result of the volume changes occurring during flushing and the application of back-pressure (corresponding to approximately 0.45% volumetric strain). Figure 3.2 presents the isotropic compression lines for the different specimen sizes tested in this study. According to the plots of Figure 3.2, the 38 mm specimens display the highest compression index (steepest compression line) followed by the 50 mm and 70 mm specimen sizes. In other words, the 70 mm specimens experienced less volumetric strain than the 38 and 50 mm specimens under the same confining stress in all tests. This indicates that larger specimens exhibit markedly stiffer isotropic compression behavior and significantly smaller compressibility during isotropic compression which is consistent with the findings from other studies (Jefferies *et al.* 1990).

As a result of the stiffer behavior of the larger specimens (70 mm), a slightly looser void ratio (2 – 3% lower  $D_{rc}$ ) was established at the end of consolidation just before shear. Accordingly, the 70 mm specimens established looser consolidation void ratios compared to the 50 mm and 38 mm specimens. On the other hand, specimens prepared at looser initial void ratios significantly deformed and collapsed after preparation and it was not possible to prepare the 50 mm and 38 mm specimens at looser initial void ratios.



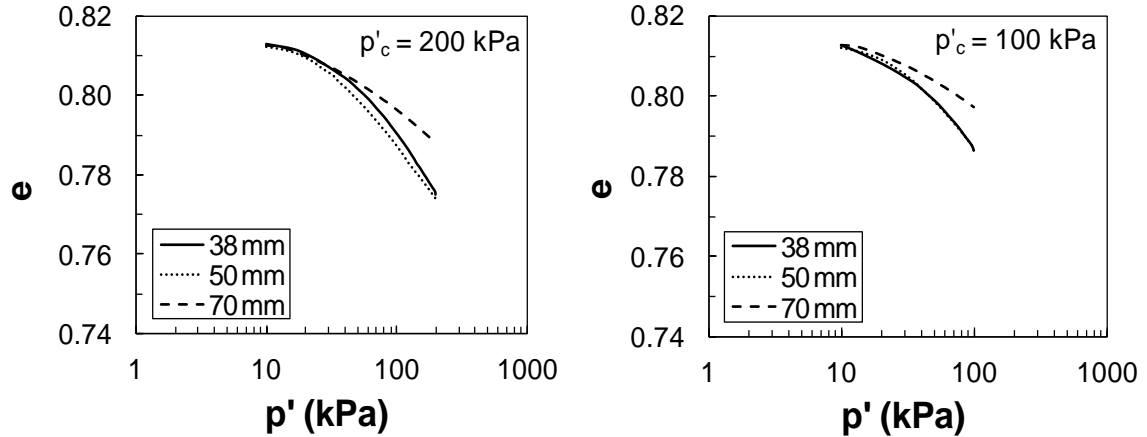


**Figure 3.2:** Effect of specimen size on the isotropic compression behavior of loose sand

### 3.3.2 Undrained shear behavior

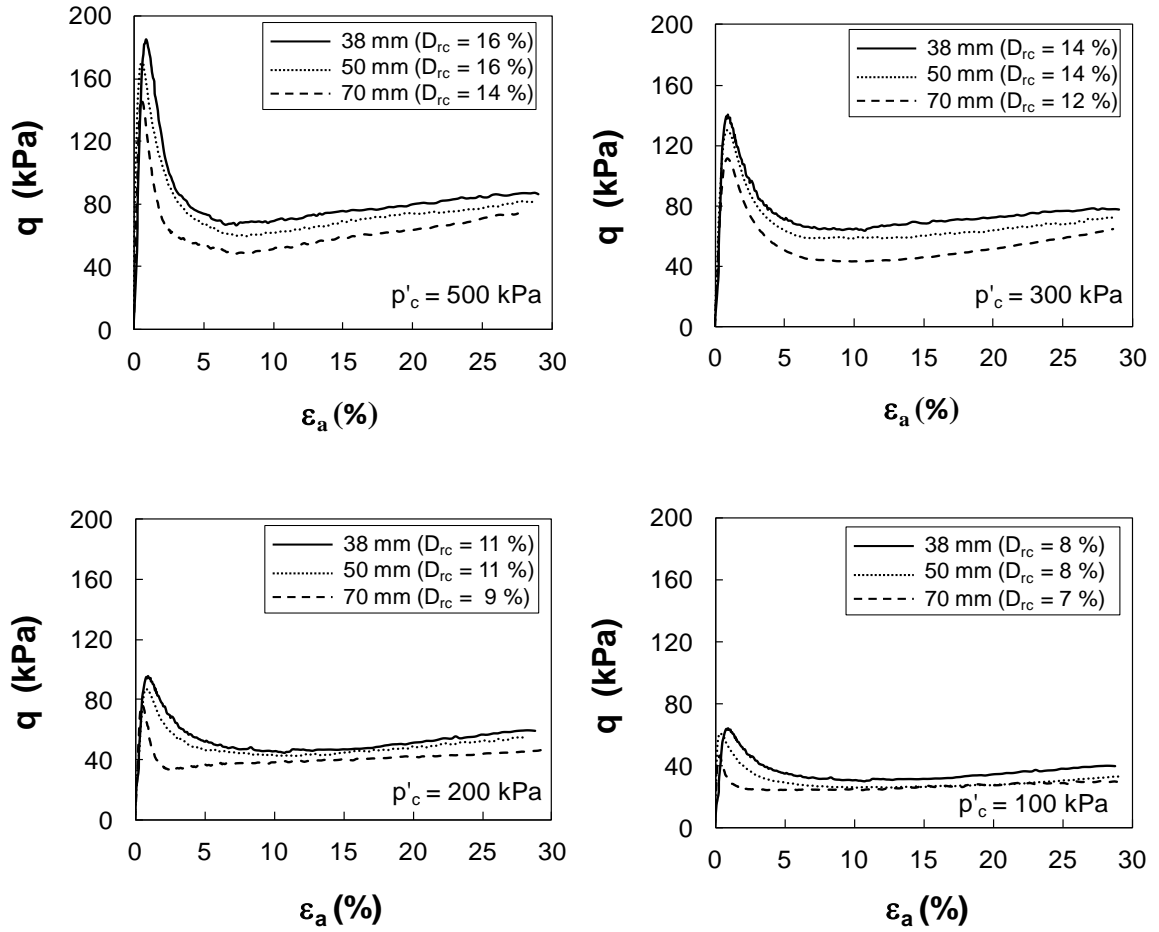
The effect of specimen size on sand behavior during undrained shear is presented in the following paragraphs with respect to undrained shear strength and excess pore water pressure generation. Figure 3.3 compares the undrained deviator stress versus axial strain behavior from the triaxial compression tests on different specimen sizes. Although, all of the specimens exhibit strain-softening behaviors, the deviator stress mobilized throughout the test is consistently larger in the smaller specimens and the peak deviator stress occurs at larger strains with decreasing specimen size.

The mechanical behavior and shear strength mobilization in cohesionless soils essentially depends on the interaction among soil particles and the amount of particle movement, rearrangement, reorientation and possible particle crushing. Accordingly, soil stress-strain response, which is a fundamental soil behavior, depends on the amount of relative displacement among soil particles and this should be essentially unrelated to the size of the specimen. Whereas on the other hand, the strain level is calculated based on normalization

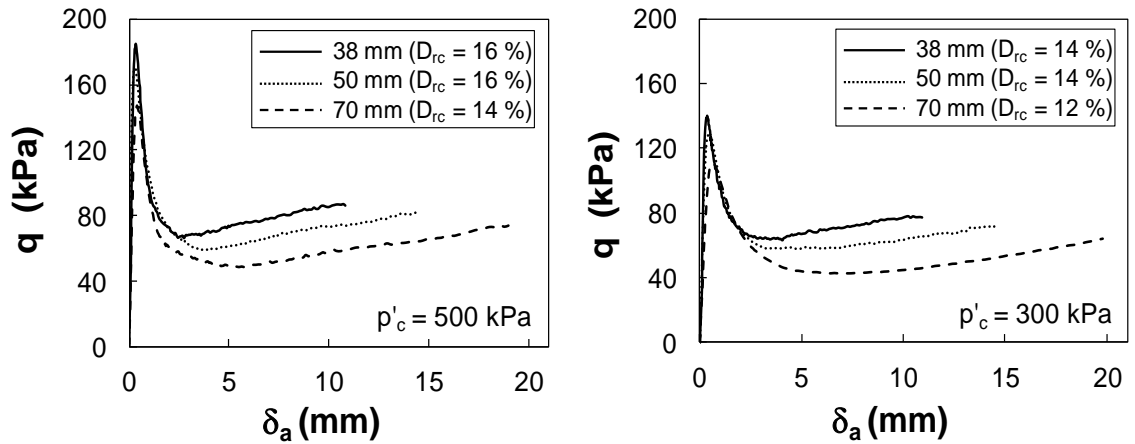
with respect to specimen dimension and, therefore, the stress-strain behaviors of specimens of different sizes could appear to be different.

Therefore, in order to remove the effect of specimen dimension from specimen deformation, the deviator stress plots of Figure 3.3 are redrawn versus the axial displacement of each specimen in Figure 3.4. Note that the axial displacements of 2.1, 1.5, and 1.2 cm represent the final axial displacements for the specimen sizes of 70, 50, and 38 mm, respectively, corresponding to the same axial strain level of 30%. According to Figure 3.4, although the peak deviator stresses now occur at almost the same axial displacement of approximately 0.7mm for all specimen sizes, the differences in deviator stresses among different specimen sizes is amplified at the same axial displacements. Although the lower deviator stress mobilized in the 70 mm specimens could be partly due to their slightly looser void ratios, the 50 mm and 38 mm diameter specimens were sheared from the same void ratios while still demonstrating specimen size effects.

On the other hand, Figure 3.5 shows similar excess pore water pressures ( $\Delta u$ ) developed during undrained shear in the different specimen sizes consolidated to the same confining stress ( $p'_c$ ). The minor differences in the initial rates of excess pore pressure generation are related to the slight differences in specimens  $D_{rc}$  however equal  $\Delta u$  are developed after an axial strain of 10% where critical state is reached. These figures imply that although the sand fabric plastic contractive tendency is the same for all specimen sizes, the mobilized strength, deviator stress, and the strain-softening behavior include an inherent specimen size dependency irrespective of the differences in the amount of deformation that is experienced by each specimen size at similar axial strains. The mechanism of this specimen size effect will be discussed after comparing the drained shear behavior of the three specimen sizes.



**Figure 3.3:** Undrained stress – strain behavior of different specimen sizes in triaxial compression tests of loose sand



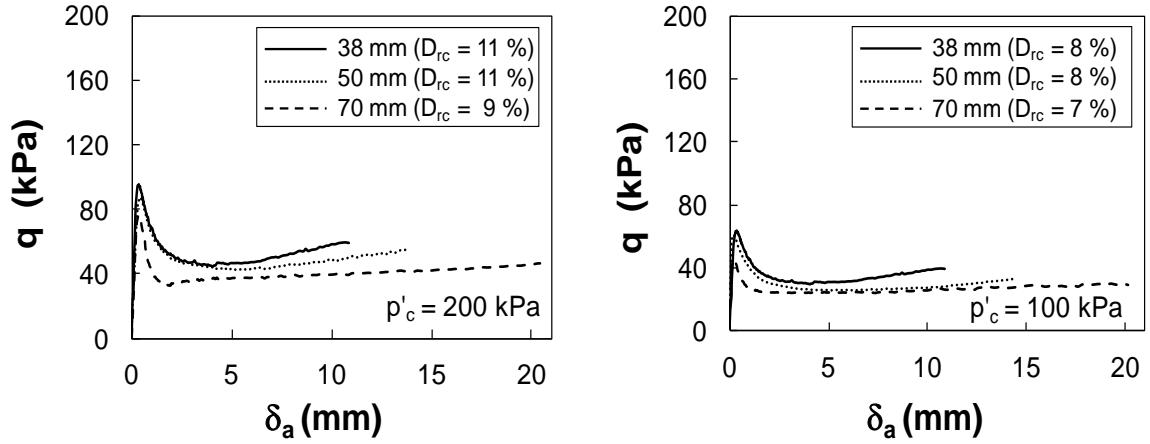


**Figure 3.4:** Undrained stress – axial displacement behavior of different specimen sizes in triaxial compression tests of loose sand

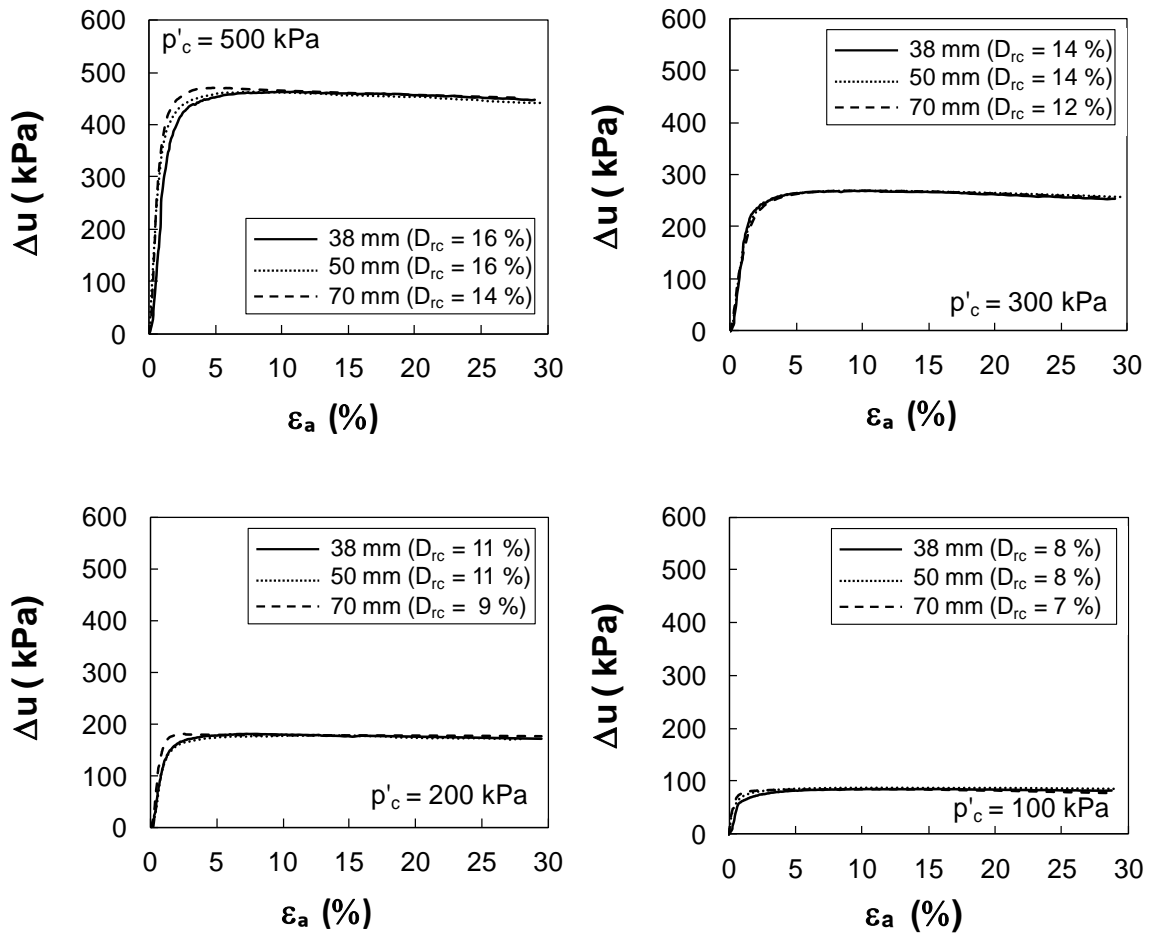


**Figure 3.5:** Excess pore water pressure developed during undrained triaxial compression tests on different specimen sizes of loose sand

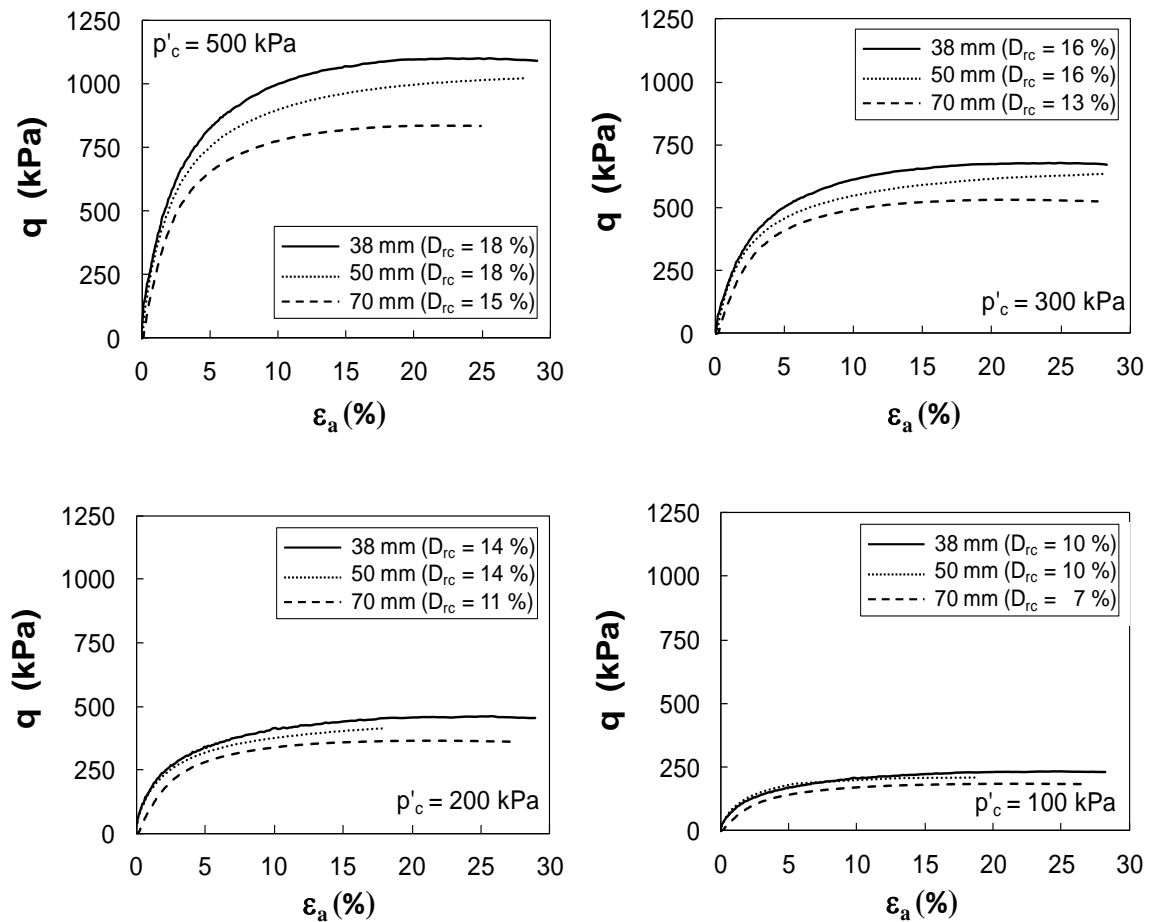


### 3.3.3 Drained shear behavior

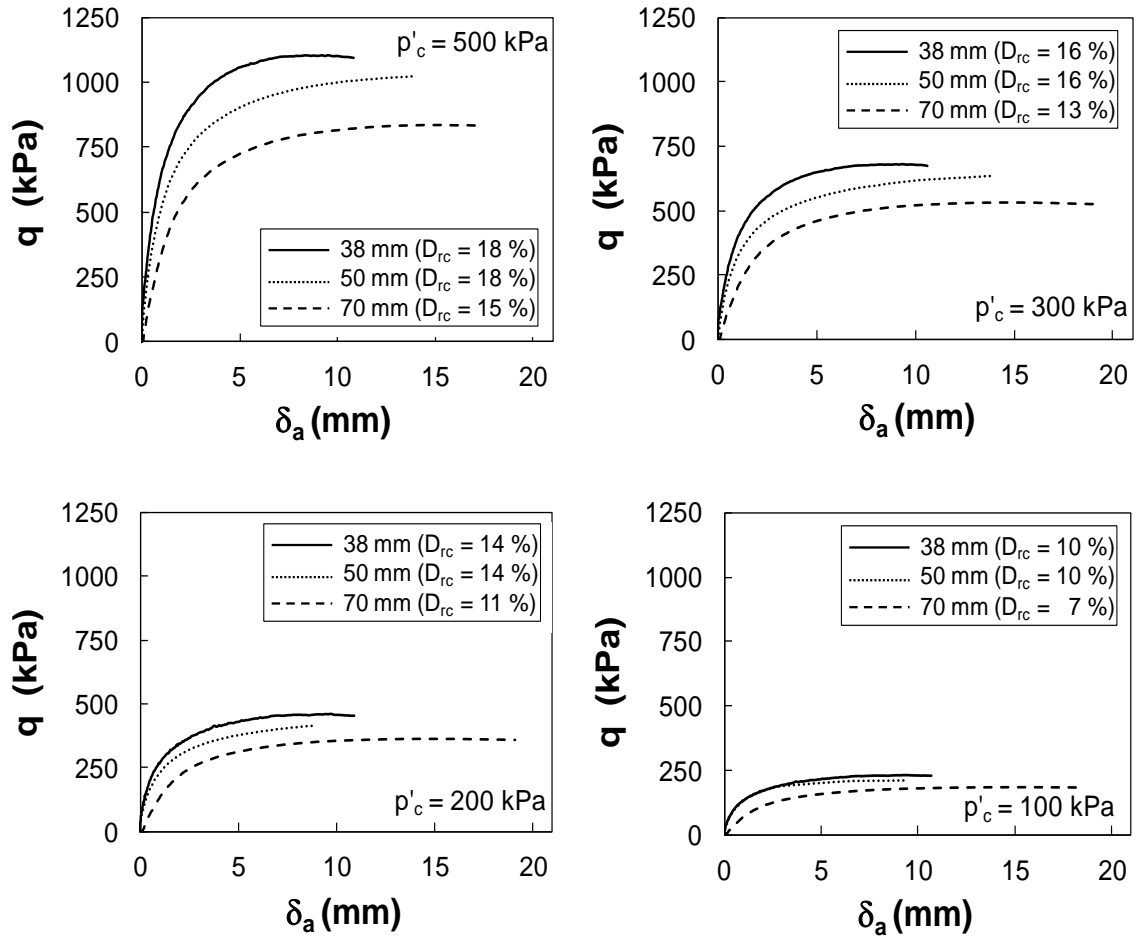
Figures 3.6 to 3.9 compare the drained behaviors of the loose sand specimens from the triaxial compression shear tests. According to Figures 3.6 and 3.7, larger initial modulus (increase in stiffness) is exhibited in the smaller specimens. This could be attributed to the higher relative density of the smaller specimens. In addition, larger deviator stresses are mobilized in the smaller specimens, which are exaggerated if axial displacements are used. Note that although the lower deviator stress of the 70 mm specimens could have been partly associated with their slightly looser void ratios, the 50 mm and 38 mm diameter specimens were sheared from the same void ratios and exhibit obvious specimen size effect. These observations are consistent with the findings from other studies (Jefferies *et al.* 1990).

However, in order to investigate the influence of specimen size on the volumetric strain behavior and volumetric contraction recorded during the drained tests, the volumetric strain versus axial strain, as well as the volumetric dilatancy ( $\Delta\varepsilon_v/\Delta\varepsilon_a$ ) versus axial strain obtained from testing specimens of different sizes are compared in Figures 3.8 and 3.9, respectively. All specimens show volumetric contraction with a steady decrease in the rate of volume reduction with axial strain (i.e. dilatancy) followed by an almost flat plateau of constant volume behavior ( $\varepsilon_v = 0$ ) at the critical state. Hypothetically, the same sand at the same  $p'_c$  and  $e_c$  should exhibit similar volumetric strains during shear. However, these plots demonstrate that volumetric strain increases with decreasing specimen size. Also, the rate of dilation increases with decreasing specimen size with the maximum occurring at a small strain of about 1% (same axial strain at which the peak undrained strength occurred). In other words, the dilatancy plots demonstrate the volumetric strain behavior of different specimen sizes with the smaller size showing more contractive behavior than the larger size.

Similar to our observation during the isotropic compression stage of the tests, the larger specimens exhibit a stiffer volumetric behavior (despite the slightly denser void ratios of the smaller 38 mm specimens) and display much less contractive potential and higher dilatancy than the smaller specimens. This progressive volumetric compressibility of the smaller specimens at large strains is the most remarkable aspect of the data regardless the effect of size on the specimens stiffness during the initial loading.



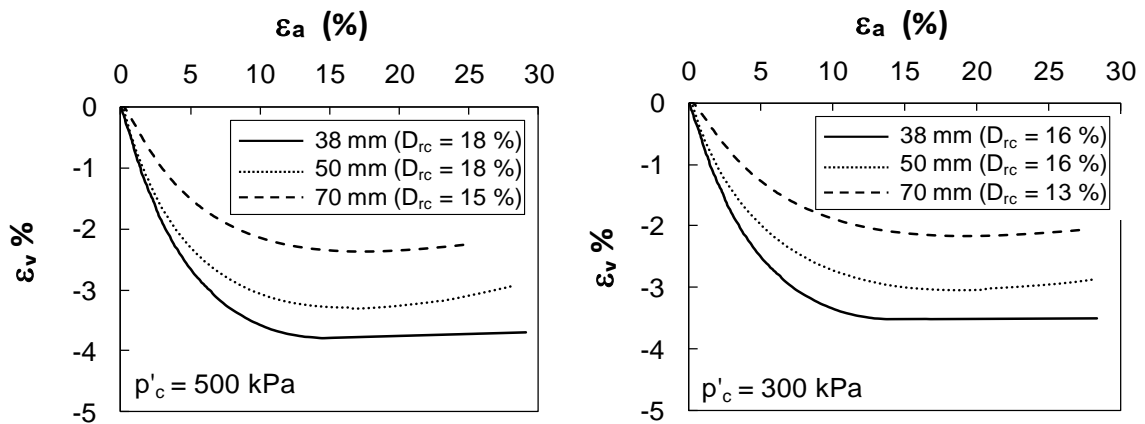
**Figure 3.6:** Drained stress – strain behavior of different specimen sizes in triaxial compression tests of loose sand

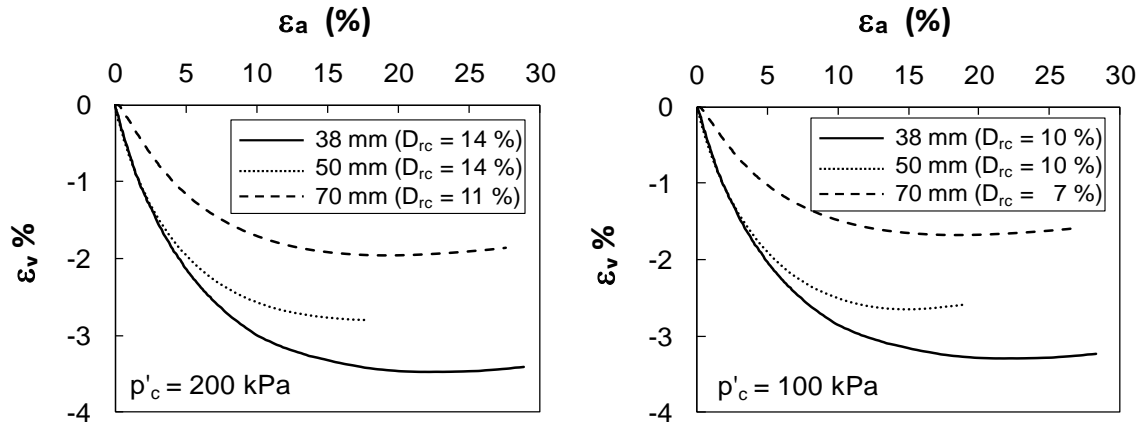


**Figure 3.7:** Drained deviator stress – axial displacement behavior of different specimen sizes in triaxial compression tests of loose sand

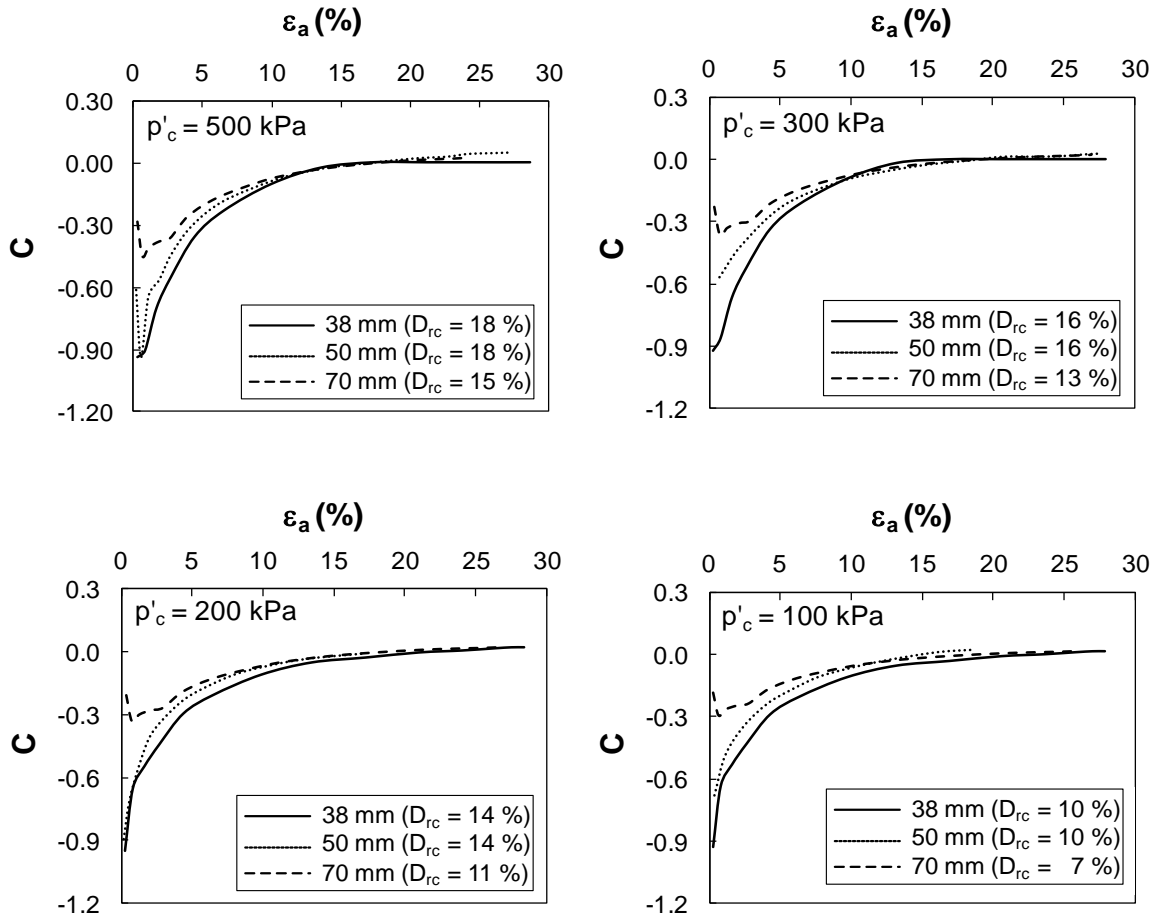
Failure of granular materials is often characterized by localization of non-uniform deformation commonly referred to as shear bands (Roscoe 1970). Loose sand specimens exhibit a complex internal failure pattern involving multiple shear bands that may not be visible without using advanced visualization techniques (Tatsuoka *et al.* 1990; Desrues *et al.* 1996; Finno *et al.* 1996; Jang and Frost 2000; Alshibli and Sture 2000). Accordingly, although no shear bands were observed at the end of the tests on the exterior surface of the triaxial specimens in this study, it is quite possible that a complex and diffuse mode of failure and shear localization (involving multiple shear bands) developed in the specimens.

In fact, the multiple shear band formation and complex localization is an inevitable response of sand to the stress state and shear path of the test, irrespective of the testing boundary conditions and specimen imperfections (Chu *et al.* 1996; Desrues *et al.* 1996). No matter how much effort is made to prevent in-homogeneity of deformation, strain localization and shear banding occur when a certain limit state is reached. Techniques such as enlarged and lubricated platens used to induce more uniform shear deformations in triaxial and biaxial tests merely delay and conceal shear localization (Lade and Wang 2011). For example, by minimizing the influence of specimen boundaries, Liang *et al.* (1997) found that a dominant shear band developed on its own (indicating material behavior) at a certain stress level. Through an extensive review of past experimental and numerical studies on shear banding and shear localization, Desrues and Chambon (2002) show that strain localization observed in laboratory tests is not an artificial effect due to imperfect test conditions and practice, and it is rather an essential aspect of material behavior which leads to localized deformation in most cases. The observed increase in stiffness and shear resistance with decreasing specimen size could be attributed to shearing along a larger number of shear bands formed in larger specimens and the differences in the available space or freedom for particle rearrangement in the specimens of different sizes.





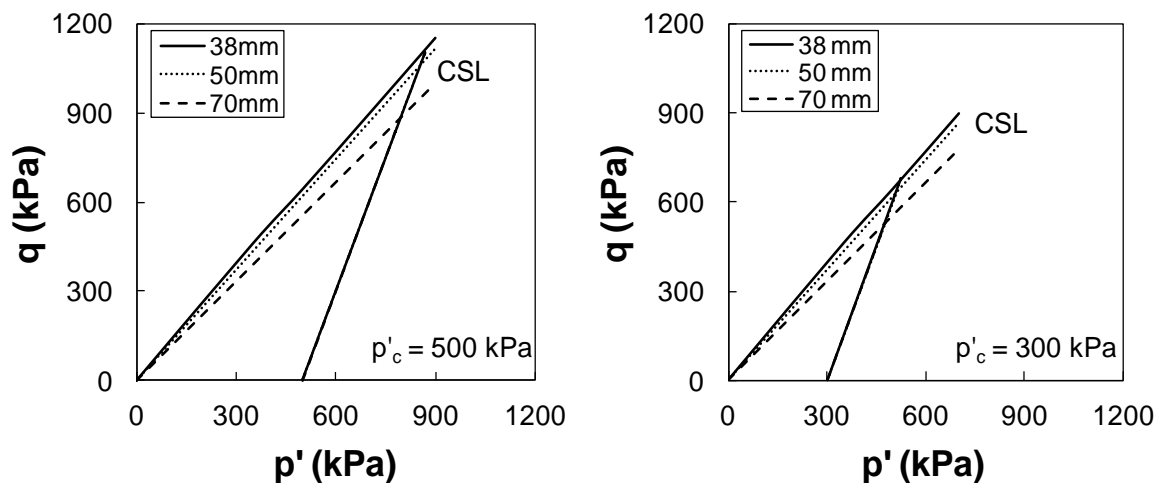
**Figure 3.8:** Volumetric strain response during drained triaxial compression tests on different specimen sizes of loose sand



**Figure 3.9:** Volumetric dilatancy response during drained triaxial compression tests on different specimen sizes of loose sand

### 3.4 Influence of Specimen Size on Effective Stress Paths

According to the stress - strain and volumetric strain plots in Figures 3.3 and 3.8, both the undrained and the drained shear tests exhibit strain-softening or contractive behavior moving towards a critical state. At the critical state, there is a unique relationship between the effective stresses, void ratio, and shear stress which is often described by the critical stress ratio line in the stress path ( $q$  versus  $p'$ ) space and the critical state line in the void ratio versus  $p'$  plane (Been *et al.* 1991) where ( $q = (\sigma_1' - \sigma_3')$ ) is the deviator stress and ( $p' = (\sigma_1' + 2\sigma_3')/3$ ) is the mean effective stress. The effective stress paths obtained from testing specimens of different sizes in the  $q$ - $p'$  plane are compared in Figures 3.10 and 3.11 for both drained and undrained conditions, respectively. It can be observed that the effective stress paths resulting from all the undrained tests of all specimen sizes reach the instability line and then move into the region of potential instability, and approach a constant stress ratio from different  $p'_c$  values, corresponding to the CSL of each specimen size. Unique critical state lines are obtained in the stress path plane for each specimen size, which become steeper with decreasing specimen size and accordingly, will affect the mobilized friction angle.



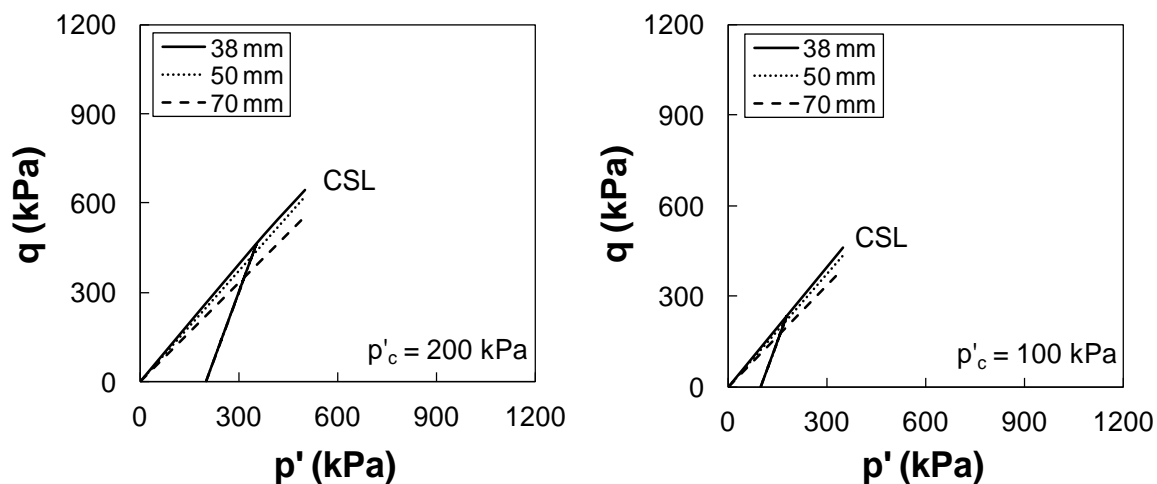


**Figure 3.10:** Effect of specimen size on drained effective stress paths

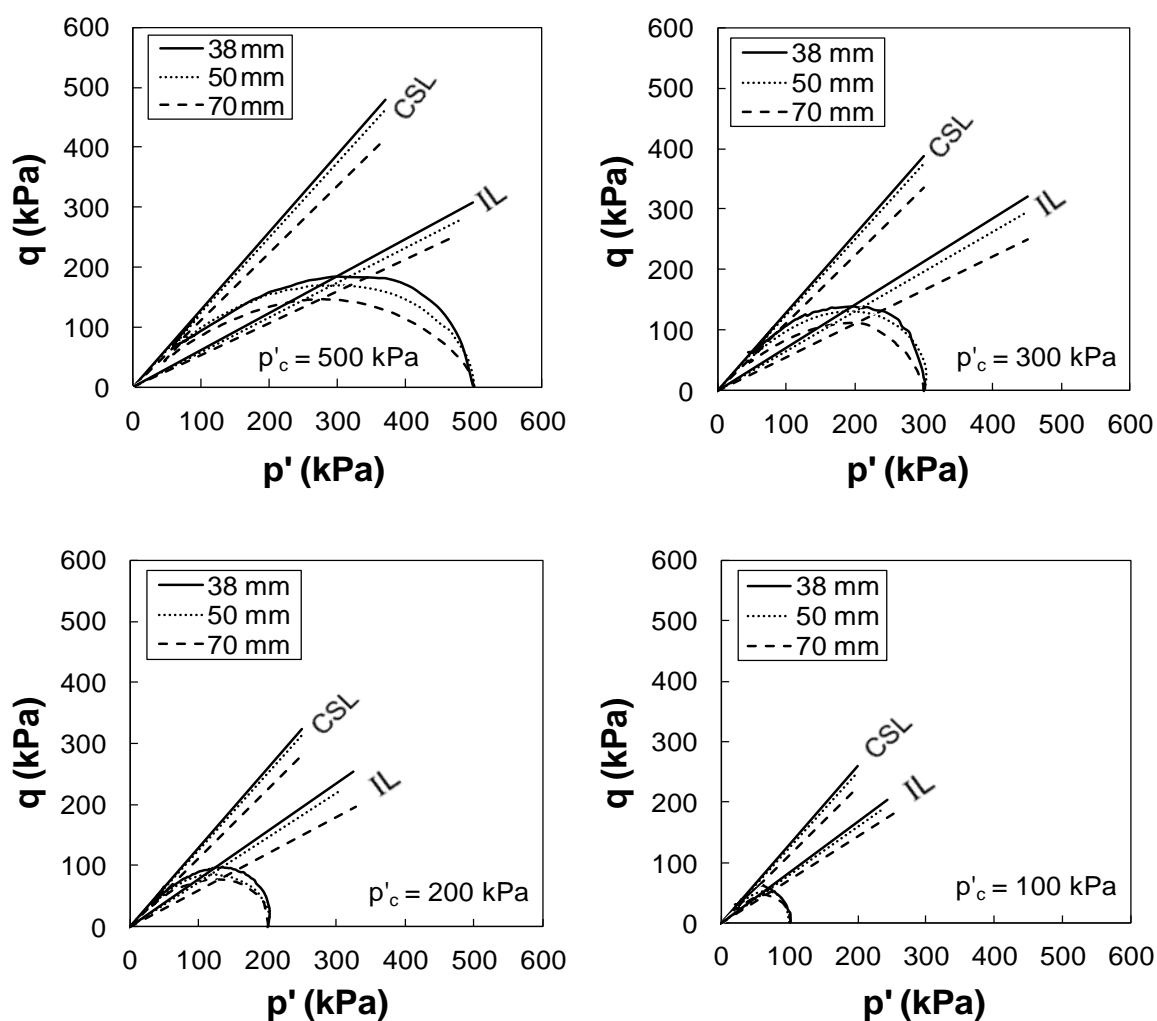


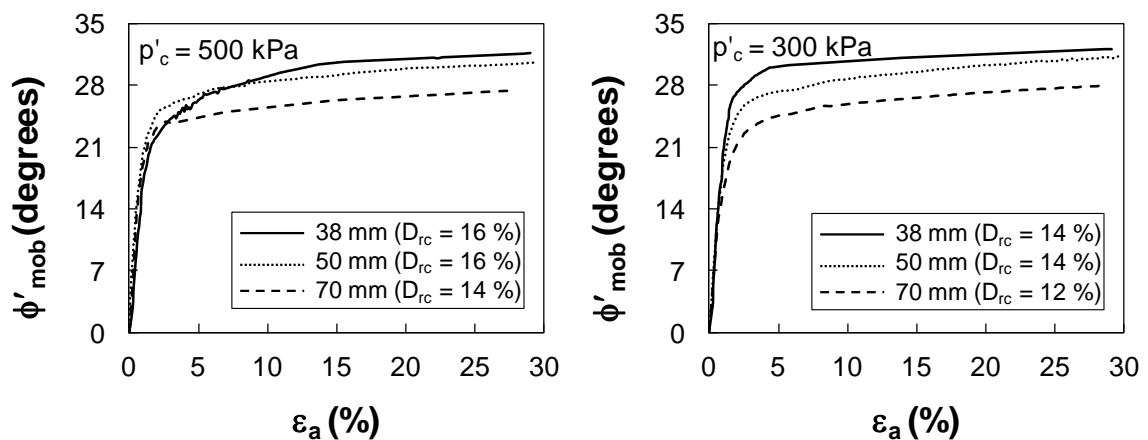
**Figure 3.11:** Effect of specimen size on undrained effective stress paths

### 3.5 Influence of Specimen Size on Effective Friction Angle

Granular soils mobilize shear resistance through its internal friction angle, and therefore, the friction angle is considered as the most important mechanical property to analyze granular soils responses to loading. The components of the mobilized friction angle during shear ( $\phi'_{\text{mob}}$ ) consist of the inter-particle sliding friction angle and the geometrical interference friction angle which can be further divided into dilation friction angle and particle rearrangement friction angle (Sadrekarimi and Olson 2011). The mobilized friction angle during shear is calculated from the effective stress ratio ( $M = q/p'$ ) using the following equation and compared for the drained and undrained shear tests on specimens of different sizes in Figures 3.12 and 3.13, respectively.

$$\phi' = \sin^{-1} \frac{3M}{(6+M)} \quad (3.1)$$

According to these figures,  $\phi'_{\text{mob}}$  in both drained and undrained shear tests steadily increases with axial strain and approaches a constant value at the critical state ( $\phi'_{\text{cs}}$ ) corresponding to the slopes of the CSLs in the stress paths of Figures 3.10 and 3.11.





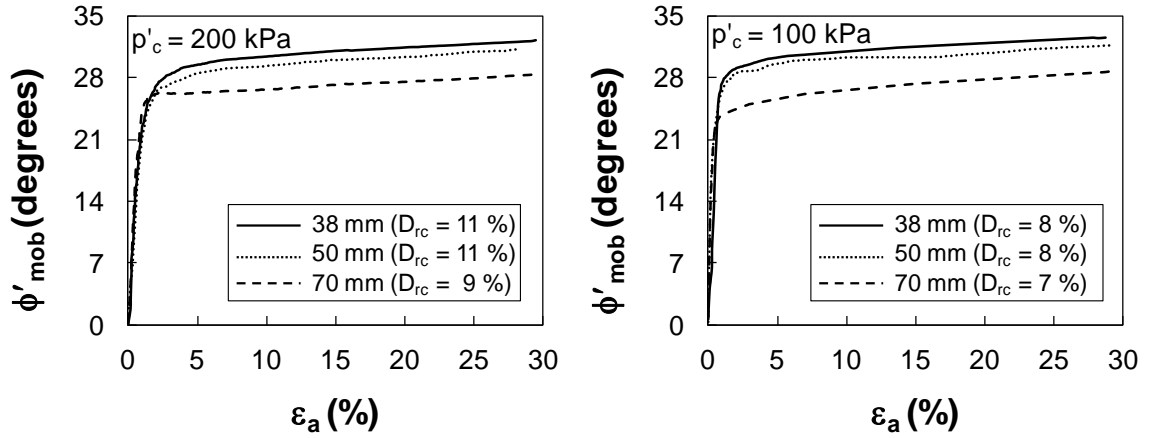


**Figure 3.12:** Effect of specimen size on  $\phi'_{mob}$  in undrained triaxial compression shear tests of loose sand

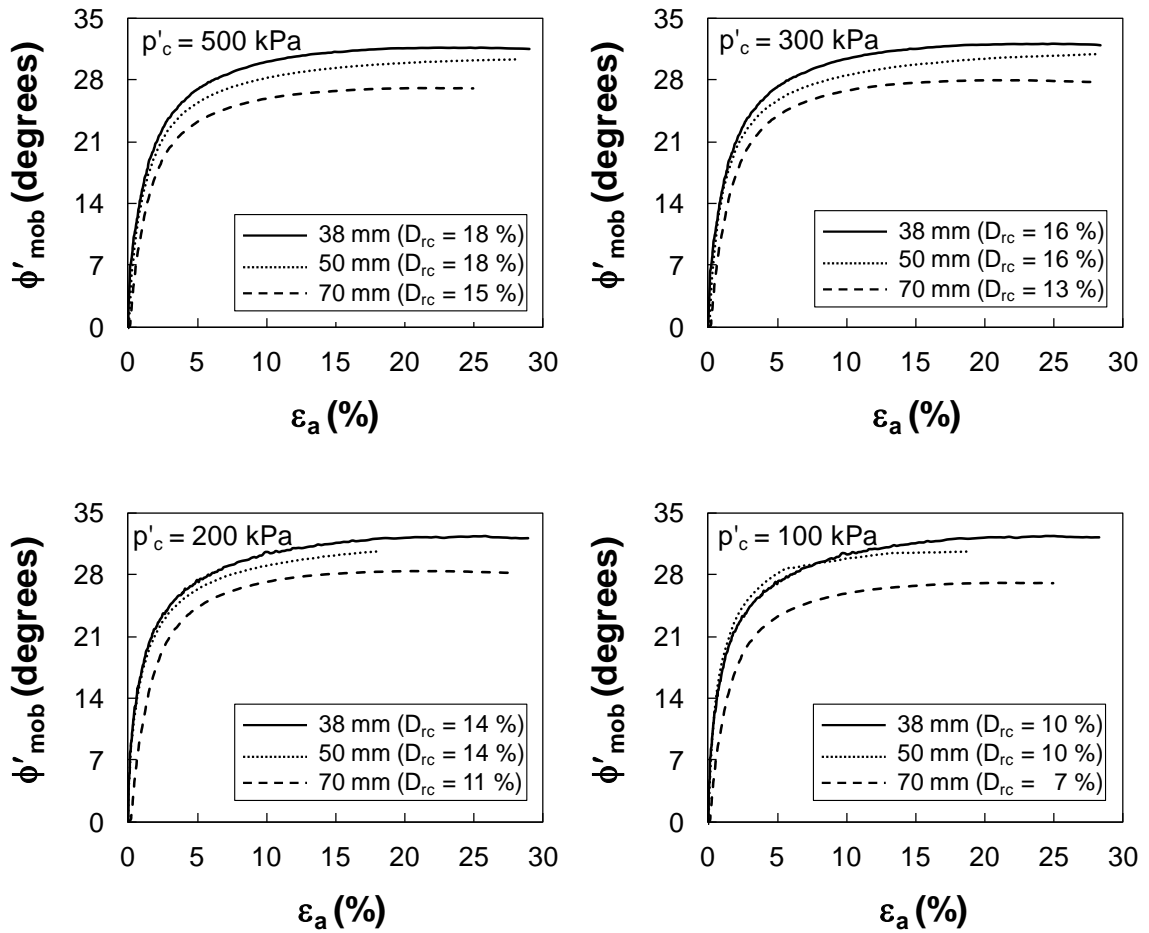


**Figure 3.13:** Effect of specimen size on  $\phi'_{mob}$  in drained triaxial compression shear tests of loose sand

The mobilized friction angle corresponding to the instability line (in Fig. 3.11) is the yield friction angle ( $\phi'_{\text{yield}}$ ) which is obtained from undrained shear tests. Table 3.3 summarizes the measured  $\phi'_{\text{yield}}$  and  $\phi'_{\text{cs}}$  for each specimen size subject to different confining stresses and drainage conditions.

**Table 3.3:** Summary of  $\phi'_{\text{yield}}$  and  $\phi'_{\text{cs}}$  for different specimen sizes

Specimen Size	Drainage Condition <sup>a</sup>	$p'_c$ (kPa)	$D_{rc}$ (%)	$\phi'_{\text{yield}}$ (degs.)	$\phi'_{\text{cs}}$ (degs.)
70 mm	D	500	15	-	27.1
		300	13	-	27.8
		200	11	-	28.2
		100	7	-	28.6
	UD	500	14	14.2	27.3
		300	12	14.7	27.9
		200	9	16.4	28.4
		100	7	18.2	28.7
50 mm	D	500	18	-	30.4
		300	16	-	31.0
		200	14	-	31.2
		100	10	-	31.4
	UD	500	16	16.2	30.6
		300	14	17.3	31.1
		200	11	18.5	31.3
		100	8	20.0	31.6
38 mm	D	500	18	-	31.5
		300	16	-	31.9
		200	14	-	32.1
		100	10	-	32.3
	UD	500	16	16.9	31.7
		300	14	18.5	32.1
		200	11	19.7	32.3
		100	8	21.1	32.5

<sup>a</sup> D: drained shear tests, UD: undrained shear test

Figure 3.14 presents the influence of  $p'_c$  and  $D_{rc}$  on the measured  $\phi'_{yield}$  and  $\phi'_{cs}$  for different specimen sizes. The effect of specimen size is clearly evident as both  $\phi'_{yield}$  and  $\phi'_{cs}$  increase with decreasing specimen size, particularly for the 38 mm and 50 mm specimens which were sheared from exactly same  $D_{rc}$  and  $p'_c$ . Besides the size of the specimens,  $\phi'_{yield}$  and  $\phi'_{cs}$  also decrease with increasing  $p'_c$  as particle interaction and rearrangement are suppressed at larger  $p'_c$ . The effect of specimen size (loose specimens) on  $\phi'_{yield}$  and  $\phi'_{cs}$  is summarized in Figure 3.15. It is often thought that  $\phi'_{yield}$  is primarily affected by the initial sand fabric and decreases with increasing  $e_c$  while  $\phi'_{cs}$  largely depends on sand mineralogy and particle shape (Sadrekarimi and Olson 2011). However, the plots of Figures 3.14 and 3.15 show that the size of the specimen can have a non-negligible effect on the  $\phi'_{yield}$  and  $\phi'_{cs}$  measured from triaxial tests. This could have significant impact in geotechnical engineering practice and designs which involve drained strength of sands.

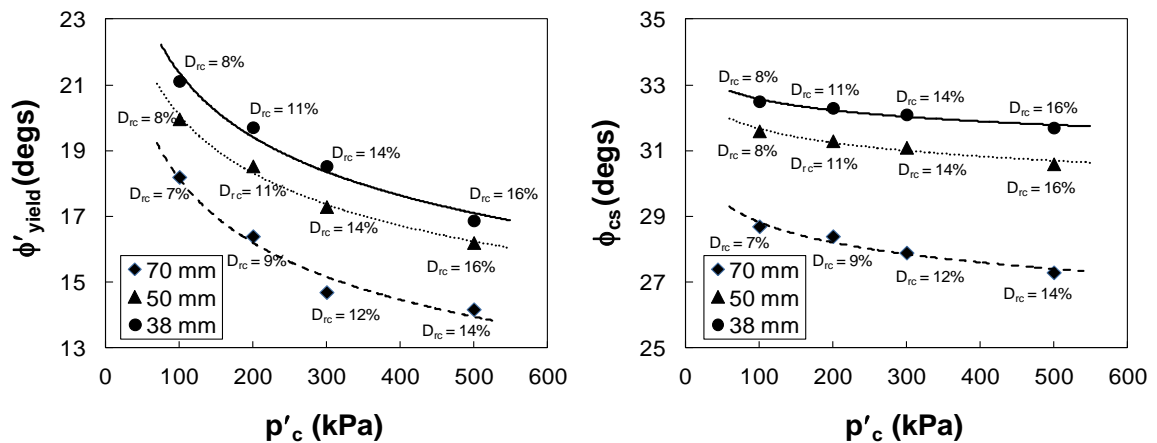


**Figure 3.14:** Effect of  $p'_c$  and  $D_{rc}$  on  $\phi'_{yield}$  and  $\phi'_{cs}$  mobilized in undrained triaxial compression tests on loose specimens of different sizes

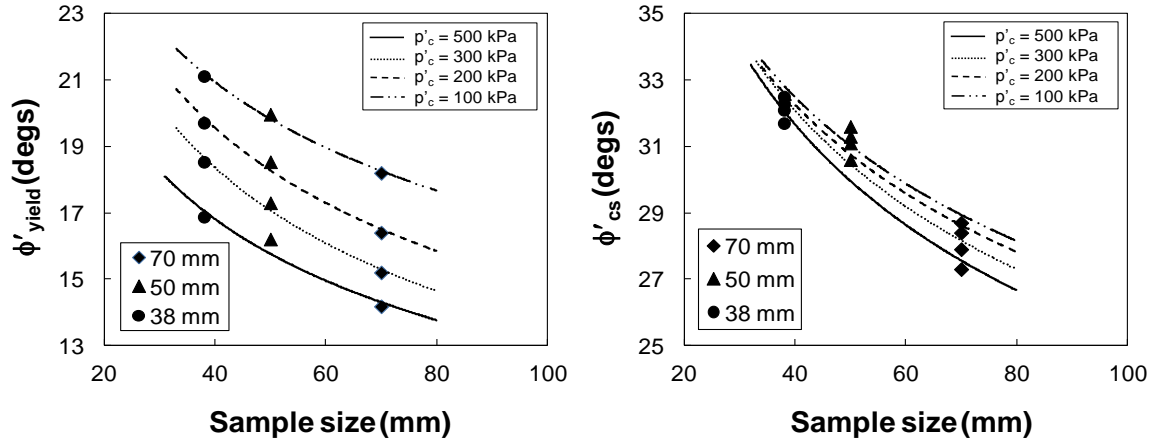


**Figure 3.15:** Effect of specimen size on  $\phi'_{\text{yield}}$  and  $\phi'_{\text{cs}}$  from undrained triaxial compression tests of loose sand

### 3.6 Influence of Specimen Size on Critical State Parameters

The effect of specimen size on the projection of the CSL in the stress path plane was presented in Figures 3.10 and 3.11 for drained and undrained shear tests, respectively. These figures indicated that the projection of the CSL in the stress path plane (i.e. the critical stress ratio line) becomes steeper with decreasing specimen size. Figure 3.16 presents the projection of the CSL in the  $e - \log(p'_c)$  plane from the undrained and drained triaxial compression tests on different specimen sizes. According to this figure, although unique CSLs are established from drained and undrained tests for each specimen size, the CSLs become steeper and largely shift to denser void ratios with decreasing specimen size from 70 mm to 38 mm specimen diameter, which reflects the stiffer response of the larger specimens observed in Figure 3.8.

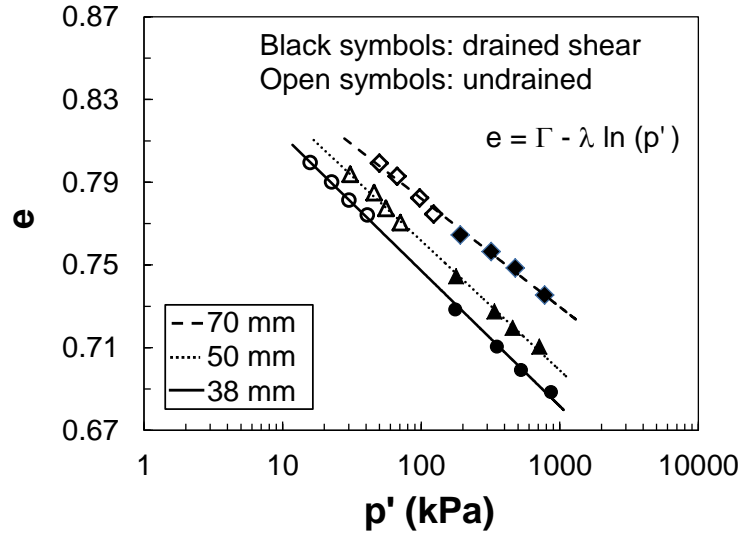


**Figure 3.16:** Effect of specimen size on the CSLs from both drained and undrained triaxial compression tests of loose sand

The slope ( $\lambda$ ) of the semi-logarithmic CSLs and the corresponding intercept value of  $e$  at  $p' = 1$  kPa in  $e - \ln p'$  space ( $\Gamma$ ) are summarized in Table 3.4. The significant change of the CSL and the critical state parameters ( $\lambda$ ,  $\Gamma$ , and  $\phi'_{cs}$ ) could have large effect in estimating soil state parameter for evaluating the liquefaction susceptibility and strain-softening behavior of cohesionless soils and the predictions of critical state constitutive models (e.g. NorSand, MIT-S1, SANISAND).

**Table 3.4:** Effect of specimen size on critical state parameters

Specimen Size	$M = q/p'_c$	$\phi'_{cs}$ (degs.)	$\lambda$	$\Gamma$
70 mm	1.12	28	0.023	0.887
50 mm	1.25	31	0.026	0.881
38 mm	1.29	32	0.028	0.878

### 3.7 Influence of Sample Size on Undrained Shear Strength

The effect of specimen size on the effective stress friction angle, which represents the drained shear strength of soils, was presented in Figures 3.12 to 3.15. Based on the Mohr-Coulomb failure theory, the undrained shear strength ( $s_u$ ) is obtained from the deviator stress ( $q$ ) as below:

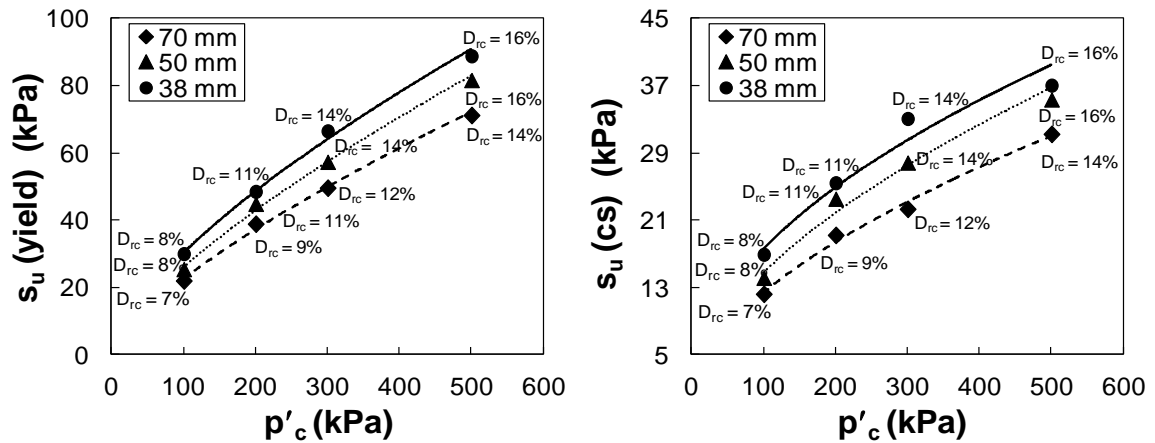
$$s_u = \frac{q}{2} \cos(\phi'_{mob}) \quad (3.2)$$

Accordingly, as presented in the deviator stress-strain plots of Figure 3.3 a peak undrained shear strength,  $s_u(\text{yield})$  is attained at an axial strain of about 1%. This is followed by significant drop of the undrained shear resistance (often called “strain-softening”) as a result of rapid increase in the excess pore pressure at constant volume. Strain-softening continues until a more-or-less constant undrained strength is mobilized at the critical state,  $s_u(\text{cs})$ . Both  $s_u(\text{yield})$  and  $s_u(\text{cs})$  depend on sand void ratio and  $p'_c$  and could vary considerably with small changes in  $e_c$ . Table 3.5 summarizes the  $s_u(\text{yield})$  and  $s_u(\text{cs})$  measured from the triaxial compression tests for each specimen size.

Figure 3.17 describes the increasing of  $s_u(\text{yield})$  and  $s_u(\text{critical})$  with  $p'_c$  for each specimen size. According to this figure,  $s_u(\text{yield})$  and  $s_u(\text{critical})$  increase not only with increasing  $p'_c$  and  $D_{rc}$ , but also with decreasing specimen size. Note that although the comparatively lower undrained shear strengths of the 70 mm specimens occurs as a result of their looser  $D_{rc}$  besides the potential effect of specimen size, since the 50 mm and 38 mm specimens were sheared from the same  $p'_c$  and  $D_{rc}$  the effect of specimen size on the undrained strengths of these specimen sizes is undeniable.

**Table 3.5:**  $s_u$ (yield) and  $s_u$ (critical) from undrained triaxial compression tests

Specimen Size	$p'_c$ (kPa)	$D_{rc}$ (%)	$s_u$ (yield) (kPa)	$s_u$ (cs) (kPa)
70 mm	500	14	71.1	31.2
	300	12	49.5	22.3
	200	9	38.8	19.2
	100	7	21.9	12.2
50 mm	500	16	81.5	35.3
	300	14	57.2	27.8
	200	11	44.7	23.5
	100	8	25.3	14.1
38 mm	500	16	88.7	37.0
	300	14	66.4	33.0
	200	11	48.4	25.4
	100	8	29.9	16.9

**Figure 3.17:** Effect of specimen size on  $s_u$ (yield) and  $s_u$ (critical) in undrained triaxial compression tests on loose sand

The critical state parameter ( $\psi_{cs}$ ) describes the void ratio change from the initial consolidation state ( $e_c$ ) to the critical state ( $e_{cs}$ ) at the same  $p'_c$  (Been and Jefferies 1985). A soil specimen at a positive  $\psi_{cs}$  ( $> 0$ ) would generally exhibit a strain-softening (during undrained shear) or contractive (in drained shear) behavior, and at a negative  $\psi_{cs}$  ( $< 0$ )

displays strain-hardening or dilative response. In order to eliminate the influence of the slight differences in  $D_{rc}$  of different specimen sizes and a clearer presentation of specimen size effect on undrained shear strengths and friction angles, the influences of  $D_{rc}$  (i.e.  $e_c$ ) and  $p'_c$  are collectively characterized by the critical state parameter ( $\psi_{cs}$ ) in Figures 3.18 and 3.19. The effect of  $p'_c$  is also incorporated in  $s_u(\text{yield})$  and  $s_u(\text{cs})$  by normalizing them with respect to  $p'_c$  in Figure 3.18. According to these figures,  $s_u(\text{yield})/p'_c$ ,  $s_u(\text{cs})/p'_c$ ,  $\phi'_{\text{yield}}$ , and  $\phi'_{\text{cs}}$  decrease with increasing  $\psi_{cs}$ . However, the decreasing trends of these parameters are widely separate for different specimen sizes with the smaller specimens mobilizing larger undrained strength ratios and effective stress friction angles. This occurs because of the large deviator stresses (in Figs. 3.3 and 3.6) as well as the higher  $\psi_{cs}$  of the smaller specimens as a result of their denser (larger  $\Gamma$ ) and steeper (larger  $\lambda$ ) CSL in Fig. 3.16.

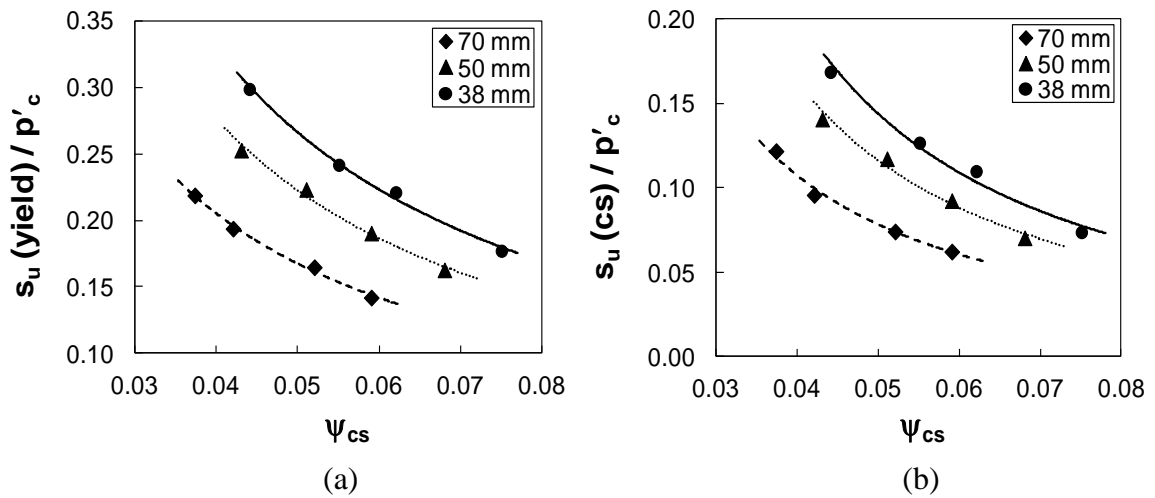


**Figure 3.18:** Effect of specimen size on the changes of: (a)  $s_u(\text{yield})/p'_c$  and (b)  $s_u(\text{critical})/p'_c$  mobilized in undrained triaxial compression tests of loose sand with  $\psi_{cs}$



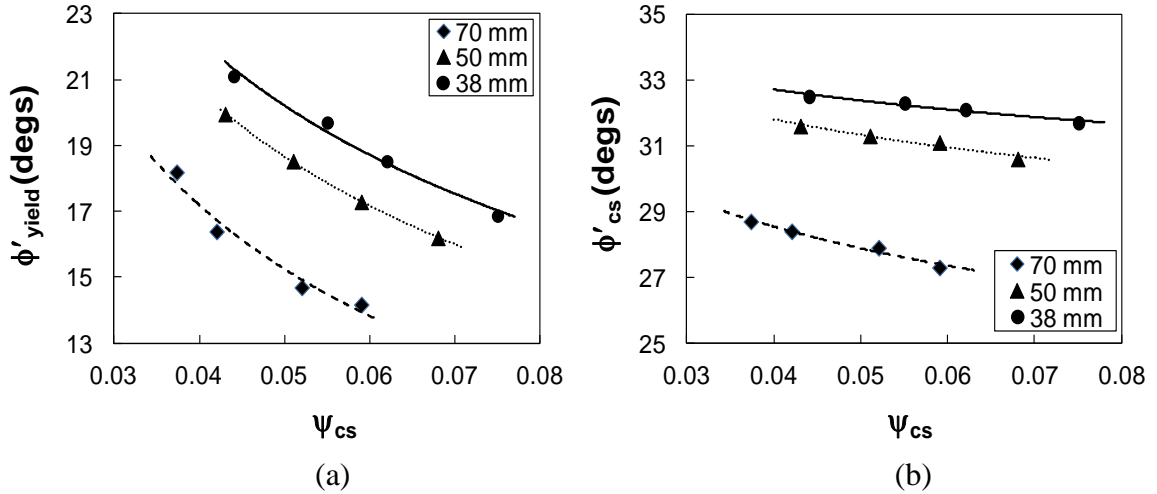


**Figure 3.19:** Effect of specimen size on: (a)  $\phi'_{yield}$  and (b)  $\phi'_{cs}$  mobilized in undrained triaxial compression tests of loose sand with respect  $\psi_{cs}$

The differences in  $s_u$  ratios and friction angles among different specimen sizes are somewhat reduced by incorporating the effect of sand compressibility  $\lambda$  in undrained shear using a critical state-compressibility ratio,  $\psi_{cs}/\lambda$  in Figures 3.20 and 3.21. The decreases of these parameters with increasing  $\psi_{cs}$  are consistent with the findings from other studies (Sadrekarimi and Olson 2011).

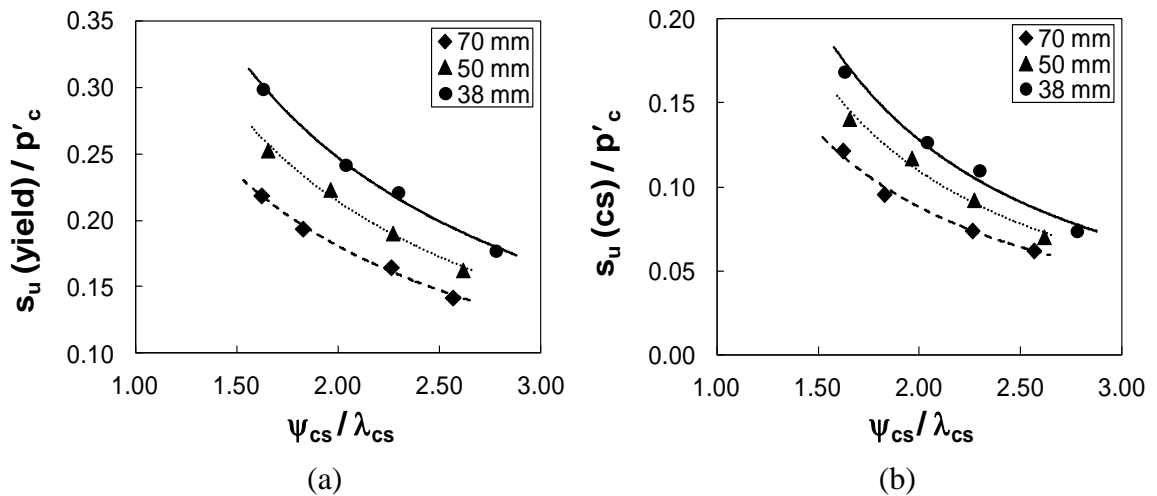


**Figure 3.20:** Effect of specimen size on the changes of: (a)  $s_u(yield)/p'_c$  and (b)  $s_u(cs)/p'_c$  mobilized in undrained triaxial compression tests of loose sand with  $\psi_{cs}/\lambda_{cs}$

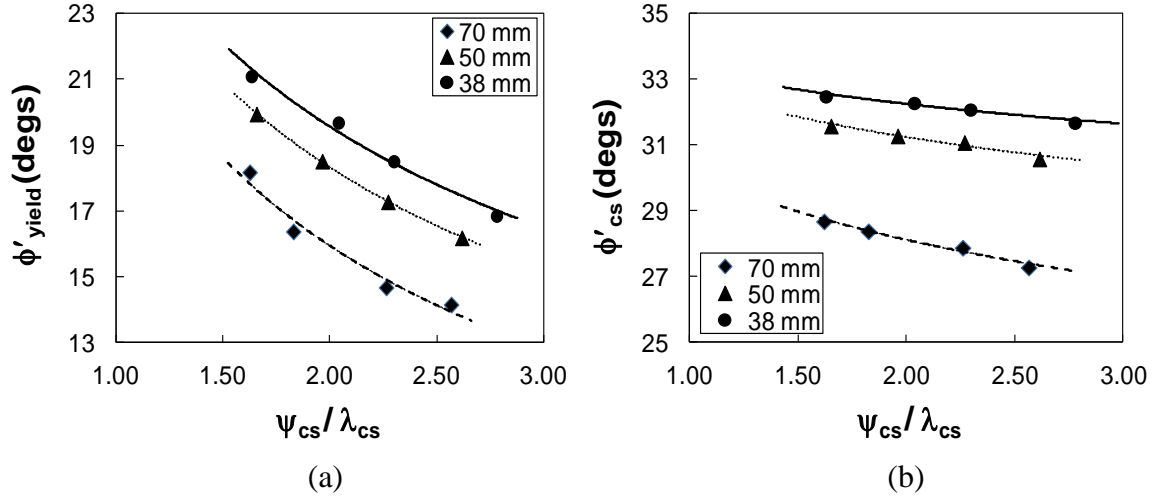


**Figure 3.21:** Effect of specimen size on: (a)  $\phi'_{yield}$  and (b)  $\phi'_{cs}$  mobilized in undrained triaxial compression tests of loose sand with respect to  $\psi_{cs}/\lambda_{cs}$

Finally, the degree of strain-softening and liquefaction flow exhibited for different specimen sizes in triaxial compression tests is compared in Figure 3.22 by the undrained brittleness index ( $I_B$ ) defined below (Bishop 1971):

$$I_B = \frac{s_u(yield) - s_u(critical)}{s_u(yield)} \quad (3.3)$$

According to Figure 3.22a, not only lower undrained strengths are mobilized in the larger specimens, but also the amount of strain-softening and  $I_B$  increase with increasing specimen size. In other words, larger specimens exhibit greater liquefaction potential and hence one may underestimate the liquefaction susceptibility potential of a saturated cohesionless soil by testing small specimen sizes. Although the differences in  $I_B$  values among different specimen sizes are reduced by accounting for the differences in specimens shearing compressibility ( $\psi_{cs}/\lambda$ ) in Figure 3.22b, the remaining difference among  $I_B$  could be essentially due to the larger number of shear bands and failure planes in a larger specimen.

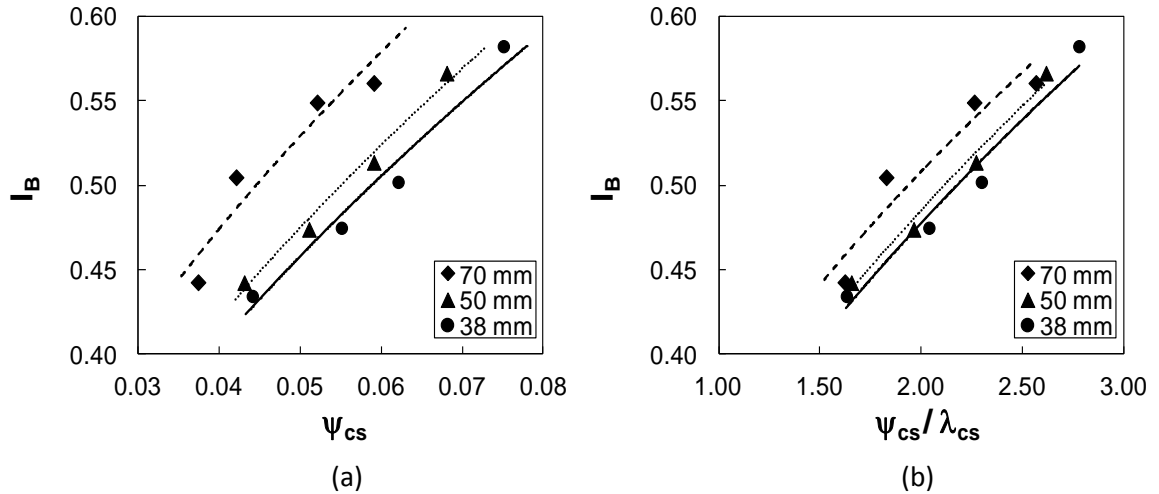


**Figure 3.22:** Effect of specimen size on  $I_B$  in undrained triaxial compression tests of loose sand with respect to: (a)  $\psi_{cs}$ , (b)  $\psi_{cs}/\lambda$

Table 3.6 summarizes the shear strength ratios ( $s_u(\text{yield})/p'_c$  and  $s_u(\text{cs})/p'_c$ ),  $I_B$ , and  $\psi_{cs}$  of the different specimen sizes from the undrained triaxial tests.

**Table 3.6:** Summary of  $\psi_{cs}$ ,  $s_u(\text{yield})/p'_c$ ,  $s_u(\text{cs})/p'_c$ , and  $I_B$  for the undrained triaxial tests

Specimen Size	$p'_c$ (kPa)	$D_{rc}$ (%)	$e_c$	$e_{cs}$	$\psi_{cs}$	$s_u(\text{yield})/p'_c$	$s_u(\text{cs})/p'_c$	$I_B$
70 mm	500	14	0.775	0.716	0.059	0.14	0.06	0.56
	300	12	0.782	0.73	0.052	0.17	0.07	0.55
	200	9	0.791	0.749	0.042	0.19	0.10	0.51
	100	7	0.797	0.760	0.037	0.22	0.12	0.44
50 mm	500	16	0.769	0.701	0.068	0.16	0.07	0.56
	300	14	0.775	0.716	0.059	0.19	0.09	0.51
	200	11	0.785	0.734	0.051	0.22	0.12	0.48
	100	8	0.795	0.752	0.043	0.25	0.14	0.44
38 mm	500	16	0.766	0.691	0.075	0.18	0.07	0.55
	300	14	0.773	0.711	0.062	0.22	0.11	0.50
	200	11	0.784	0.729	0.055	0.24	0.13	0.48
	100	8	0.794	0.75	0.044	0.30	0.17	0.43

### 3.8 Discussion

The micromechanical and particle-scale mechanisms associated with the observed specimen size effects were not investigated in this study and could be required in future work to investigate the role of the larger number of particles and hence, particle contacts mechanism on the observed lower stiffness and smaller volumetric contraction of the larger specimens during isotropic compression (in Fig. 3.2) and drained shear (in Fig. 3.8). While the drained and undrained shear strengths of the larger specimens were reduced as a result of shearing along a larger number of shear bands. Similar results have been documented by other studies on the effect of specimen size in triaxial compression tests (Scott 1987; Been and Jefferies 1991; Hu *et al.* 2010; Chew *et al.* 2011).

Specimen size effect on the shear strength parameters can affect the design and analysis of many geotechnical applications. For example, different instability zones can affect the evaluation of liquefaction triggering resistance of soils as liquefaction and pre-failure instability under undrained condition have often been considered as the triggering factors of loose granular slopes. The predication of sand behavior using critical state constitutive models depends on the critical state parameter and the different critical state parameters obtained from the testing of different specimen sizes can affect the modeling predictions for soil response. In addition, the static slope stability analysis as well as the seismic analysis due to an earthquake shaking can be directly affected by the different shear strength parameters. Lastly, the differences in the measured effective friction angles can affect soil bearing capacity and hence, the design of shallow footings on granular soil as well as the design and stability analysis of retaining wall structures.

Besides the fact that a larger specimen provides a better representation of field soil behavior, the smaller friction angles and undrained shear strengths mobilized in a larger specimen are more critical and should be used with caution for design as discussed above. However, the associated cost and the practical size of triaxial testing devices limit specimen size. Accordingly, several studies have proposed minimum sizes for direct shear or triaxial specimens. For example, the ASTM D3080 standard testing method for direct shear testing of soils requires a minimum specimen thickness of six times the maximum particle diameter ( $D_{\max}$ ) as well as a minimum specimen width of 10 times  $D_{\max}$ . Similarly, ASTM D 4767 and D 7181 standard methods for triaxial undrained and drained compression tests require cylindrical specimens with a minimum diameter of 33 mm and average height to diameter ratio between 2 and 2.5. The largest particle size shall be smaller than 1/6 the specimen diameter. Furthermore, Scarpelli and Wood (1982) and Bareither *et al.* (2008) respectively suggested using shear box lengths of at least 100 and 93 times the mean particle diameter ( $D_{50}$ ) in direct shear testing while other studies suggested shear box widths or diameters no less than 50 (Cerato and Lutenegeger 2006) or 60 (Wang and Gutierrez 2010) times  $D_{\max}$ . The 38, 50, and 70 mm specimen sizes used in the triaxial tests of this study were respectively 173, 227, and 318 times  $D_{50}$  and 57, 74, and 104 times  $D_{\max}$  of the tested sand. While these ratios are larger than the criteria proposed by past studies, it was shown here that the effect of specimen size did not disappear or even reduce with increasing specimen diameter. Although a minimum specimen size or sand particle diameter ( $D_{50}$  or  $D_{\max}$ ) at which specimen size effect disappears was not found in this study, the results indicate that the triaxial compression test results are still sensitive to specimen size at specimen to sand particle diameter ratios of 100 (based on  $D_{\max}$ ) and 320 (based on  $D_{50}$ ). Figure 3.23 shows the average changes of  $s_u$ ,  $\phi'_{\text{yield}}$ , and  $\phi'_{\text{cs}}$  with percentage deviation of a triaxial specimen's

diameter (D) from a 70 mm-diameter specimen (the larger specimen diameter in this study).

The following correlations are curve-fitted to these data:

$$\Delta s_u(\%) = -0.668 \Delta D(\%) \quad (3.4)$$

$$\Delta \phi'_{yield}(\text{deg.}) = -0.0704 \Delta D(\%) \quad (3.5)$$

$$\Delta \phi'_{cs}(\text{deg.}) = -0.0942 \Delta D(\%) \quad (3.6)$$

Therefore, a minimum specimen diameter for triaxial compression tests should be at least  $100 \times D_{\max}$  or  $320 \times D_{50}$  (of the test sand) in order to obtain representative strength parameters. However, the above equations indicate that with every 10% decrease in specimen size (from a typical specimen diameter of 70 mm); the undrained strength could be overestimated by about 6.7%. In addition, the mobilized yield and critical state friction angles could be overestimated by about  $0.71^\circ$  and  $0.94^\circ$ , respectively.

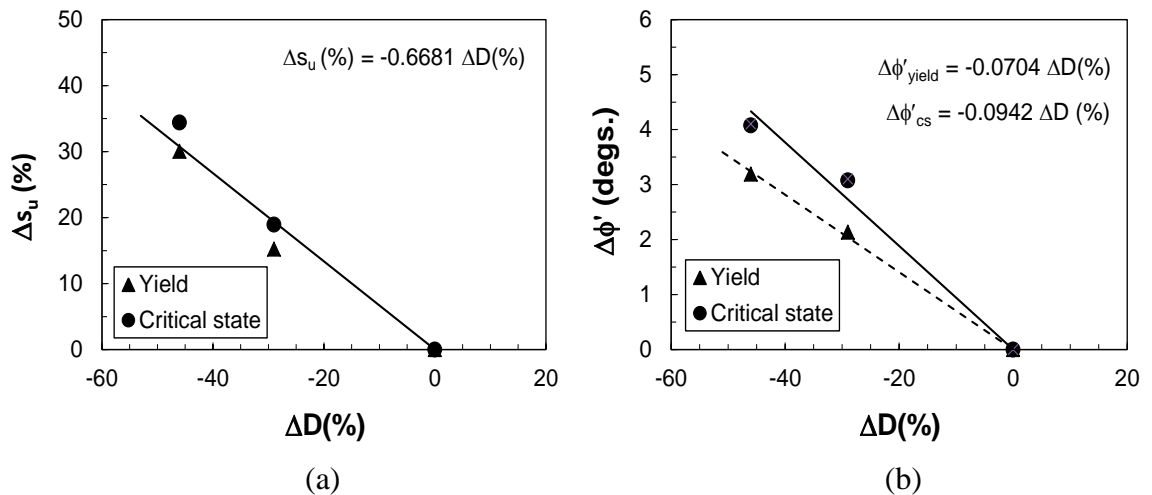


**Figure 3.23:** Changes in (a)  $s_u$ (%) and (b)  $\phi'$ (degrees) with percent changes of specimen diameter (D) from  $s_u$  and  $\phi'$  mobilized in a 70 mm loose specimen

### 3.9 Conclusion

The main objective of this study is to investigate the specimen size effect on loose sand behavior in triaxial compression tests. An experimental program of 24 static drained and undrained triaxial compression tests were conducted on three specimen sizes (38, 50, and 70 mm) of an Ottawa sand to determine whether specimen size effects exist or not. The triaxial test results illustrated the significance of sample size on loose sand shear behavior. The larger specimens showed stiffer isotropic compression behavior and significantly smaller compressibility than the smaller specimens. During shear, the smaller specimens exhibited steeper CSL, indicating a higher compressibility, exhibited higher modulus, and mobilized larger internal friction angles and shear strengths. The geometrical scale as well as the large number of shear bands and failure planes (the shear zone characteristics) in larger specimens could have produced the significant effect of specimen size on the observed behavior.

This influence of sample size on sand behavior, particularly on the internal friction angle is very important as the friction angle is the most vital mechanical property of sands and it directly affects many aspects in geotechnical engineering practice (design of shallow footings on granular soils, slope stability analysis, design of retaining structures). In order to reduce specimen size and scale effects, triaxial testing of larger specimens is recommended as it also provides a better representation of field soil behavior. Based on the results of this study, it is recommended, to use sand samples with a minimum diameter no less than 320 times  $D_{50}$  and/or 100 times the maximum particle size in triaxial shear testing. Two equations are presented to estimate the deviation of undrained shear strengths and mobilized friction angles for samples of different sizes from a typical specimen size of 70 mm.

## References

- Alshibli, K. A., and Sture, S. (2000). "Shear band formation in plane strain experiments of sand" *J. Geotech. & Geoenviron. Eng.*, Vol. 126 (6), pp: 495–503.
- Araei, A., Soroush, A., and Rayhani, M. (2010). "Large scale triaxial testing of rounded and angular rock materials" *Scientia Iranica*, Vol. 17 (3), pp: 169-183.
- Arslan, H., Sture, S., and Batiste, S. (2010). "Engineering properties of Lunar soil stimulant" *J. Aerospace Eng.*, Vol. 23 (1), pp: 70-84.
- ASTM, D2487-06 "Standard practice for classification of soil for engineering purposes (Unified Soil Classification System)" ASTM International, West Conshohocken, PA.
- ASTM, D4253-06 "Standard test methods for maximum index density and unit weight of soils using vibratory table" ASTM International, West Conshohocken, PA.
- ASTM, D4767-11 "Standard test method for consolidated un-drained triaxial compression test for soils" ASTM International, West Conshohocken, PA.
- ASTM, D7181-11 "Standard test method for consolidated drained triaxial compression test for soils" ASTM International, West Conshohocken, PA.
- Baldi, G., and Nova, R. (1984). "Membrane penetration effects in triaxial testing" *J. Geotechnique*. Vol. 110 (3), pp: 403-420.
- Bareither, C. A., Benson, C. H., and Edil, T.B. (2008). "Comparison of shear strength of sand backfills measured in small scale and large scale direct shear tests" *Can. Geotech. J.* Vol. 45, pp: 1224-1236.
- Been, K., and Jefferies, M. G. (1985). "A state parameter for sands" *J. Geotechnique*. Vol. 35. pp: 99-112.
- Been, K., Jefferies, M. G., and Hachey, J. E. (1991). "The critical state of sands" *J. Geotechnique*. Vol. 41(3), pp: 365–381.
- Bishop, A.W. (1971). "Shear strength parameters for undisturbed and remoulded soil specimens in stress-strain behaviour of soils" *Proceedings of the Roscoe Memorial Symposium, University of Cambridge, UK.* pp: 3–58.
- Bishop, A. W., and Green, G. E. (1965). "The influence of end restraint on the compression strength of a cohesionless soil" *J. Geotechnique*. Vol. 15 (3), pp: 243- 266.
- Bishop, A. W., and Henkel, D. J. (1962). "The measurement of soil properties in the triaxial test" *St. Martin's Press, Inc., New York*, 225 pp.
- Castro, G. (1969). "Liquefaction of sands" Ph.D. Thesis, Harvard University, Cambridge.
- Cerato, A.B., and Lutenecker, A.J. (2006). "Specimen size and scale effects of direct shear box tests of sands" *J. Geotech. Testing*. Vol. 29 (6), pp: 1-10.
- Chew, S. H., and Bharati, S. K. (2011). "Effect of large diameter sample testing for offshore site investigation" *Pan-Am. CGS. Geotechnical Conference*. pp: 1-6.
- Chu, J., Lo, S. C. R., and Lee, I. K. (1992). "Strain softening behavior of granular soil in strain-path testing". *J. Geotech. Eng.*, Vol. 118 (2), pp: 191-209.



- Chu, J., Lo, S. C. R., and Lee, I. K. (1996). "Strain softening and shear band formation of sand in multi-axial testing" *J. Geotechnique*. Vol. 46 (1), pp: 63-82.
- Dangus, J., Desrues, J., and Foray, P. (1988). "Triaxial testing of granular soil under elevated cell pressure" *ASTM STP 977*, pp: 290-310.
- Desrues, J., and Chambon, R. (2002). "Shear band analysis and shear moduli calibration", *International Journal of Solids and Structures*, 39: 3757 – 3776.
- Desrues, J., Chambon, R., Mokni, M., and Mazerolle, F. (1996). "Void ratio evolution inside shear bands in triaxial sand specimens studied by computed tomography" *J. Geotechnique*. Vol. 46 (3), pp: 529–546.
- Farbodfar, H. (2013). "Studying sand size and scale effects on its shear behavior" M.Eng. project. University of Western Ontario.
- Fear, C., and Robertson, P. (1995). "Estimating the undrained strength of sand: a theoretical framework" *Can. Geotech. J.* Vol. 32, pp: 859-870.
- Finno, R. J., Harris, W. W., Mooney, M. A., and Viggiani, G. (1996). "Strain localization and undrained steady state of sand" *J. Geotech. Eng.*, Vol. 122 (6), pp: 462–473.
- Frossard, E., Hu, W., Dano, C., and Hicher, P. Y. (2011). "Rockfill shear strength evaluation: a rational method based on size effects" *J. Geotechnique*. 14, pp: 1-13.
- Frost, J. D. and Jang, D. J. (2000). "Evolution of sand microstructure during shearing" *J. Geotech. & Geoenviron. Eng.*, Vol. 126 (2), pp: 116-130.
- Frost, J. D., and Park, J. Y. (2003). "A critical assessment of the moist tamping technique" *J. Geotech. Testing*. Vol. 26, pp: 1-14.
- Garga, V. (1988). "Effect of sample size on shear strength of basaltic residual soils" *Can. Geotech. J.* Vol. 25, pp: 478-487.
- Garga, V., and Zhang, H. (1997). "Volume changes in undrained triaxial tests on sands" *Can. Geotech. J.* Vol. 34, pp: 762-773.
- Hazarika, H., Igarashi, N., and Yamada, Y. (2011). "Behavior of granular and compressible geomaterial under cyclic loading" 5<sup>th</sup> Conference of Earthquake Geotech. Eng. Santiago, Chile. pp: 1-12.
- Hettler, A and Vardoulakis, I. (1984). "Behaviour of dry sand tested in a large triaxial apparatus" *J. Geotechnique* Vol. 34 (2), pp: 183-198.
- Hight, D. W. and Leroueil, S. (2003) "Characterisation of soils for engineering purposes" *Proc. of the characteris. & Eng. Properties of Natural Soils*, Vol. 1, pp: 255–360.
- Hu, W., Dano, C., Hicher, P., Touzo, J., and Derkx, F. (2010). "Effect of Sample Size on the Behavior of Granular Materials" *J. of Geotech. Testing*, Vol. 34 (3), pp: 1-12.
- Islam, M., Siddika, A., Hossain, B., Rahman, A., and Asad, M. (2011). "Effect of particle size on the shear strength behavior of sands" *Proc. of the Conference of Eng. Research. Sylhet, Bangladesh*. pp: 1-11.
- Jang, D. J., and Frost, J. D. (2000). "Use of image analysis to study the microstructure of a failed sand specimen" *Can. Geotech. J.* Vol. 37, pp: 1141–1149.

- Jefferies, M. and Been, K. (2006). "Soil liquefaction: a critical state approach" Taylor & Francis, New York, London, 479 pp.
- Jefferies, M. G., Been, K., and Hachey, J. E. (1990). "Influence of scale on the constitutive behavior of sand" *Cand. Geotech. Confererence*. pp: 263-273
- Konrad, J. M. (1990). "Minimum undrained strength of two sands" *J. Geotech. Eng.*, Vol. 116 (6), pp: 932–947.
- Ladd, C. C. (1978). "Preparing test specimen using undercompaction" *J. Geotech. Testing*. Vol.1, pp: 16-23.
- Lade, P. V., and Wang, Q. (2011). "Effect of boundary conditions on shear banding in true triaxial tests on sand," *J. Geotech. Eng.* Vol. 42 (4), pp: 19 – 25.
- Lee, K. L. (1978). "End restraint effects on undrained static triaxial strength of sand". *J. Geotech. Eng.*, Vol.104 (6), pp: 687–704.
- Lee, K. L., Seed, H. B. (1967). "Drained strength characteristics of sands" *J. Soil Mech. and Found.*, Vol. 93 (SM6), pp: 117- 141.
- Liang, L., Saada, A. S., Figueroa, J. L., and Cope, C. T. (1997). "The use of digital image processing in monitoring shear band development", *Geotechnical Testing Journal*, ASTM, 20(3): 324 – 339.
- Liang, Z. Z., Tang, C. A., and Wang, S. Y. (2009). "Numerical simulation of scale effect of jointed rock masses" *Society for Rock Mechanics (Singapore)*, pp: 521 – 530.
- Marachi, N. D., Chan, C. K., Seed, H. B., and Duncan, J. M. (1969). "Strength and deformation characteristics of rockfill materials". Report No. TE-69 (5), Dept. of Civil Engineering, Univ. Of California, Berkeley, Berkeley, CA.
- Marsal, R. J. (1967). "Large-scale testing of rockfill materials" *J. Soil Mech. and Found. Div.* Vol. 93 (SM2), pp: 27–44.
- Moayed, R. Z., and Alizadeh, A. (2011). "Effects of shear box size on the strength for different type of silty sands in direct shear tests" *Unsaturated Soils: Theory and Practice*, Kasetsart University, Thailand, pp: 265 – 271.
- Nakao, T., and Fityus, S. (2008). "Direct shear testing of a marginal material using a large shear box" *J. Geotech. Testing*, Vol. 31 (5), pp: 1-11.
- Oie, M., Sato, N., Okuyama, Y., Yoshida, T., Yoshida, T., Yamada, S., and Tatsuoka, F. (2003). "Shear banding characteristics in plane strain compression of granular materials" *J. Soil Mech. and Found. Eng.*, Vol. 4, pp: 597-606.
- Okuyama, Y., Yoshida, T., Tatsuoka, F., Koseki, J., Uchimura, T., Sato, N., and Oie, M. (2003). "Shear banding characteristics of granular materials and particle size effects on the seismic stability of earth structure" *J. Soil Mech. and Found.* 4, pp: 607-707.
- Palmeira, E. M. and Milligan, G. W. E. (1989). "Scale effects in direct shear tests on sand" *J. Soil Mech. and Found. Eng.*, Vol. 1 (1). pp: 739–742.
- Parsons, J. D. (1936). "Progress Report on an investigation of the shearing resistance of cohesionless soils" *Int. Conf. Soil Mech. Found. Eng.*, Vol. 2, pp: 133-138.

- Po-Kai, W., Matsushima, k., and Tatsuoka, F. (2007). "Effects of specimen size and some other factors on the strength and deformation of granular soil in direct shear tests" *J. of Geotech. Testing*, Vol. 31 (1), pp: 167-183.
- Rowe, P.W., and Barden, L. (1964). "Importance of free ends in triaxial testing" *J. soil mech. and found.*, Vol. 90 (1), pp: 1–27.
- Sadrekarimi, A., and Olson, S.M. (2010). "Shear band formation observed in ring shear tests on sandy soils". *J. of Geotech. & Geoenviron. Eng.*, Vol. 136 (2), pp: 366–375.
- Sadrekarimi, A., and Olson, S.M. (2011). "Yield strength ratios, critical strength ratios, and brittleness of sandy soils from laboratory tests" *Can. Geotech. J.* 48, pp: 493–510.
- Sadrekarimi, A., and Olson, S.M. (2011). "Critical state friction angle of sands" *J. Geotechnique*, Vol. 61 (9), pp: 771–783.
- Scarpelli, G. and Wood, D. M., (1982). "Experimental observations of shear band patterns in direct shear tests." *Con. on Deformation and Failure of Granular M.*, pp: 22-35.
- Scott, R. F. (1969). "Mechanical properties of lunar surface materials" *J. of Geophys. Res.*, 73 Vol. 3, pp: 177-191.
- Scott, R. F. (1987). "Failure" *J. Geotechnique*. Vol. 37 (4), pp: 423-466.
- Seif el Dine, B., Dupla, J., and Frank, R. (2009). " Mechanical characterization of matrix coarse soil with large triaxial size" *Can. Geotech. J.* 47, pp: 425–438.
- Shen, H., (2001). "Sample size effects on constitutive relations of granular materials, a numerical simulation study with 2-D flow of disks" *J. Eng. Mech.* pp: 978-986.
- Sladen, J. A and Oswell, J .M (1989). "The behaviour of very loose sand in the triaxial compression test" *Can. Geotech. J.* Vol. 26, pp: 103-113.
- Tatsuoka, F. (1997) "Deformation and strength characteristics of granular materials" Research center, Tokyo University of Science. pp: 1-100.
- Wang, J., and Gutierrez, M. (2010). "Discrete element simulations of direct shear specimen scale effects" *J. Geotechnique*, 60 (5): 395 – 409.
- Wong, C. K. (1999). "Mobilized strength components of Athabasca oil sand in triaxial compression" *Can. Geotech. J.* Vol. 36, pp: 718–735.
- Wood, D. M. (1990). "Soil Behaviour and Critical State Soil Mechanics" Cambridge University Press, Cambridge.
- Wu P, Matsushima K. and Tatsuoka F. (2007). "Effects of specimen size and some other factors on the shear strength and deformation of granular soils in direct shear tests" *J. of Geotech. Eng.*, Vol. 31(1), pp: 45-64.
- Yamamuro, J.A., and Lade, P.V. (1997). "Static liquefaction of very loose sands" *Can. Geotech. J.*, Vol.34, pp: 905–917.
- Yoshida, T. and Tatsuoka, F. (1997). "Deformation property of shear band in sand subjected to plane strain compression and its relation to particle characteristics" *Conference on Soil Mech. and Found. Eng.*, Hamburg. Vol. 14 (1), pp: 237 – 240.
- Zhang, H. and Garga, V. K. (1997). "Quasi-steady state: a real behaviour" *Can. Geotech. J.* Vol. 34 pp: 749–761.

## Chapter 4

### 4 Influence of Triaxial Specimen Size in Engineering Practice

#### 4.1 Introduction

Granular soils are widely employed as backfill material for earth embankment dams, trenches, highway embankments, and earth-retaining structures, as they provide high shear strength, and suitable compaction and drainage properties. For these soils, the friction angle plays a prominent role in their strength and stability behaviors. Accurate assessment of shear strength parameters for these soils is required for analysis and design of soil structures (e.g. earth dams, retaining walls, foundations, slopes) involving these soil types. However, the size of the specimen used to determine soil parameters can have a significant impact on the parameters selected for analysis or design, making it difficult to extrapolate laboratory test results to real field situations. Most practicing engineers are unaware of the significant effect of specimen size. Therefore, this phenomenon is either totally neglected in using laboratory test results on a small specimen in engineering design and analysis, or laboratory test results are simply distrusted and the design or analysis is based on empirical interpretations of in-situ tests (e.g. SPT or CPT) which could also involve a wide range of uncertainties.

Several investigators have studied the scale effect in practical engineering problems (DeBeer 1963 and 1965, Meyerhof 1982, Eid 1987, Tatsuoka *et al.* 1991, Sakai 1997, Lehane *et al.* 2005, Bareither *et al.* 2011). For example, DeBeer (1963) studied the influence of the width and the depth of a wedge (representing a strip footing) on the ultimate bearing capacity of an incompressible material. He calculated the ultimate bearing capacity of a dense Mol sand under the penetration of a wedge with different widths (varying from 0.5cm to 100cm) and

at different depths (varying from 0 to 20m). The results of the performed calculations indicated that the ultimate bearing capacity at a given depth was very sensitive to the width of the foundation and increased with decreasing the foundation width. Furthermore, DeBeer (1965) compiled, from the literature, the results of model-scale square and circular footing tests and derived an empirical equation that indicated the decreasing of the bearing capacity factor,  $N_\gamma$ , with increasing the foundation width. Similarly, many other studies have also documented the effect of the footing size on  $N_\gamma$  (Shiraishi 1990, Zhu *et al.* 2001, Ueno *et al.* 2001, Okamura *et al.* 2002, Cerato and Lutenecker 2007.etc). Meyerhof (1982) compared the ultimate bearing capacity of piles, and proposed an empirical reduction factor for the ultimate resistance of larger pile diameters. Eid (1987) developed a large scale calibration chamber and conducted an extensive experimental program of cone penetration tests to study the effect of cone diameter on the measured tip and sleeve frictional resistances in Monterey sand samples. He found that cone tip resistance was lower for larger cones in both loose and dense samples. Using centrifuge model tests, Lehane *et al.* (2005) examined the effect of pile diameter on the unit shaft friction developed in sand and observed that the effective lateral stresses significantly reduced with increasing pile diameter. Bareither *et al.* (2011) investigated the immediate compression behavior of municipal solid wastes in laboratory compression cells of different diameters and observed a higher compressibility for the larger specimens. They also compared the measured laboratory results with those from field-scale experiments and found that the immediate compression index was identified in a shorter time in the laboratory compression tests compared to that from the field-scale experiments.

In this study, the observed increase of sand shear strength and friction angle with decreasing specimen size in triaxial compression tests on three different specimen sizes are used to

explain some of the aforementioned scale effects, investigate specimen size effects in engineering analysis of slope stability and liquefaction, the design of foundations and retaining walls, as well as the calibration of soil constitutive models. Each analysis is carried out with reference to real engineering cases when possible or examples of actual field structures.

## 4.2 Experimental Data

Static triaxial compression tests were performed on loose sand specimens with different specimen sizes using an automated stress path triaxial compression testing system. These experiments were conducted on a uniformly-graded clean quartz sand from Ottawa, Illinois. This sand is composed of round to sub-round particles with a specific gravity of 2.65 and maximum and minimum void ratios of 0.821 and 0.487, respectively measured using the ASTM standards D854 and D4243, respectively. The sand is classified as Fine Sand, SP as per the ASTM D2487 standard procedure (the unified soil classification system) with mean grain size ( $D_{50}$ ) of 0.22 mm. Three different specimen diameters of 38, 50, and 70 mm were prepared with a slenderness ratio ( $h/d$ ) of 1 to minimize strain localization and non-uniform deformations at large strains. In order to produce very loose specimens which would exhibit entirely contractive or strain-softening behaviors in both drained and undrained shear tests, all the specimens were prepared by moist tamping. In order to minimize the density variations and void ratio non-uniformities within the specimens, the under compaction technique introduced by Ladd (1978) was used for specimen preparation. Furthermore, the specimen end platens were adequately enlarged and lubricated in order to accommodate the radial expansion of the specimen at large shear strains and thus minimize the effect of

specimen boundaries and end restraints on the specimens' stress-strain behaviors. It was found that the initial modulus and the mobilized shear strength decreased with increasing specimen size, while volumetric compressibility during isotropic compression and drained shear increased with reducing specimen diameter. These results are used to investigate the application of triaxial test results from different specimen sizes on engineering analysis and design of soil structures and explain some of the scale effects observed in past studies.

### 4.3 Sample Size Effect on Liquefaction Triggering Analysis

Figure 4.1 illustrates the instability (IL) lines from the undrained triaxial compression tests of this study on the three different sizes of loose Ottawa sand specimens. The IL, which is developed by connecting the peak strengths of the undrained stress paths for a certain void ratio, separates the potentially unstable stress states from the stable stress states (Lade 1992) and constitutes the triggering stress condition for soil liquefaction. A soil specimen would fail with a rapid reduction of its undrained strength when the undrained stress path crosses the IL (i.e. "liquefaction"). This phenomenon is often characterized by a sudden collapse under undrained conditions accompanied by a rapid increase in pore pressure. An undrained critical shear strength,  $s_u(\text{critical})$  and the critical state line (CSL) is subsequently reached at large shear strains.

According to Figure 4.1, IL becomes steeper with decreasing specimen size which will have significant implications for liquefaction triggering and stability analysis. Liquefaction of loose, saturated granular soil triggered by either monotonic, cyclic, or shock loading is a major cause of destruction and damage of constructed facilities. As liquefaction is triggered when the effective stress path crosses the IL, the liquefaction triggering resistance increases

with decreasing specimen size. Therefore, as the larger specimen (70 mm) is a closer replicate of a field soil sample, the in-situ liquefaction potential would be underestimated as a larger amount of excess pore water pressure is required for liquefaction with the triaxial test results of the smaller 38 mm specimens.

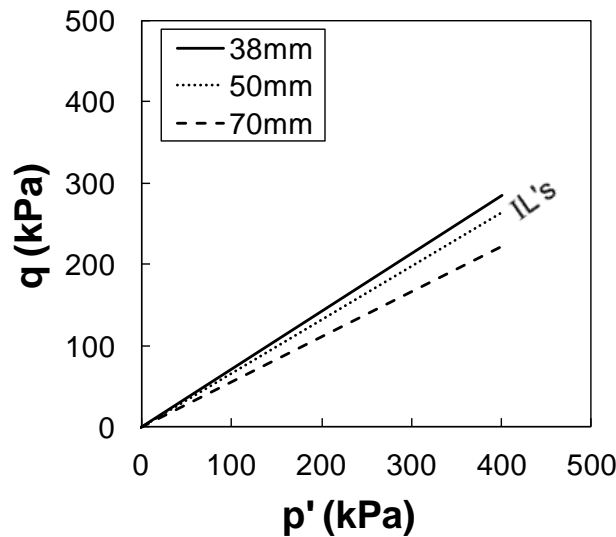


**Figure 4.1:** IL of different specimen sizes from undrained triaxial compression tests

#### 4.4 Sample Size Effect on the Calibration of a Soil Constitutive Model

Modeling of soil constitutive behavior as an elastic-plastic material has been the main area of development by many researchers (Lade 1972, Lade and Duncan 1975, Nova and Wood 1979, Baladi *et al.* 1980, Lade 1980, Frantziskonis and Somasundaram 1986, Jefferies 1993, Jefferies and Shuttle 2002). The main components of an elastic-plastic model are the elastic properties of soil, a yield surface, a flow rule, and a hardening law. Currently, most constitutive models for sands are based on the critical state theory, for example the MIT-S1 (Pestana and Whittle 1999), SANISand (Manzari and Dafalias 1997), UBCSand (Byrne *et*



*al.* 1995), and the NorSand models (Jefferies 1993). In these models the CSL is used in describing soil behaviour at large strains. An important advantage of critical-state constitutive models is their ability to predict soil behavior over a wide range of void ratios and confining pressures using a single set of parameters.

NorSand (Jefferies 1993) is an isotropically hardening - isotropically softening generalized critical state model that captures particulate soil behavior over a wide range of void ratios. NorSand provides a simple computational platform to capture the salient aspects of liquefaction in all its forms. This model uses the critical state parameter to capture soil behavior, and in fact the Cam Clay model is a special case of NorSand. The primary advantages of NorSand over some other critical soil models is that it uses fewer material properties which are easily measured in conventional triaxial laboratory tests, and it has been validated for a wide range of sands and stress paths, including plane strain. It is therefore a general and validated soil model suitable for parametric studies of sand behavior as well as for practical engineering. Since cohesionless soils can exhibit virtually unlimited normal compression lines at different initial void ratios (Ishihara et al. 1975; Been et al. 1991; Pestana and Whittle 1995; Jefferies and Been 2006), the hardening of the yield surface cannot be necessarily tied to its initial void ratio. Accordingly, these two parameters are realistically decoupled in the formulation of NorSand.

NorSand models the behavior of cohesionless soil over a range of accessible void ratios using seven model parameters including three parameters to model soil plasticity using the CSL ( $\Gamma$ ,  $\lambda$ , and  $M$ ), two parameters for modeling the hardening of the yield surface ( $H$ ,  $N$ ,  $\chi$ ), and two parameters which model soil elastic behavior within the yield surface. The effect of specimen size on the predictions of critical state-based constitutive models is investigated

here by calibrating the parameters of the NorSand model based on the experimental results of this study for the three specimen sizes of 38, 50, and 70 mm. The procedure used to establish these parameters is described below. The CSL parameters are defined from the slope and position of this line in the void ratio –  $p'$  space ( $\Gamma, \lambda$ ) and the stress-path diagram (M) as shown in Figure 4.2.

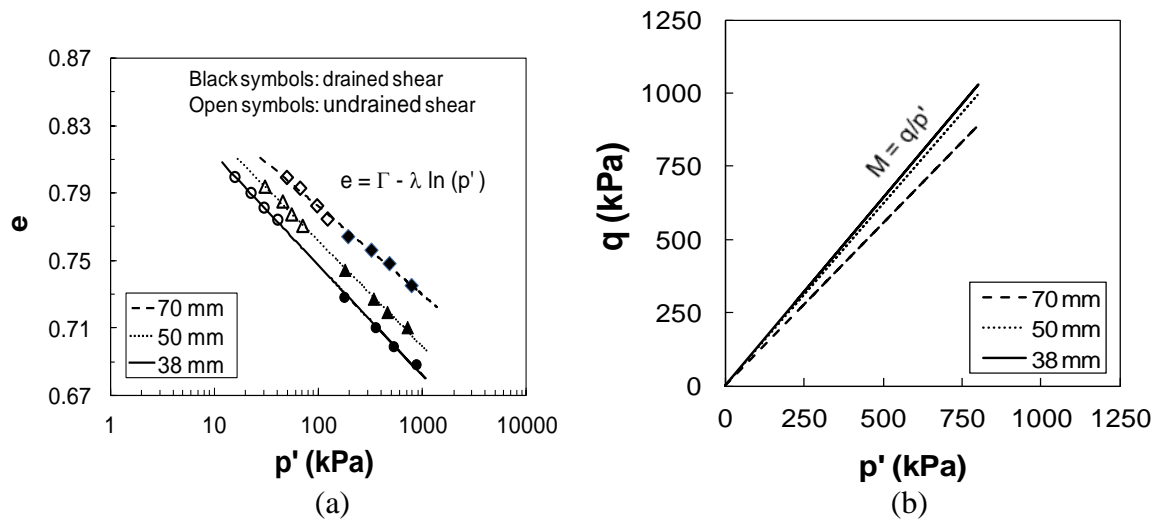


**Figure 4.2:** Critical state lines for different specimen sizes in (a) void ratio –  $p'$  diagram, and (b) stress path plot

As a result of the decoupling of the size of the yield surface from void ratio, a plastic hardening parameter ( $H$ ), essentially independent of soil void ratio, is used to control the size of the yield surface. The plastic hardening parameter,  $H$  is determined iteratively by a trial and error procedure to match the stress-strain and stress paths from triaxial tests. The calibrated values of  $H$  for each specimen size are plotted against  $\psi$  as shown in Figure 4.3. The corresponding trend line for each specimen size is presented in the form of  $H = a - b\psi$ . It can be observed that at the same state parameter, the smaller specimen exhibits higher plastic hardening modulus than the larger specimen.

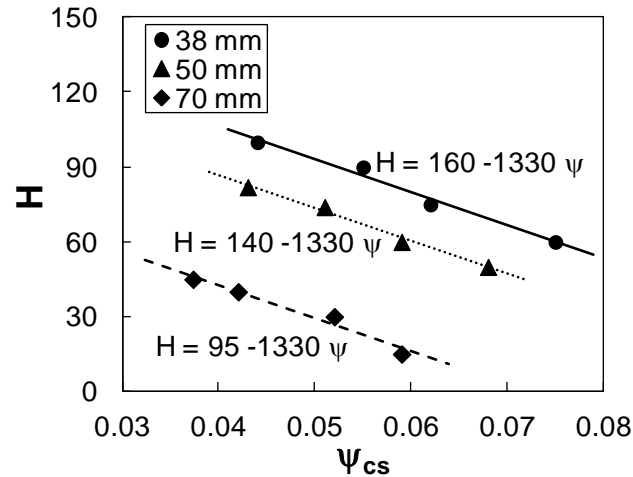


**Figure 4.3:** Plastic hardening modulus as a function of  $\psi$  for each specimen size

Among the parameters which describe the yield surface,  $\chi_{tc}$  is a model property that describes maximum soil dilatancy ( $D_{max}$ ) as a function of the critical state parameter ( $\psi$ ). The dilatancy parameter  $\chi_{tc}$  is more significant in dense samples and takes greater values with increasing soil density (Jefferies and Shuttle 2002). The dilatancy at peak deviator stress ( $D_{max}$ ) was obtained directly from the volumetric strain data of drained shear tests. The slope of the  $D_{max} - \psi$  trendline in Figure 4.4 defines the dilatancy parameter for each specimen size where  $D_{max} = -\chi_{tc} \psi$ .

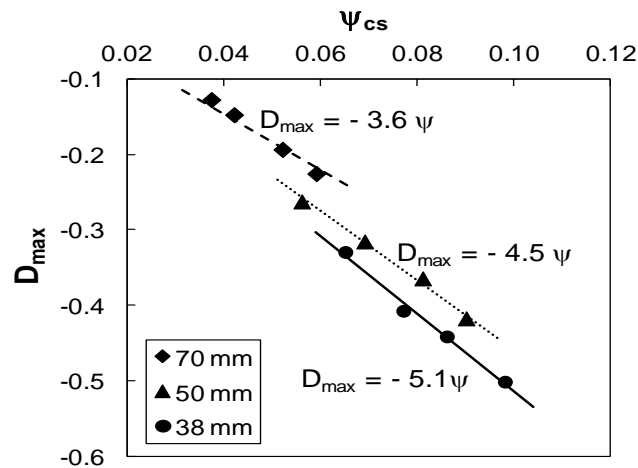


**Figure 4.4:** Dilatancy as a function of  $\psi$  for each specimen size

It can be observed from Fig. 4.4 that the dilatancy parameter  $\chi_{tc}$  increases with decreasing specimen size. This can be attributed to the smaller compressibility of the larger specimens during drained shearing.

Finally, elasticity is modeled using a shear rigidity number ( $I_r = G_{\max}/p' = 100 - 600$ ) and a constant Poisson's ratio,  $\nu$  (0.1 – 0.3). A Poisson ratio  $\nu$  of 0.34 was determined from the axial deformation and volume change of the specimen during isotropic consolidation. Although  $\nu$  does not vary greatly from one soil to another and is often constant for a particular soil,  $I_r$  is ideally determined from shear wave velocity measurements using bender elements located on a triaxial specimen, or from unload-reload cycles with local strain measurements. Since none of these measurements were made in the experimental program here,  $I_r$  was determined similar to the calibration process used for defining the plastic hardening modulus. As plastic shear strains govern soil behavior beyond the initial loading,  $I_r$  has a relatively minor effect on the post-peak soil behavior. The model parameters for each specimen size are summarized in Table 4.1.

**Table 4.1:** Summary of NorSand calibration parameters

Specimen Size	M	$\Gamma$	$\lambda$	$I_r$	H	$\chi_{tc}$
70 mm	1.12	0.887	0.023	20	95 - 1330 $\psi$	3.6
50 mm	1.25	0.881	0.026	20	140 - 1330 $\psi$	4.5
38 mm	1.29	0.878	0.028	20	160 - 1330 $\psi$	5.1

Using the parameters of Table 4.1, NorSand can describe soil shearing behavior moving to the critical state with shear strain in accordance with the fundamentals of the critical state soil mechanics. NorSand captures the post-peak shear localization of cohesionless soils by

imposing a maximum upper limit on the plastic hardening behavior of the soil. Strain-softening ensues when this limit is reached and the soil within the shear accelerates to critical conditions. NorSand predictions are obtained by implementing the model in a MicroSoft Excel spreadsheet and using the macro programming capability of VBA for the numerical solution of the associated differential equations of NorSand. Figures 4.5 to 4.7 compare the stress-strain and stress path plots of NorSand with those from the triaxial compression tests on each specimen size for  $p'_c = 500$  kPa.

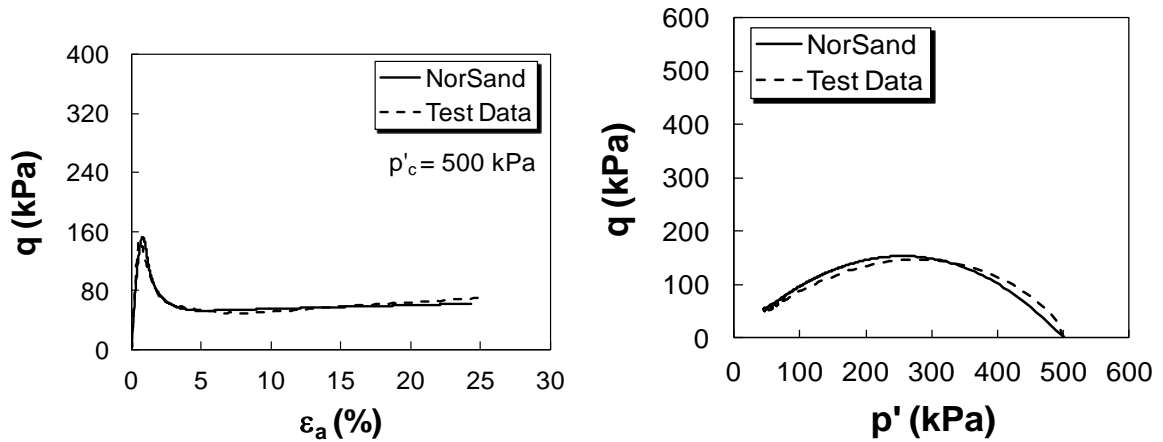


**Figure 4.5:** Comparison of Ottawa sand behavior in triaxial shear tests on 70 mm specimens with NorSand predictions

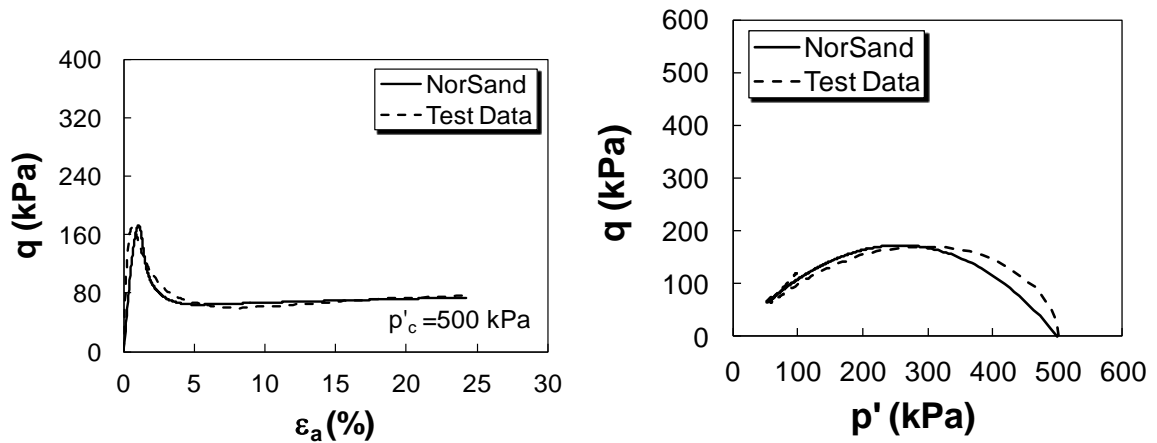


**Figure 4.6:** Comparison of Ottawa sand behavior in triaxial shear tests on 50 mm specimens with NorSand predictions

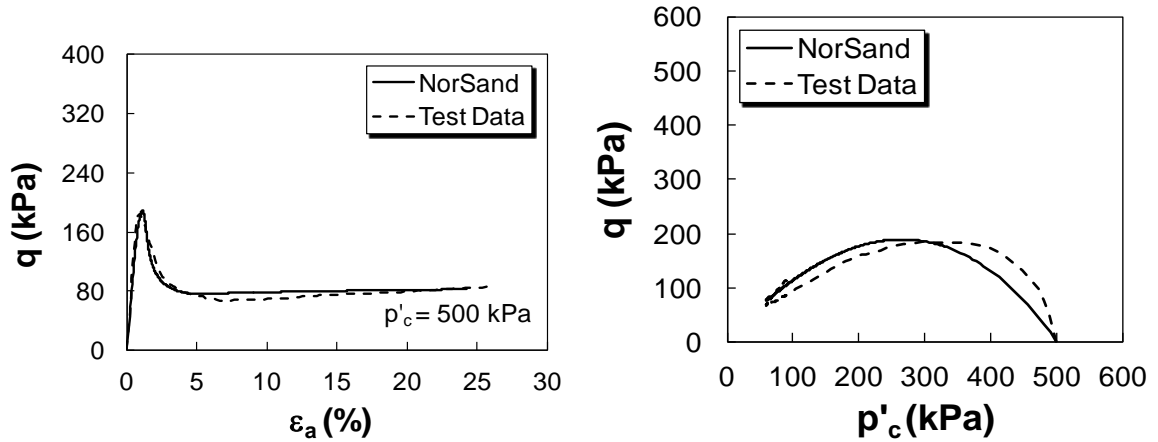


**Figure 4.7:** Comparison of Ottawa sand behavior in triaxial shear tests on 38 mm specimens with NorSand predictions

Overall, NorSand replicates the experimental data on very well and therefore the calibrated model could be employed to captures the influence of void ratio and confining stress on the behaviour of Ottawa sand.

To investigate the effect of specimen size on the predictions of a soil constitutive model (e.g. NorSand), the parameters of Table 4.1 are used in NorSand to estimate the stress-strain behaviours of Ottawa sand at  $e_c = 0.77$  and  $p'_c = 400$  kPa in Figure 4.8. The plots demonstrate that model calibration from different specimen sizes could significantly affect modeling predictions (e.g. the peak and critical state strengths) for a certain soil at the same void ratio and  $p'_c$ . Accordingly, large errors could arise in the application of constitutive models calibrated based on small specimens (e.g. 38 mm in this study) for predicting the behavior of in-situ soils, modeling larger soil masses and field applications.

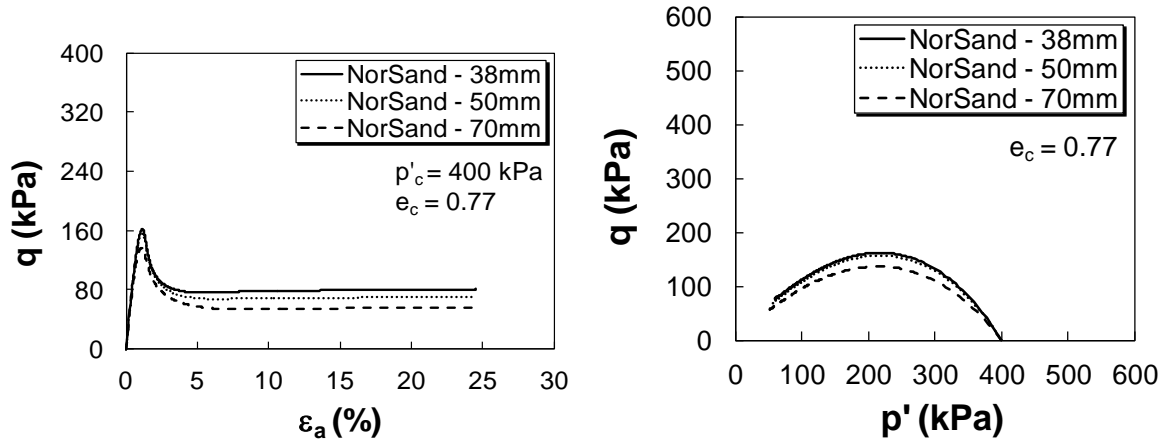


**Figure 4.8:** Effect of specimen size on modeling sand behavior with NorSand

NorSand is further used to compare the undrained peak (or yield),  $s_u(\text{yield})$  and critical,  $s_u(\text{critical})$  strengths for different specimen sizes in Figure 4.9. Similar to Figure 4.8, Figure 4.9 also indicates that both of these strength parameters are significantly overestimated using the calibration parameters of the smaller specimen (38 mm). Such overestimations could lead to a false assessment of the safety of a soil structure (slope, foundation, retaining wall) or unsafe designs using numerical analysis with advanced soil constitutive models.

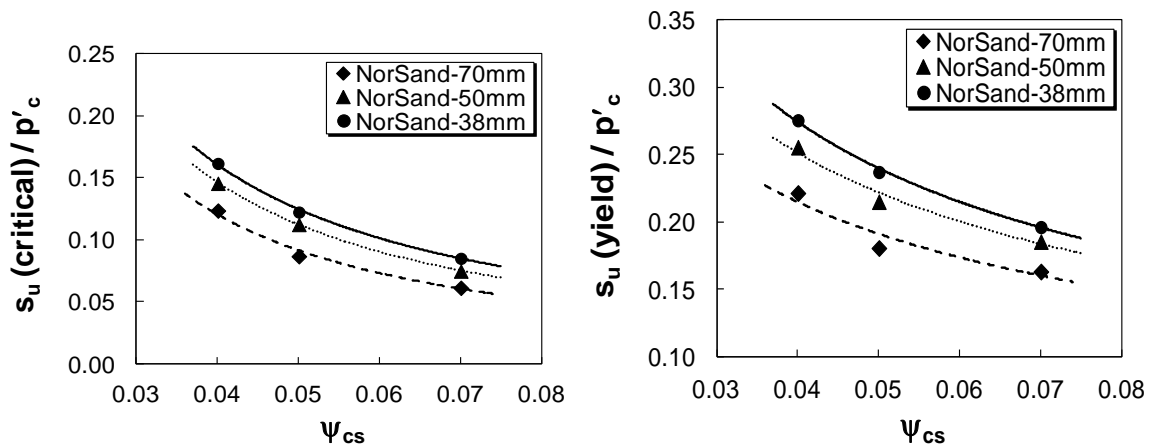


**Figure 4.9:** Effect of specimen size on  $s_u(\text{critical})/p'_c$  and  $s_u(\text{yield})/p'_c$  estimations by the NorSand soil model

## 4.5 Sample Size Effect on Consolidation Settlement

Granular soils are relatively pervious materials that have high in-situ permeability and their compressibility characteristics are much less than those of cohesive soils. Accordingly, their consolidation is always assumed negligible compared to those of more compressible cohesive soils. However, the immediate compression of sands could be important in the design and analysis of critical structures (nuclear power plants, advanced laboratories) to minimize settlements. Figure 4.10 shows that the Ottawa sand would exhibit a much stiffer compression behavior in large specimens (70 mm). Since no particle crushing was found in any of our triaxial tests, we expect that this difference in compressibility resulted from the larger number of particles and particle contacts in the larger specimen. Accordingly, the specimen size from which soil compressibility is obtained, could affect settlement calculations as with smaller specimens, the immediate settlement could be overestimated.

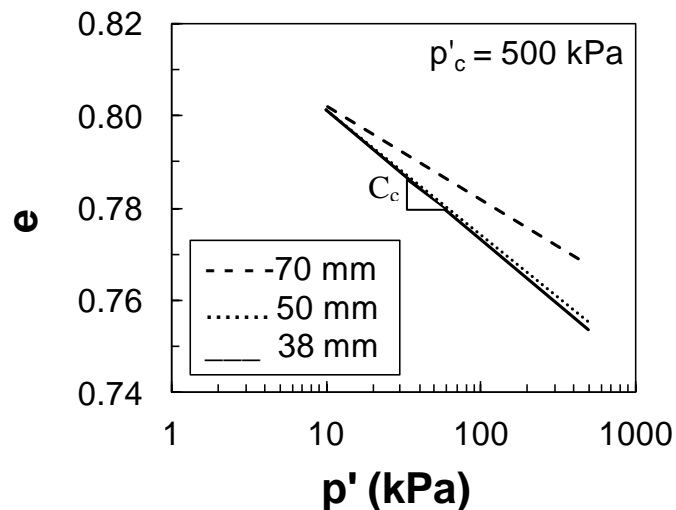


**Figure 4.10:** Isotropic compressibility of different specimen sizes



## 4.6 Sample Size Effect on Slope Stability Analysis

In spite of improvements in recognition, prediction, mitigation, and warning systems, economic losses and casualties due to landslides continue to grow as a result of increasing development of landslide-prone areas due to population pressures (Seed 1979). Intense rainfall, rapid snowmelt, and water-level change are the most common causes of slope failures in addition to the failures occurring due to earthquakes, abnormal precipitations, hurricanes, etc. Landslides triggered by earthquakes often caused more damages, destructions, and casualties than the earthquakes themselves (Duncan 2005). Therefore, landslides represent a significant element of many major disasters and inadequate design and errors or uncertainties involved in the estimation of external factors (loads, pore pressure changes, and earthquake accelerations) and/or internal factors (soil cohesion, friction angle, and undrained shear strength) could be a major reason that leads to these failures. The accuracy of shear strength parameters has a high priority to the geotechnical engineers for the analysis of such slope failures or the design of new embankment slopes, earth dams, etc.

The critical state friction angle ( $\phi'_{cs}$ ) is used to analyse the stability of slopes in granular soils, except in very rapid loading (e.g. earthquakes, blasting, vibrations, flow-slides) of saturated granular soils where shear-induced excess pore pressure accumulates and the undrained shear strength ( $s_u$ ) would apply. The CSL slope in the stress path diagram of Figure 4.2 reflects  $\phi'_{cs}$ . Accordingly, the steeper CSL of the smaller specimen would result in the false perception of a higher stability and safety of a field slope, while being less stable or even at failure based on a more representative  $\phi'_{cs}$  from the larger specimen.

To demonstrate the influence of specimen size on static and seismic stability of cohesionless soil slopes, the shear strength parameters from the triaxial compression tests on different

specimen sizes are used for the slope stability analysis of the Lower San Fernando Dam (LSFD).

LSFD is an earth embankment dam constructed during 1912 to 1915 in Los Angeles, California. The dam was a 43 m high dam with a reservoir capacity of about 25 million m<sup>3</sup> which was constructed using the hydraulic filling method (Seed *et al.* 1975). LSFD suffered significant damage following the February 9<sup>th</sup>, 1971 San Fernando earthquake as a result of liquefaction flow failure associated with strength losses and development of very high pore-water pressure in the hydraulically filled sandy soil of its upstream slope (Seed *et al.* 1975, Lee *et al.* 1975, Castro *et al.* 1992). The cross section of the dam prior to the failure is shown in Figure 4.11.

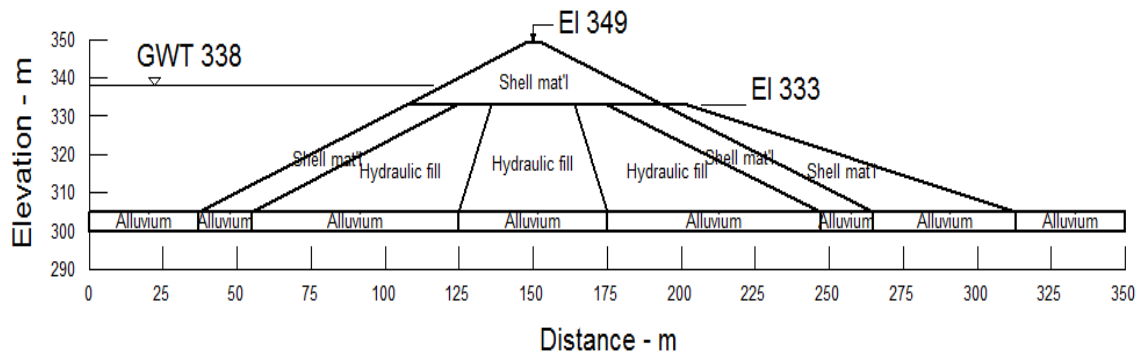


**Figure 4.11:** Pre-failure cross section of LSFD (Seed *et al.* 1975)

LSFD as a typical geometry of an embankment dam that underwent liquefaction flow failure is an adequate case to analysis the slop stability using different shear strength parameters of the tested loose Ottawa sand. In this study, the drain and undrained stability of the LSFD is analyzed using the  $\phi'_{cs}$  (for drained analysis),  $s_u(\text{yield})$  and  $s_u(\text{critical})$  (for undrained analysis) from the triaxial test of this study. Limit equilibrium analyses (Spencer 1967) are

performed using the Slope/W (Version 7) software package from GeoStudio Ltd and the factors of safety are compared for the stability of the slopes.

#### 4.6.1 Static Slope Stability Analysis

Drained stability analyses corresponding to a static loading condition, were conducted using  $\phi'_{cs}$  for the three specimen sizes of 70, 50, and 38mm in the Mohr-Coulomb failure criterion. The analyses were carried out for the original cross section of the LSFD in Figure 4.11 and assuming a uniform material (Ottawa sand) for the entire hydraulic fill dam with a total unit weight of  $15.3 \text{ kN/m}^3$ . A separate steady-state seepage analysis was initially performed using Seep/W for more precise calculation of the effective stresses existing in the dam. The minimum factors of safety using the strength parameters of different specimen sizes are summarized in Table 4.2 and the analysis diagrams are included in Appendix B.

#### 4.6.2 Seismic Slope Stability Analysis

Undrained stability analyses were conducted for the seismic stability of the LSFD during the 1971 San Fernando earthquake. It is assumed that the entire hydraulic fill was constructed at a density corresponding to  $\psi = 0.05$  and the undrained shear strength ratios corresponding to  $\psi = 0.05$  are used. The seismic acceleration as a pseudo-static acceleration was applied in Slope/W where the average acceleration of the sliding mass was estimated as 0.2 using (Makdisi and Seed's 1978) plot. The method described by Olson and Stark (2003a) is used for the liquefaction triggering and flow slide stability analyses. In this method,  $s_u(\text{yield})/p'_c$  is used to determine the critical failure surface along which a larger portion of the hydraulic fill material would liquefy under the combined seismic and static (self-weight) loads.

Therefore, the liquefied slices are identified as those in which  $s_u(\text{yield})/p'_c$  is exceeded by the total driving shear stress at the base of the slide. A separate stability analysis is subsequently conducted using  $s_u(\text{critical})/p'_c$  for the liquefied slices and  $s_u(\text{yield})/p'_c$  for those which did not liquefy without including the seismic loads in order to assess the stability of the LSFDF against liquefaction flow failures. Table 4.2 summarizes the factors of safety obtained for each specimen size in both static and seismic analyses.

**Table 4.2:** Factor of safety against static and seismic loads of different specimen sizes

Specimen Size	FOS (Static S. Analyses)	FOS (Seismic S. Analyses)
70 mm	1.58	0.89
50 mm	1.75	1.05
38 mm	1.89	1.14

According to Table 4.2 specimen size has a significant impact on the computed factor of safety with the smaller specimen producing a higher factor of safety as a result of the differences existing in the effective stress friction angles and the undrained shear strengths of different specimen sizes. With a smaller specimen size, the slope is safe ( $\text{FOS} > 1$ ) while with using the strengths from a larger specimen the slope would fail ( $\text{FOS} < 1$ ). The analysis diagrams are included in Appendix B.

The factors of safety for the three specimen sizes in both drained and undrained conditions are plotted versus the sample size in Figure 4.12 which illustrates the significance of scale effect and sample size on the stability analyses and safety of slopes. Testing larger

specimens is recommended and the specimen size effects should be considered in landslides risk assessment.

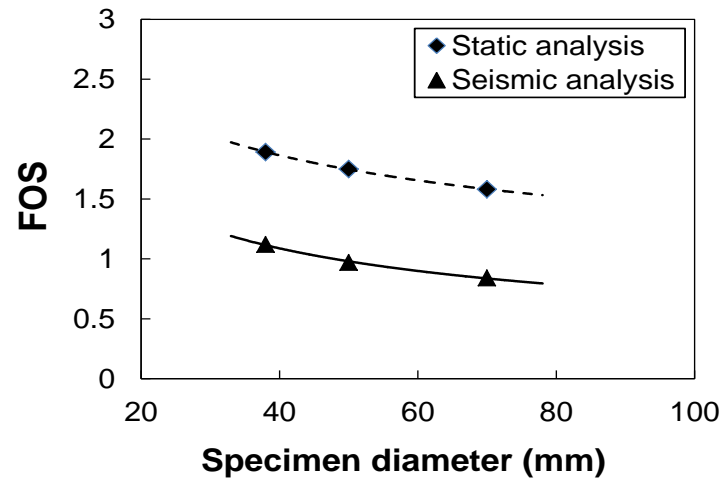


**Figure 4.12:** Specimen size effect on factors of safety (FOS) from static and seismic slope stability analyses

## 4.7 Sample Size Effect on Bearing Capacity of Shallow Foundations

Shallow foundations including spread footing and mat foundations are often constructed on the ground surface or at a shallow depth beneath the ground to transmit the structural loads to the ground over a suitably large area. The proper design of a shallow foundation is to ensure that the structural load is carried safely by the underlying soil. The ultimate bearing capacity ( $q_{ult}$ ) is the critical applied pressure at which the soil mass beneath the foundation will theoretically collapse if exceeded. Vesic (1973, 1975) proposed a general bearing capacity formula as below which is widely used in engineering practice:

$$q_{ult} = c' N_c + \gamma' D N_q + 0.5 \gamma' B N_\gamma \quad (4.1)$$

Where  $N_c$ ,  $N_q$ , and  $N_\gamma$  are bearing capacity factors,  $B$  and  $D$  are width and depth of the foundation,  $c'$  and  $\gamma'$  are the effective cohesion and unit weight. Additional correction factors could be introduced to account for the foundation shape, depth, load inclination, base inclination, and ground inclinations.

Several researchers have investigated the scale effect of different foundation sizes on the bearing capacity factor  $N_\gamma$  for shallow foundations (DeBeer 1965, Habib 1974, Shiraishi 1990, Zhu *et al.* 2001, Ueno *et al.* 2001, Okamura *et al.* 2003, Cerato and Lutenecker 2007). DeBeer (1965) was the first to observe that the bearing capacity factor  $N_\gamma$  decreases with an increase in foundation width, and related this to the greater friction angle mobilized beneath large foundations. Habib (1974) did analytical analysis and observed that the bearing capacity of sands was sensitive to the width of the footing rather than the size of the sand particles. He found that smaller footings had a greater bearing capacity. Zhu *et al.* (2001) present numerical and physical modeling (with centrifuge tests) studies of scale effect on the bearing capacity of strip and circular footings on dense silica sands. Their findings indicate that the bearing capacity of both strip and circular footings increase with decreasing footing size. Ueno *et al.* (2001) reappraised the footing size effects on the prediction of ultimate bearing capacity of strip and circular surface footings. They considered the relationship between the footing width and the strength parameters of the underlying granular soil. They developed a rational method (using FEM) to estimate the soil shear parameters based on the stress range under the footing at failure. In addition, they introduced an extended slip line method with variable footing widths for estimating the ultimate bearing capacity which increased with decreasing footing width. Okamura *et al.* (2003) studied the effects of shape and size of footings on the bearing capacity and deformation characteristics of dense

Toyoura sand. They performed a series of centrifuge loading tests on rectangular footings with aspect ratios from 1 to 5 at two different centrifugal accelerations. They observed that the bearing capacity factor  $N_\gamma$  decreased with an increase in the footing width irrespective of footing shape. Cerato and Lutenegeger (2007) further evaluated the trend of decreasing  $N_\gamma$  with increasing footing width by testing a large range of model-scale square and circular footing sizes, ranging in width from 0.025 to 0.914 m, on two compacted well-graded sands at three relative densities. Their results indicated that  $N_\gamma$  was dependent on the width of the footing for both square and circular footings with the smaller footings exhibiting higher  $N_\gamma$  values, and the impact increased with increasing sand relative density. Tatsuoka *et al.* (1991) related the effect of footing size effect on  $N_\gamma$  to the stress-level dependency of sand mechanical properties (as also suggested by DeBeer 1965) and the relative size of sand particles compared to the footing width (B). Accordingly, Kusakabe (1995) suggested testing footing sizes with  $B/D_{50}$  ratios higher than 50–100 to avoid the particle size effect while Cerato and Lutenegeger (2007) reinstated the effect of stress level as the observed footing-size dependency of  $N_\gamma$ . Based on this mechanism, the mobilized friction angle in the underlying soil decreases with increasing mean stress under larger footings.

The effect of specimen size is demonstrated using Equation (4.1) for the calculation of  $q_{ult}$  based on the triaxial test results of this study. For a shallow foundation resting on the surface ( $D = 0$ ) of a sandy soil ( $c' = 0$ ), Equation (4.1) reduces to the following relationship:

$$q_{ult} = 0.5 \gamma' B N_\gamma \quad (4.2)$$

Where the bearing capacity factors  $N_\gamma$  and  $N_q$  are obtained as below (Vesic 1975):

$$N_{\gamma} = 2(N_q + 1) \tan \phi' \quad (4.3)$$

$$N_q = e^{\pi \tan \phi'} \tan^2 (45 + \phi'/2) \quad (4.4)$$

Table 4.3 and Figure 4.13 show the effective friction angles ( $\phi'_{cs}$ ) and the calculated  $N_{\gamma}$  values for each specimen size.

**Table 4.3:** Bearing capacity factor based on  $\phi'_{cs}$  of different specimen sizes

Specimen Size	$\phi'_{cs}$ (degrees)	$N_{\gamma}$
70 mm	28	16.7
50 mm	31	26.0
38 mm	32	30.2

According to Figure 4.13, differences in  $\phi'_{cs}$  from the differences in specimen size can have a profound impact on the bearing capacity factor  $N_{\gamma}$  with the smaller specimens producing higher  $N_{\gamma}$  values. For example, an increase of  $4^{\circ}$  in the friction angle from the 70 mm to the 38 mm specimen diameter led to 80% increase in  $N_{\gamma}$ . Accordingly, the allowable bearing capacity could be significantly overestimated using the strength parameters of small specimens (e.g. 38 mm), which could lead to less safe foundation dimensions and the possibility of unaccounted large settlements associated with ground failure. An additional correction factor could be devised to reduce  $N_{\gamma}$  obtained from laboratory tests on small specimens and account for specimen size effect.



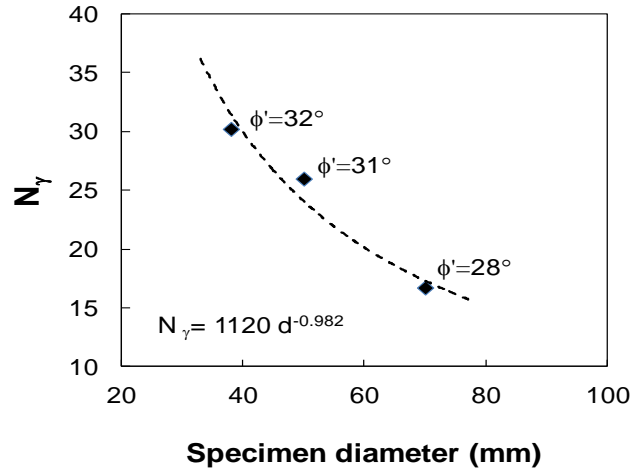


**Figure 4.13:** Bearing capacity factor as a function of specimen size

The specimen size effect observed in the triaxial compression tests is similar to the particle size mechanism introduced by Tatsuoka *et al.* (1991) and Kusakabe (1995). In both situations, a larger number of particles and particle contacts become involved in a larger specimen (in the triaxial tests) or beneath a larger footing, which reduces the overall amount of the mobilized shear resistance. This result also agrees with the observation of Eid (1987) where the cone penetration resistance was lower for larger cones and with Lehane *et al.* (2005) who observed that the effective lateral stresses significantly reduced with increasing pile diameter.

## 4.8 Sample Size Effect on Lateral Earth Pressure

The design of earth retaining walls, abutments, mechanically stabilized earth walls, and reinforced soil slopes is a challenging geotechnical problem (Holtz *et al.* 2001). The basic design approach for these structures is to design against sliding, overturning, or bearing

capacity failure. In all of these phases of design, the lateral active earth pressure coefficient,  $k_a$ , plays a vital role in the stability analyses which is defined as:

$$K_a = \tan^2 \left( 45 - \phi'_{cs}/2 \right) \quad (4.5)$$

The measured  $\phi'_{cs}$  for different sample sizes are employed to calculate  $k_a$ , and to demonstrate the specimen size effect on lateral earth pressures in Figure 4.14.

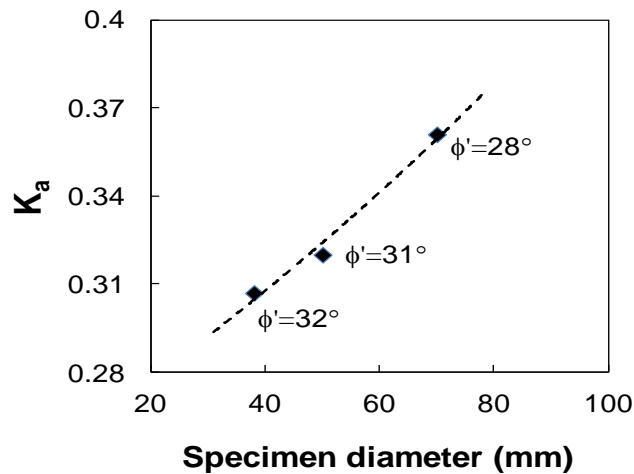


**Figure 4.14:** Lateral active earth pressure coefficient,  $k_a$ , as function of specimen size

Accordingly, the  $\phi'_{cs}$  differences realized as a result of differences in specimen size could significantly affect the lateral earth pressures and therefore the sliding and overturning analysis and design of retaining structures. Therefore, obtaining the soil strength properties by testing of larger specimens allows for building safer structures.

## 4.9 Conclusion

Scale effects have been observed in many practical implications by several researchers and illustrated in this study with different approaches. The shear strength parameters obtained from testing samples with different sizes could largely affect almost all geotechnical engineering applications in which soil shear strength and friction angle play important roles. The results of using shear strength parameters of three different specimen sizes indicated that the liquefaction triggering resistance increases with decreasing specimen size, large errors could arise in the application of constitutive models, uncertainty in stability analyses and safety of slopes and retaining structures, and the bearing capacity factor  $N_\gamma$  increases with decreasing specimen size. Accordingly, testing smaller specimens could lead to falsely higher liquefaction triggering resistance and the liquefaction potential would be underestimated, unsafe designs using numerical analysis with advanced soil constitutive models, higher static and seismic factors of safety in slope stability analyses, less safe foundation dimensions, and a falsely higher factor of safety in designing retaining structures. These outcomes highlight the significant influence of specimen size on the geotechnical engineering design and the importance of selecting an appropriate sample size in geotechnical laboratories. Testing larger specimen sizes allows an accurate shear behavior, better representation of field deformations, and building safer structures. In addition to the observation of many researchers on the behavior of most model-scale footing tests that cannot be directly correlated to the behavior of full-scale tests and the existing application of performing model-scale tests at a lower density than a corresponding prototype footing for accurate prediction of sand behavior.

## References

- ASTM, D2487-06 “Standard practice for classification of soil for engineering purposes (Unified Soil Classification System)” ASTM International, West Conshohocken, PA.
- ASTM, D4253-06 “Standard test methods for maximum index density and unit weight of soils using vibratory table” ASTM International, West Conshohocken, PA.
- ASTM, D4767-11 “Standard test method for consolidated un-drained triaxial compression test for soils” ASTM International, West Conshohocken, PA.
- ASTM, D7181-11 “Standard test method for consolidated drained triaxial compression test for soils” ASTM International, West Conshohocken, PA.
- Bareither, C. A., Benson, C. H., and Edil, T. B. (2011). “Compression behavior of municipal solid waste: Immediate compression” *J. Geotech. & Geoenviron. Eng.*, Vol. 10 (3), pp: 1-54.
- Been, K., Jefferies, M. G., and Hachey, J. E. (1991). “The critical state of sands” *J. Geotechnique*. Vol. 41 (3), pp: 365–381.
- Byrne, P. M., Roy, D., Campanella, R. G., and Hughes, J. (1995). “Predicting liquefaction response of granular soils from pressuremeter tests” *ASCE, Geotech. Special Publication*. Vol. 56, pp: 122-135.
- Castro, G., Seed, R. B., and Keller, T. O. (1992). “Steady state strength analysis of loser San Fernando Dam slide” *J. Geotech. Eng.*, Vol. 29 (6), pp: 406-427.
- Cerato, A. B., and Lutenecker, A. J. (2007). “Scale effects of shallow foundation bearing capacity on granular material” *J. Geotech. & Geoenviron. Eng.*, Vol. 133 (10), pp: 1192 - 1202.
- De Beer, E. E. (1963). “The scale effect in the transposition of the results of deep-sounding tests on the ultimate bearing capacity of piles and caisson foundations” *J. Geotechnique*. Vol. 13 (1), pp: 39–75.
- De Beer, E. E. (1965). “The scale effect on the phenomenon of progressive rupture in cohesionless soils” *Proc., 6th Int. Conf. on Soil Mech. and Found. Eng.*, Vol. 2(3–6) Montreal, Canada, pp: 13–17.
- Duncan J. M., and Wright S.G. (2005). “Soil strength and slope stability” John Wiley & Sons, Hoboken, New Jersey.
- Eid, W. K. (1987). “Scalling effect in cone penetration testing in sand” PhD Thesis. Virginia Polytechnic Institute and State University.
- Frantziskonis, G., Desai, F., and Somasundaram, S. (1986). “Constitutive model for non-associative behavior” *J. Eng. Mech.* Vol. 112 (9), pp: 932-946.
- Habib, P. A. (1974). “Scale effect for shallow footings on dense sand” *J. Geotech. Eng.* Vol. 100 (GT1), pp: 95–99.
- Hettler, A., and Gudehus, G. (1988). “Influence of the foundation width on the bearing capacity factor” *J. of Soils Found.*, Vol. 28 (4), pp: 81–92.
- Holtz, R., D. (2001). “Geosynthetics for soil reinforcement” 9<sup>th</sup> Spencer J. Buchanan lecture.

- Holtz, R. D., Shang, J. Q., and Bergado, D. T. (2001a) "Soil Improvement", Chapter 15 in *Geotech. and Geoenviron. Handbook*, pp: 429-462.
- Imam, S. M., Morgenstern, N. R., Robertson, P. K., and Chan, D. H. (2005). "A critical state constitutive model for liquefiable sand" *Can. Geotech. J.* Vol. 42 (3), pp: 830-855.
- Ishihara, K., Tatsuoka, F., and Yasuda, S. (1975). "Undrained deformation and liquefaction of sand under cyclic stresses" *J. Soil Found.*, Vol. 15(1), pp: 29-44.
- Jefferies, M. G. (1993). "Nor-Sand: A simple critical state model for sand" *J. Geotechnique*. Vol. 43 (1), pp: 91-103.
- Jefferies, M. and Shuttle, D. A., (2002). "Nor-Sand: Features, calibration and use" *J. Geotechnique* Vol. 113 (2), pp: 204-237.
- Jefferies, M. and Been, K. (2006). "Soil liquefaction: a critical state approach" Taylor & Francis, New York, London, 479 p.
- Kramer, S. L. (1996). "Geotechnical Earthquake Engineering" Prentice Hall, Inc., Upper Saddle River, New Jersey
- Kusakabe, O. (1995). "Chapter 6: Foundations." *Geotechnical centrifuge technology*, R. N. Taylor, ed., Blackie Academic & Professional, London, pp: 118-167.
- Ladd, C. C. (1978). "Preparing test specimen using undercompaction" *J. of Geotech. Testing*. Vol.1, pp: 16-23.
- Lade, P. V. (1980). "Elasto-plastic stress-strain model for sand" *J. Geotech. Eng.*, Vol. 106 (4), pp: 628-648.
- Lade, P. V. (1992). "Static instability and liquefaction of loose fine sandy slopes" *J. Geotech. Eng.*, Vol. 118 (1), pp: 51-72.
- Lade, P. V., and Duncan, J. M. (1975). "Elastoplastic stress-strain theory for cohesionless soil" *J. Geotech. Eng.*, Vol. 101 (10), pp: 1037-1053.
- Lee, K., L. (1975). "Properties of soil in the San Fernando hydraulic fill dams" *J. Geotech. Eng.*, Vol. 101 (8), pp: 801-819.
- Lee, K. L., Seed, H. B., Idriss, I. M., and Makadisi, F. I. (1975). "Properties of soil in the San Fernando Hydraulic Fill Dams" *J. Geotech. Eng.* GT8, pp: 801-821.
- Lehane, B. M., Gaudin, C., and Schneider, J. A. (2005). "Scale effects on tension capacity for rough piles buried in dense sand" *J. Geotechnique*. Vol. 55 (10), pp: 709 – 719.
- Manzari, M. T., and Dafalias, Y. F. (1997). "A critical state two surface plasticity model for sands" *J. Geotechnique*. Vol. 47 (2), pp: 255-272.
- Mesri, G., and Vardhanabhuti, B. (2009). *Compression of granular materials*. *Can. Geotech. J.* Vol. 46(4), pp: 369-392.
- Meyerhof, G. G. (1948). "An investigation of the bearing capacity of shallow footings on dry sand" *Proc., 2nd Int. Conf. on Soil Mech. and Found. Eng.*, Rotterdam, The Netherlands, Vol. 1, pp: 237-243.
- Nova, R., and Wood, D. M. (1979). "A constitutive model for sand in triaxial compression" *Int. J. Num. Analy. Meth. Geomech.*, Vol. 3 (2), pp: 255-278.

- Okamura, M., Mihara, A., Takemura, J., and Kuwano, J. (2003). "Effects of footing size and aspect ratio on the bearing capacity of sands subjected to eccentric loading" *J. of Japanese Geotechnical*. Vol. 2 (23), pp: 43-56.
- Olson, S. M., and Stark, T. D. (2001). "Liquefaction analysis of Lower San Fernando Dam using strength ratios" *Proc. 4<sup>th</sup> Inter. Conference in Geotech. Earthquake Eng. and Soil Dynamics*. p 4.05.
- Olson, S. M., and Stark, T. D. (2003a). "Yield strength ratio and liquefaction analysis of slopes and embankments" *J. Geotech. & Geoenviron. Eng.* 129 (8), pp: 727–737.
- Pestana, J. M., Whittle, A. J. (1995). "Compression model for cohesionless soils" *J. Geotechnique*. Vol. 45 (4), pp: 611-631.
- Pestana, J. M., Whittle, A. J. (1999). "Formulation of a unified constitutive model for clays and sands" *Int. J. 43 Numer. Anal. Meth. Geomech*, Vol. 23, pp: 1215-1243.
- Sadrekarami, A. (2011). "An alternative mechanism for earthquake-induced displacement of the lower San Fernando Dam" *Georisk, Assessment and management of risk for engineering systems and geohazards*, Taylor and Francis, First article, pp: 1-12.
- Seed, H.B., Lee, K. L., Idriss, I. M., and Makdisi, F.I (1975a). "The slides in the San Fernando Dams during the earthquake of Feb. 9, 1971" *J. Geotech. Eng. Division*, Vol. 101 (7), pp: 651-688.
- Seed, H. B., (1979). "Consideration in the earthquake-resistant design of earth and rockfill dams" *J. Geotechnique*. Vol. 29 (3), pp: 215-263.
- Shiraishi, S. (1990). "Variation in bearing capacity factors of dense sand assessed by model loading tests" *J. Soils Found.*, 30 (1), pp: 17–26.
- Spencer, E. (1967). "A method of analysis of the stability of embankments assuming parallel inter-slice forces" *J. Geotechnique*. Vol. 15, pp: 11-26.
- Tatsuoka, F., Goto, S., Tanaka, T., Tani, K., and Kimura, Y. (1997). "Particle size effects on bearing capacity of footing on granular material" *Proc. Int. Conf. on Deformation and Progressive Failure in Geomech.*, IS Nagoya '97, pp: 133–138.
- Tatsuoka, F., Okahara, M., Tanaka, T., Tani, K., Morimoto, T., and Siddiquee, M. S. A. (1991). "Progressive failure and particle size effect in bearing capacity of a footing on sand" *J. of Geotechnique*. Vol. 27 (2), pp: 788–802.
- Ueno, K., Miura, K., Kasakabe, O., and Nishimura, M. (2001). "Reappraisal of size effect of bearing capacity from plastic solution" *J. Geotech & Geoenviron. Eng.*, 127(3): pp: 275 – 281.
- Vesic, A. S. (1973). "Analysis of ultimate loads of shallow foundations" *J. Soil Mech. and Found.*, 99 (1), pp: 45–73.
- Vesic, A.S. (1975). "Bearing capacity of shallow foundations" *Found. Eng. Handbook*, 1st ed., pp: 121-147.
- Wood, D. M. (1990). "Soil Behaviour and Critical State Soil Mechanics" Cambridge University Press, Cambridge.
- Zhu, F., Clark, J., and Philips, R. (2001). "Scale effect on strip and circular footings resting on dense sand" *J. of Geotech. & Geoenviron. Eng.*, Vol. 127 (7), pp: 613–622.

## Chapter 5

### 5 Summary and Conclusions

The comprehensive experimental study performed in this research was accomplished in order to solve the problem of sample size. In the testing program three different sample sizes are used to investigate the effect of specimen size on very loose sand behavior in triaxial testing which illustrated the significance of sample size on sand shear behavior. A clear effect of specimen size on the yield and critical state friction angles, critical state parameters, and the yield and critical strengths were presented. The larger specimens showed stiffer isotropic compression behavior and significantly smaller compressibility than the smaller specimens. During shear, the smaller specimens exhibited steeper CSL, indicating a higher compressibility, exhibited higher initial modulus, and mobilized larger internal friction angles and shear strengths. The geometrical scale as well as the large number of shear bands and failure planes (the shear zone characteristics) in larger specimens could have produced the significant effect of specimen size on the observed behavior.

The experimental errors affecting the shear behavior of loose sand have been thoroughly reviewed in this research, which illustrated the significant effects of end restraint and triaxial data corrections on sand shearing behavior. The non-uniform deformations at large strain, which is often required to achieve critical state, may significantly affect the critical strength of sands. It was demonstrated that lubricated and enlarged end platens are helpful mechanisms to minimize the effects of end restraint and promote uniform deformations during shear. As a result of these improvements, accurate volume change in drained shear tests as well as lower deviator stresses and higher pore pressures were measured in the undrained shear tests. It was found that rough end platens could result in an average of 10%

and 4 degree overestimation in the critical strength and critical state friction angle, respectively. The importance of lubrication was found to increase with increasing specimen density. While lubrication improved specimens' deformation uniformity, it did not completely eliminate them and the final specimen shapes were slightly parabolic and an area correction conforming to the shape of the deformed specimens was used to account for this barreling deformation of the specimen and correct the measured axial stress on the specimens. Accordingly, the critical strength and critical state friction angle was further reduced by an average of 24% and 9 degrees, respectively. The bedding error due to the compression of the latex membrane used in the enlarged platens technique increased the measured axial strain by an average of 2.5%. It was further indicated that neglecting membrane resistance would lead to overestimation of the critical strength by an average of 8% and the friction angle by 3 degrees. The overall combined errors could overestimate the critical strength and friction angle of the tested loose sand as much as 42% and 15 degrees, respectively, if not corrected. Another important factor affecting the behavior of sands is its void ratio. The volume change during back pressure saturation and due to membrane penetration could significantly affect the critical void ratio and the location of the critical state line. The results of volume change analyses indicated that ignoring the volume change during saturation could lead to an overestimation of the sample void ratio up to 0.01 which corresponds to about 3% in terms of relative density. The membrane penetration into the surface cavities lead to an overestimation of specimens volume change during consolidation and thus the void ratio by about 0.003 which represents 0.9% changes in specimen's relative density. The relatively minor influence of membrane penetration on the volumetric strain could be related to the fine gradation ( $D_{50} = 0.22$  mm) of the tested sand that minimized the penetration of the membrane into the surface irregularities among the sand particles. The



area correction at large strains was the most significant source of error observed in this comprehensive study which requires necessary corrections for triaxial shear testing of loose sands.

Scale effects in many practical implications are illustrated in this research with different approaches. The results of using shear strength parameters of three different specimen sizes indicated that the liquefaction triggering resistance increases with decreasing specimen size, large errors could arise in the application of constitutive models, uncertainty in stability analyses and safety of slopes and retaining structures, and the bearing capacity factor  $N_\gamma$  increases with decreasing specimen size. Accordingly, testing smaller specimens could lead to falsely higher liquefaction triggering resistance and the liquefaction potential would be underestimated, unsafe designs using numerical analysis with advanced soil constitutive models, higher static and seismic factors of safety in slope stability analyses, less safe foundation dimensions, and higher factor of safety in designing retaining structures.

These outcomes highlight the significant influence of specimen size on the geotechnical engineering design in which soil shear strength and friction angle play important roles. In order to reduce specimen size and scale effects, triaxial testing of larger specimens is recommended as it also provides a better representation of field soil behavior. Based on the results of this study, it is recommended, to use sand samples with a minimum diameter no less than 320 times  $D_{50}$  and/or 100 times the maximum particle size in triaxial shear testing. Two equations are presented to estimate the deviation of undrained shear strengths and mobilized friction angles for samples of different sizes from a typical specimen size of 70 mm. The interesting finding of this research, open the door for a comprehensive study of the scale effect on different sands with different gradation, and different mean particle sizes.

Appendix A  
(Sensors Calibration Factors)

### PRESSURE SENSOR CALIBRATION

Date: August 9, 2013

**Sensor Information:**

Type:	Pressure Sensor
Mfgr:	Geotac
Model:	SQ226
Serial No:	PS2-288
Range:	200 psi

**Standard Information:**

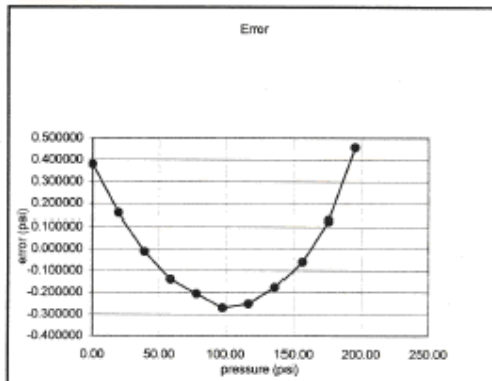
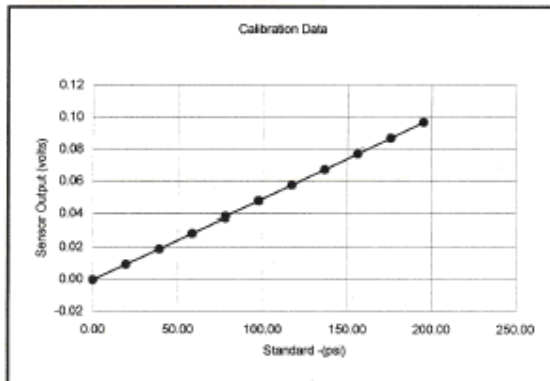
Type:	Digital Readout
Mfgr:	Geotac
Serial No:	PS-3012
ID:	
Last Calibration:	

Sensor Exctiation (volts): 9.918106079

**Calibration Results:**

Corr. Coefficient:	0.999992483
Slope (volts/in):	0.000497823
Intercept (volts):	-0.000189822
Calibration Factor	19922.94437
(in/Vs/Ve):	
Offset (volts):	-0.000189822

Standard (psi)	Sensor Output (volts)	Zero Adjusted Sensor Output (volts)	Best Fit Line Sensor Output (volts)	0.00 Best Fit Line error (volts)	0.46 Best Fit Line error (psi)	0.23 Accuracy %FS
0.00	-0.0005176	0	-0.000189	0.000189	0.379857	0.194657
19.48	0.00906742	0.00958497	0.009506	0.000078	0.157632	0.080778
38.97	0.01868886	0.01920641	0.019213	-0.000005	-0.012387	0.006348
58.47	0.02833067	0.02884823	0.028918	-0.000070	-0.140978	0.072244
77.97	0.03800613	0.03852368	0.038527	-0.000103	-0.206892	0.105919
97.50	0.04769388	0.04821144	0.048346	-0.000135	-0.270895	0.138717
116.98	0.05740293	0.05792048	0.058046	-0.000125	-0.251989	0.129131
136.49	0.0671512	0.06766875	0.067757	-0.000088	-0.177150	0.090780
155.95	0.07689771	0.07741527	0.077445	-0.000030	-0.060495	0.031001
175.48	0.08671143	0.08722899	0.087167	0.000062	0.125033	0.064073
195.07	0.09662867	0.09714623	0.096918	0.000228	0.457865	0.234632



### Load Cell Calibration Certificate

Date of Shipment 12/8/2011  
 Capacity 2000 lb  
 Input Resistance 464 Ohms  
 Excitation 10.00 VDC  
 Test Temp 73.2 degrees F  
 Linearity (% of R.O.) 0.027  
 ID Number 474042  
 Recommended Range 0 to 2000 lb  
 Output Resistance 353 Ohms  
 Relative Humidity 36.0%

Applied Load Pounds	Load Cell Reading (mV / V)	
	Tension	% Full Scale*
0	0.0000	0.000%
400	0.3991	0.016%
800	0.7981	0.027%
1100	1.0971	0.023%
1500	1.4959	0.024%
2000	1.9939	0.000%
0	0.0000	

Note: Error Calculated On Best Fit Straight Line Method

Calibration Factor: -1002974.811 lbs/V/V  
 Correlation Coefficient: 0.99999995

Note: Load cell calibration factor is valid for 1 year after shipment date

#### Calibration Equipment Used

Dead Weight: 3 klb  
 Traceability Number: 8511-09

Digital Multimeter:  
 HP Model Number: 34401A S/N US36133125

Calibrated By: Victor Garcilazo

Calibrated using equipment traceable to NIST in accordance with ISO/IEC 17025:2005 and ANSI/NCSL Z540-1-1994.

### LINEAR POSITION SENSOR CALIBRATION

Date: November 8, 2011

**Sensor Information:**

Type:	LPT
Mfr:	Geotac
Model:	LPT3
Serial No:	LPT-854
Range:	3 inch

**Standard Information:**

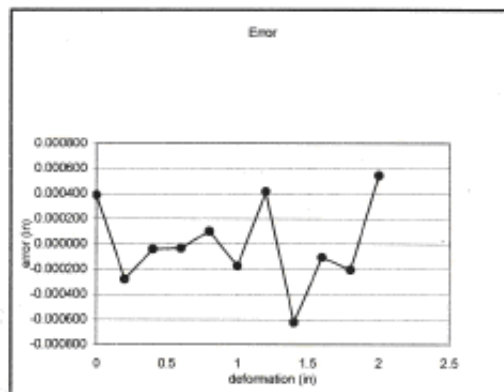
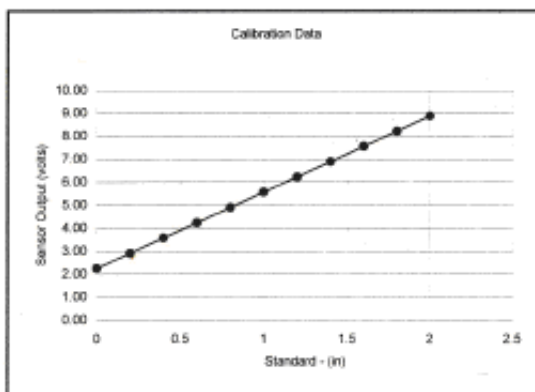
Type:	Gage block
Mfr:	HDT
Serial No:	21298
ID:	
Last Calibration:	

Sensor Excitation (volts): 10.0309

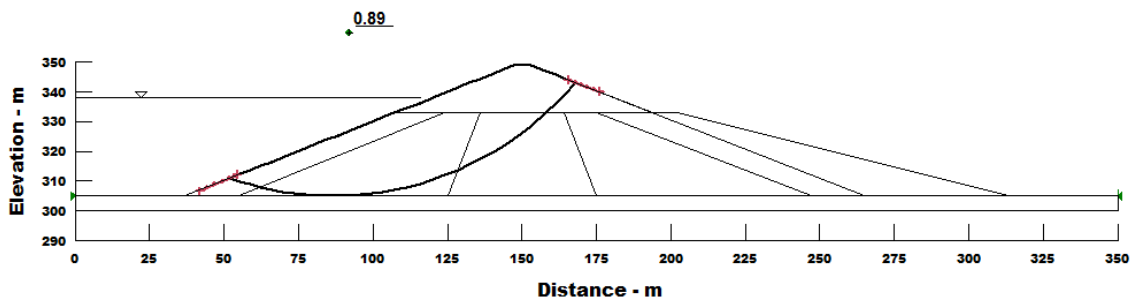
**Calibration Results:**

Corr. Coefficient:	0.999999865
Slope (volts/in):	3.319043136
Intercept (volts):	-0.00129759
Calibration Factor (in/Vs/Ve):	~ 0.2226463
Offset (volts):	-0.00129759

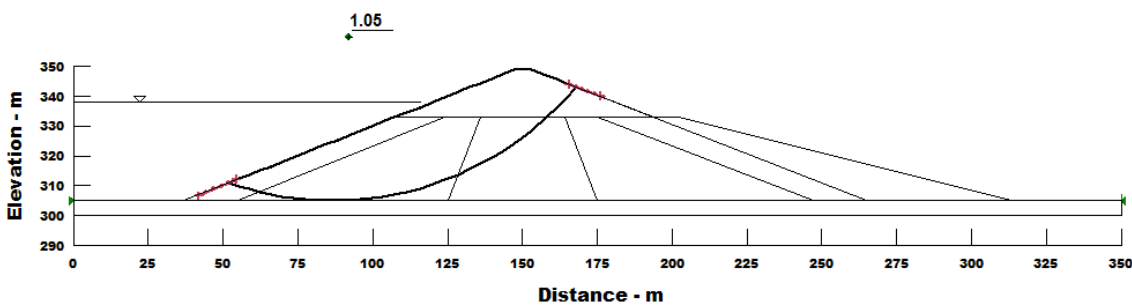
Standard (in)	Sensor Output (volts)	Zero Adjusted Sensor Output (volts)	Best Fit Line Sensor Output (volts)	0.00 Best Fit Line error (volts)	0.00 Best Fit Line error (in)	0.03 Accuracy %FS
2	8.886399	6.638601	6.636789	0.001812	0.000546	0.027300
1.8	8.220097	5.972299	5.972960	-0.000661	-0.000205	0.010259
1.6	7.556619	5.308821	5.309171	-0.000350	-0.000106	0.005279
1.4	6.891096	4.643298	4.645363	-0.002065	-0.000622	0.031103
1.2	6.230734	3.982936	3.981554	0.001382	0.000416	0.020815
1	5.564969	3.317171	3.317746	-0.000575	-0.000173	0.008685
0.8	4.902074	2.654276	2.653937	0.000339	0.000102	0.005108
0.6	4.237816	1.990018	1.990128	-0.000110	-0.000033	0.001661
0.4	3.573987	1.326189	1.326320	-0.000131	-0.000039	0.001968
0.2	2.90939	0.661592	0.662511	-0.000919	-0.000277	0.013844
0	2.247798	0	-0.001298	0.001298	0.000391	0.019546



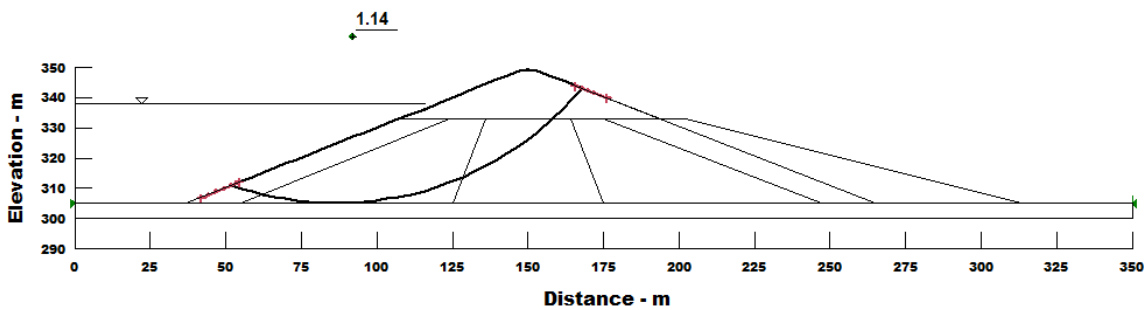
Appendix B  
(Stability Analyses - LSFD)



(a) - Result of 70 mm specimen

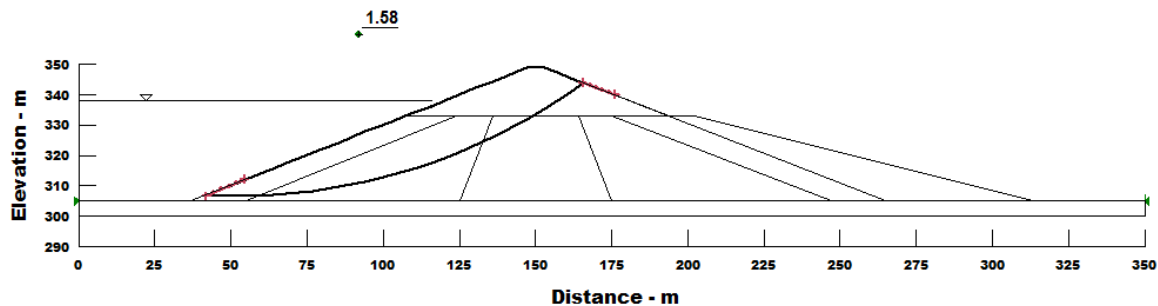


(b) - Result of 50 mm specimen

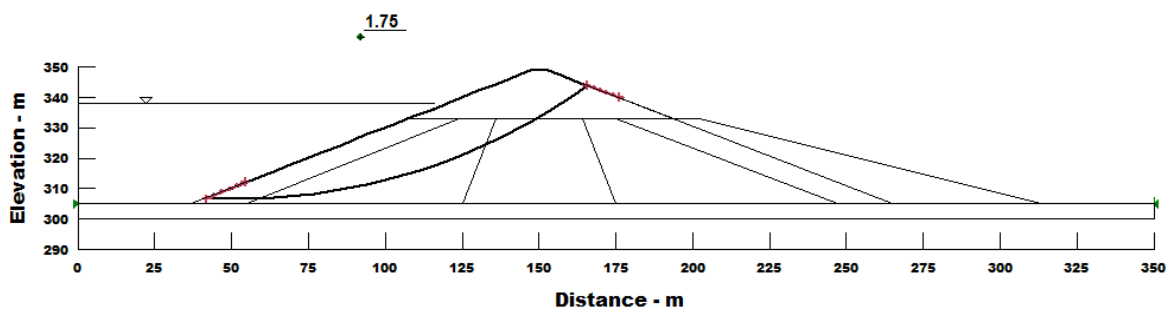


(c) - Result of 38 mm specimen

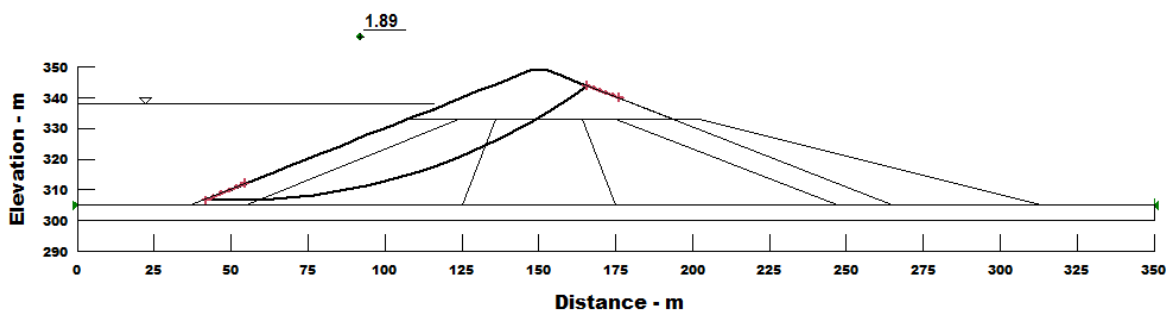
**Figure B.1:** FOS for seismic stability analyses using different specimen sizes



(a) - Result of 70 mm specimen



(b) - Result of 50 mm specimen



(c) - Result of 38 mm specimen

**Figure B.2:** FOS for static stability analyses using different specimen sizes



## Curriculum Vitae

**Name:** Tarek Omar

**Post-secondary  
Education and  
Degrees:** Ain-Shams University  
Cairo, Egypt  
1979-1984 B.A.

The University of Western Ontario  
London, Ontario, Canada  
2012-2013 M.A.

**Honours and  
Awards:** Quality Design Award  
Abu Dhabi, 2010-2011

Construction Excellence Award  
Dubai, 2007-2008

Young Consultant Award  
UK, 2002-2003

**Related Work  
Experience** Research Assistant / Teaching Assistant  
The University of Western Ontario  
London, Ontario, Canada  
2012-2013

Project Director  
Hyder Consulting Ltd. (UK)  
Abu Dhabi Branch, UAE  
1998-2011

Geotechnical Engineer  
Dorsch Consulting Ltd. (Germany)  
Abu Dhabi Branch, UAE  
1991-1998

**Publications:**

**Omar, T.**, Osouli, A., and Sadrekarimi, A. "Influence of Specimen Size in Engineering Practice" Proceedings of the ASCE, Geotechnical Special Publication, GeoCongress 2014, Atlanta, Georgia USA. February 23-26. Submitted; June 2013, Accepted; August 2013.